UNIVERSITAT DE BARCELONA

Ancestral roles of IκB proteins in *Caenorhabditis elegans*

David Ricardo Ahumada Brena

Programa de Doctorat en Biomedicina, Facultad de Medicina,
Universitat de Barcelona

Ancestral roles of IκB proteins

in *Caenorhabditis elegans*

Memòria presentada per

David Ricardo Ahumada Brena

per optar al grau de

Doctor

per la Universitat de Barcelona

UNIVERSITAT DE BARCELONA

Tesi doctoral realitzada sota la direcció del Dr. Julián Cerón Madrigal

Realitzada al Programa de Gens, Malaltia i Teràpia del l'Institut
d'investigació Biomèdica de Bellvitge (IDIBELL)

IDI BELL

El director,	El tutor,	L' autor,
Dr. Julián Cerón Madrigal	Dr. Francesc Vinyals Canals	David Ricardo Ahumada Brena

Barcelona, Juny de 2021

A mi familia mexicana y española

Acknowledgments

Raticos de nfki-1

Hacia el final de la primavera del 2016, poco antes del inicio de la Eurocopa, desde el otro lado del charco yo ya estaba pendiente de lo que sucedía en el Viejo Continente, aunque no precisamente en cuando al fútbol.

Yo era un muchacho oaxaqueño motivado que había empezado a tener minutos en equipos pequeños de la Masía mexicana que, aunque cortos de presupuesto, nos inculcaban la pasión y el respeto por la buena ciencia, pero que sabíamos que era difícil vivir en nuestras tierras por falta de inversión, pocas plazas de posgrado, una extenuante burocracia y, cómo no, escándalos de corrupción. Así que, aunque sabía que probablemente en ningún lado existe el paraíso científico, comencé a buscar clubes en España, la tierra natal de mi abuela.

Quería jugar con los grandes, quería aprender lo que es desayunar, comer y cenar pensando en lo que te salió en un experimento, aprender cuándo valía la pena atacar con todo lo que daba para resolver una pregunta; saber cuándo una retirada a tiempo es una victoria, sobre todo en aquellas sesiones de microinyección; entender que la ciencia es poner escalones y que de la manera más Cholista posible, conviene

mentalizarse a que vamos partido a partido. Todo esto y muchas más enseñanzas no sólo profesionales sino personales, y que he de decir que han llegado en el momento preciso cuando las necesitaba, las he aprendido gracias a ti, Julián. En ti he tenido la fortuna no sólo de encontrar un gran mentor, sino además un gran amigo. Así que me gustaría aprovechar estas líneas para agradecerte todos los "*up to you"*, "*enjoy life"*, también las jaladas de orejas necesarias de vez en cuando, y corroborarte que tus esfuerzos, trabajo y el corazón generoso que le pones a todo seguirán con cada uno de tus doctorandos. Gracias también a Joan, capitán del BigSpinLab con el que pude coincidir en mis meses de cesión por ese club. También agradecer a todo el BigSpinLab por acogerme como uno más desde el minuto 1.

En una buena dinámica de equipo tiene gran mérito el entrenador, pero quizá hasta un poco más lo tienen los jugadores, y cómo no, hasta la suerte. En este sentido, yo he tenido una suerte extraordinaria por los compañeros de equipo que me han tocado, siendo no sólo unos verdaderos *cracks* en la ciencia, sino también dominando tácticas avanzadas de levantamiento de jarras de *Turia* y un exquisito manejo del maravilloso, pero peligroso, deporte de cerrar bares.

Gracias a vosotros, las tardes largas de pinchadas, preparación de *lab meetings* (donde está la verdadera felicidad), arduas discusiones filosóficas de "interpretación de

datos", y posiblemente cualquier acontecimiento más o menos relevante que nos sucedió en el lab (o fuera), fue muchísimo más agradable, divertido y enriquecedor. Los quiero muchísimo (sí, hemos llegado ya a este *level* del texto) y me enorgullece pensar en lo mucho que hemos crecido juntos, y lo que nos falta. Sois mi familia española y mudarse lejos de casa para empezar una nueva vida ha sido muchísimo más fácil en gran parte por vosotros. Ahora, antes de que comencéis a preguntaros si en serio sólo voy a poner unas líneas generales sobre vosotros, comienzo con el marcaje personal (en orden de aparición, al estilo de peli de *Woody Allen*):

Dmytro, poca broma, a ti te conocí en el máster y hemos pasado de, por alguna extraña razón pensar que no hablábamos español y comunicarnos en inglés, a ser compis de lab, ahora de piso, y por azares del destino a veces seguir comunicándonos en inglés *for no reason*. Gracias por ser ese gran amigo que está siempre ahí para ayudarte, por todas las *pláticas*, los consejos y demostrarme que siempre vale la pena ser noble y bondadoso.

Carmenaure, tú me enseñaste el maravilloso arte de trabajar con nuestro nematodo favorito y luego hemos disfrutado divulgando *apostólicamente* juntos sus muchas cualidades, pero también me mostraste que la alegría siempre está dentro de ti, y que sólo tienes que dejarla bailar un poco de *salsa* para que se expanda hasta alcanzar a los que quieres. Muchas

gracias por todos esos valiosos *momentos-stickers* que hemos compartido. Gracias también por presentarme a Ale, que es un tipazo y amigo al que también le debo mucho.
Jeivy, maestro de las pinchadas y del karaoke, contigo siempre he compartido este sentimiento *expat* que curiosamente nos separa 7 husos horarios, sólo que en direcciones opuestas, de nuestras familias. Muchas gracias por todos los buenos momentos dentro y fuera del lab, las anécdotas de *Alta Galicia,* y por armonizar el lab con tus sesiones *a capella.* Tiene poco que volaste a jugar la *Champions* con el CRG, y ya se nota tu ausencia en el *IDIBELL Arena*.

Precisamente hablando de ausencias, Xénia, en las vitrinas del museo del equipo están expuestos todos los trofeos y premios que tu paso por el club nos ha dejado, eres una crack y me enorgullece haber compartido vestuario contigo, gracias por tantas enseñanzas científicas y por todos los otros premios que ganamos juntos fuera de las poyatas, tales como el *Trofeo Campari,* el *Mundialito de La Granadella*, y la *Copa Colonia-Düsseldorf.* Ha sigut un autèntic plaer.

Quiero extender también un agradecimiento enorme a nuestros compañeros de estadio, los grandes fichajes del IDIBELL: Leire, Laura, Clara, Juanjo, Edgard, Valentina, Júlia, Edgar, Isa, Paula, Mariona, Miguel, Núria, a mis compañeros

del Comité de PhDs, y todos con los que pude compartir campo, se crece más entrenando con los mejores.

Mención especial para mi excompañero de Cerón lab y siempre amigo Lluís, tú fuiste mi primer verdadero amigo español y ahora no sólo compartimos muchísimas vivencias inolvidables como el *Primavera* (ojo al que se viene), el *Mad Cool*, los viajes a Mallorca, los inicios de estos raticos de *nfki-1* y los dolores de cabeza en la caracterización de los fenotipos, sino que por si fuera poco formamos nuestra banda de indie rock *DNA Dàmage* junto con el buen Filip, *też jesteś kochany, cabrón*. Pocas personas han estado tan acertadas en los momentos en los que realmente lo necesitaba, eres un gran amigo y me da *un chingo* de gusto saber que seguiremos añadiendo capítulos a esta historia, y ojalá algún concierto de *DNA Dàmage.* ¡A que molaría!

Fuera del campo también he sido muy afortunado al haber podido compartir los primeros 3 años de este viaje con dos de mis mejores amigos desde México, Raz y Roy.
Raz, gracias por transmitirme esa pasión por la bioinformática, ahora cada vez más informática jajaja, por mostrarme el valor de la constancia y lo que se necesita para triunfar profesionalmente. Por si fuera poco, por ser un gran amigo y siempre recomendarme pelis *chidas*.
Roy, gracias por enseñarme que, citándote: "*Lo que importa es la actitud, wey*". Por tantos consejos, pláticas y anécdotas

cagadas que siempre quedarán y seguirán sorprendiéndonos en los guiones de *Los Escritores*. Con ustedes dos creamos ya no sé cuántas temporadas de excelentes vivencias tipo *sitcom*, y la batalla del doctorado siempre fue más fácil de afrontar sabiendo que estarían en casa para recibirme con una chela.

También quiero dedicar estas líneas, que nunca serán suficientes, para agradecer a Ivonne, amigui eres de las mejores sorpresas que me ha dado Barcelona. Gracias por todo lo que me has enseñado, por ayudarme a deconstruirme y entender muchas cosas sobre feminismo y sobre la vida, eres un gran ejemplo para mí por tu valentía, perseverancia y calidez. Gracias por hacerme sentir que de pronto nuestro México está más cerquita.

Это текст на русском языке был сделан специально для того чтобы вы могли быстрее найти ту часть в которой говорится о Вас.
Dasha, perhaps my greatest luck of these years has been meeting you and being able to share this time, and the long journey that we have ahead, with a person as magnificent as you. Thank you for reminding me that kind, empathetic, and caring love as the one we share, is the vital force that moves our lives. It is true what they say, that when you least expect it, love knocks at your door. Certainly, I wasn't expecting that the

door would be knocked from inside, and that I was already so close of the happiness that I was about to find. Love you.

También quiero agradecer enormemente a Nicol, tú viviste esa época de escritura intensiva de tesis durante la ya de por sí difícil etapa de confinamiento, y siempre estuviste ahí para animarme, compartir un vinito o cava y salirme del mundo de los gusanitos.

Aprovechando que hablo de la desconexión del mundo gusanero, quiero agradecer también a Bryan, Aby, Coca, JP, Adriana, Brendis, Pedrinho, Chamo, Mar y Rafa de la Facultad de Farmacia, ustedes me recordaron que hay vida fuera del lab y que en los *brunchs* no sólo se come.

Cruzando de vuelta el charco, siempre tengo presentes a mis grandes hermanos de toda la vida Tebo, Javi, Cane y Daniel. Quiero que sepan que a pesar de lo mucho que los extraño, me da mucho gusto darme cuenta de que nuestras amistades son y serán capaces de superar las vicisitudes de los años y de la distancia. Espero poder verlos pronto.

Finalmente, y como cumbre de estos largos, pero necesarios agradecimientos, quiero agradecer a mi familia. Sin ustedes nada de esto hubiera sido posible. Gracias por siempre haberme otorgado el amor y apoyo que he podido necesitar, por todos los sacrificios que hicieron para que yo pudiera

aspirar a cosas mejores, por la libertad y la confianza para impulsarme a seguir mis sueños, aunque esto represente volar lejos y vernos crecer desde la distancia. Gracias por inculcarme los valores necesarios para ser una persona de bien y por saberme querido y quererlos siempre. Mamá, tu amor es infinito y lo siento siempre cerca de mí. Abuelita, tú fuiste la conexión inicial entre los dos mundos en los que vivo ahora y vivir en tu país hace que siempre te tenga en mis pensamientos. Tatos, tu bondad y tus consejos me acompañan a donde voy y he notado que hay incluso lecciones de vida que me diste y que sigo descubriendo. Gracias por todo. A Ella, Moss, Connie, Arturo, Ramón y Mario, porque de cada uno de ustedes he aprendido mucho y en estos años de lejanía física nunca han permitido que me sienta solo. Los quiero a todos.

Mención final a todos los pequeños gusanitos, wild types y mutantes, que dieron sus vidas sin saberlo por este proyecto que intenta acercarnos a conocer un poco más sobre los procesos biológicos que están involucrados en el desarrollo del cáncer.

ABSTRACT

ABSTRACT

Mammalian Inhibitor-of-kappa-B (IκBs) proteins exert their main function as negative regulators of NF-κB, a central signaling pathway controlling immunity and inflammation. An alternative chromatin role for IκBs has been shown to affect stemness and cell differentiation. However, the involvement of NF-κB in this function has not been excluded. NFKI-1 and IKB-1 are IκB homologs in *Caenorhabditis elegans*, which lacks NF-κB nuclear effectors. We found that *nfki-1* and *ikb-1* mutants display developmental defects that phenocopy mutations in Polycomb and UTX-1 histone demethylase, suggesting a role for *C. elegans* IκBs in chromatin regulation. Further supporting this possibility *(i)* we detected NFKI-1 in the nucleus of cells; *(ii)* NFKI-1 and IKB-1 bind to histones and Polycomb proteins, *(iii)* and associate with chromatin *in vivo*, and *(iv)* mutations in *nfki-1* and *ikb-1* alter chromatin marks. Based on these results, we propose that ancestral IκB proteins modulate chromatin marks with an impact on development.

RESUM

Les proteïnes dels mamífers Inhibidors de kappa B (IκB) exerceixen la seva funció principal com a reguladors negatius de NF-κB, una via central de senyalització que controla la immunitat i la inflamació. S'ha demostrat que un paper alternatiu de cromatina per IκBs afecta la *stemness* i la diferenciació cel·lular. Tot i això, la participació de NF-κB en aquesta funció no ha estat exclosa. NFKI-1 i IKB-1 són homòlegs de IκB en *Caenorhabditis elegans*, al qual no tenen efectes nuclears de NF-κB. Hem trobat que les mutants de *nfki-1* i *ikb-1* mostren defectes de desenvolupament que fenocopian les mutacions en Polycomb i la histone desmetilasa UTX-1, el que suggereix un paper per a les IκBs de *C. elegans* en la regulació de la cromatina. Afavorint encara més aquesta possibilitat (i) es va a detectar NFKI-1 al nucli de cèl·lules; (ii) NFKI-1 i IKB-1 s'uneixen a les histones i a les proteïnes Polycomb *in vitro*, (iii) i s'associen amb la cromatina *in vivo*, i (iv) mutacions en *nfki-1* i *ikb-1* alteren les marques de cromatines. A partir d'aquests resultats, proposem que els proteins IκB ancestrals modulin marques de cromatina amb un impacte en el desenvolupament.

KEY WORDS

KEYWORDS

IκB

NF-κB

C elegans

Development

Epigenetics

CRISPR

Cancer

INDEX

INDEX

LIST OF FIGURES AND TABLES

LIST OF FIGURES

LIST OF ABBREVIATIONS

LIST OF ABBREVIATIONS

Ank R	Ankyrin repeats domain
BCL-10	B cell lymphoma 10
bp	Base pair
Ca	Calcium
Cas	CRISPR-associated nuclease
CBM	CARD protein BCL-10-MALT1
cDNA	Complementary DNA
ChIP	Chromatin immunoprecipitation
CRISPR	Clustered regularly-interspaced short palindromic repeats
crRNA	CRISPR RNA
DCPM	Depth of coverage per million mapped reads
DEG	Differentially expressed gene
DIC	Differential interphase contrast
DNA	Deoxyribonucleic acid
DSB	Double-strand break
dsRNA	Double-stranded RNA
DTC	Distal tip cell
ECM	Extracellular matrix
EED	Embryonic Ectoderm Development
EGFP	Enhanced green fluorescent protein

EZH2	Enhancer of Zeste Homolog 2
FP	Fluorescent protein
GO	Gene Ontology
H3K27me3	Trimethylation of the lysine 27 of the histone H3
H3K36me3	Trimethylation of the lysine 36 of the histone H3
H3K4me3	Trimethylation of the lysine 4 of the histone H3
HAT	Histone acetyltransferase
HDAC	Histone deacetylase
HDR	Homology directed repair
HMT	Histone methyl transferase
Hox	Homeobox
IgG	Immunoglobulin G
IKK	IκB kinase complex
IRAK	interleukin-1 receptor-associated kinase
IκB	Inhibitor of kappa B
K	Lysine
kDa	Kilodaltons
L1/L2/L3/L4	Larvae 1/2/3/4
LPS	Lipopolysaccharide
LRR	Leucine-rich repeat domain
MALT1	Mucosa-associated lymphoid tissue lymphoma translocation protein 1
MAPK	Mitogen-Activated Protein Kinase
Mb	Megabases

ml	Milliliters
mm	Millimeters
MOM	More Of MS (refers to the MeSoderm embryonic founder lineage)
mRNA	Messenger RNA
msp	Major sperm protein
MyD88	Myeloid Differentiation primary response 88
N_2	Liquid Nitrogen
NaCl	Sodium Chloride
NEMO	NF-κB essential modulator
NES	Nuclear export sequences
NF-κB	Nuclear factor kappa-light-chain-enhancer of activated B cells
NGM	Nematode Growth Medium
NHEJ	Non-homologous end-joining
NLS	Nuclear localization signal
NPC	Nuclear pore complexes
NSD	Nuclear receptor-binding SET Domain
nt	Nucleotide
ORF	Open reading frame
PAM	Protospacer adjacent motif
PAMP	Pathogen-associated molecular pattern
PCA	Principal component analysis
PCR	Polymerase chain reaction

PIK	Pelle/IL-1 receptor associated Kinase (IRAK)
PMK	P38 Map Kinase family
PRC2	Polycomb repressive complex 2
PS-IκBα	Phosphorylated and SUMOylated IκBα
PTM	Post-translational modification
RDE	RNAi defective
RHD	Rel homology domain
RNA	Ribonucleic acid
RNA-seq	RNA sequencing
RNAi	RNA interference
SARM	Sterile Alpha and Armadillo Motif
SCF βTrCP	β-TrCP F-box-containing component of a Skp1-Cullin-F-box (SCF)-type E3 ubiquitin-protein ligase complex
Ser	Serine
sgRNA	Single guide RNA
siRNA	Small interfering RNA
SN	Supernatant
ssDNA	Single-stranded DNA
t-SNE	t-distributed Stochastic Neighbor Embedding
TAD	Trans activation domain
TAK1	Transforming growth factor beta activated kinase 1
TCR	T-cell receptors

TIR	Toll/interleukin-1 receptor domain
TLR	Toll-like receptor
TMD	Transmembrane domain
TNFα	Tumor necrosis factor alpha
TOL	Toll *Drosophila* gene family. Toll is a German slang term for “fantastic”
TPM	Transcripts per million
tracrRNA	Trans-activating RNA
TRAF	TNF Receptor Associated Factor
TRF	TNF Receptor Associated Factor (TRAF) homolog
WT	Wild type
µl	Microliters
µm	Micrometers

INTRODUCTION

I1. The NF-κB pathway

I1.1. Discovery and biological relevance

In the eighties, Ranjan Sen and David Baltimore discovered the first of a set of transcription factors that have since been acknowledged to be evolutionarily conserved and interconnected to many biological pathways (Sen and Baltimore, 1986a; Zhang et al., 2017)

Since then, these factors have proven to orchestrate a plethora of fundamental biological processes as development, innate and adaptive immune responses, and cellular homeostasis. Accordingly, deregulation of their functions can lead to various forms of cancer, autoimmunity and chronic inflammatory syndromes (Baltimore, 2011; Sen, 2011).

These factors were named NF-κB (nuclear factor kappa-light-chain-enhancer of activated B cells) because of the specific and very limited context in which were originally identified (Sen and Baltimore, 1986a; Sen, 2011).

In the first paper in 1986, Sen and Baltimore used a simple electrophoresis mobility-shift assay for the identification of a DNA-binding factor in B lymphocytes that specifically

recognizes the sequence 5'-GGGRNWYYCC-3' (N, any base; R, purine; W, adenine or thymine; Y, pyrimidine) (later named κB site) of an enhancer element located in the gene that encodes the immunoglobulin κ light chain (Sen and Baltimore, 1986a; Lenardo et al., 1989). The same year, they proved that this activity is inducible and that, greatly surpassing their initial expectations, its expression is not only restricted to the B cell lineage, but also widely expressed in very diverse cell types (Sen and Baltimore, 1986b; Hayden and Ghosh, 2008; Sen, 2011).

Then, it was shown that the inactive form of NF-κB is reclused in the cytoplasm and can be liberated by treatment of cytoplasmic extracts with a detergent, later discovered to be different proinflammatory molecules (Patrick A. Baeuerle and Baltimore, 1988; Hayden and Ghosh, 2008). This last discovery led to the purification of their most known inhibitors, which were named the IκB proteins, for inhibitors-of-kappa-B (P A Baeuerle and Baltimore, 1988; Ghosh and Baltimore, 1990).

As time has passed, what appeared a simple induction process mediated by proinflammatory molecules has turned out to implicate many intermediate factors and processes including protein-protein dimerization, post-translational modifications as phosphorylation or polyubiquitination, and chromatin

modifications (Hayden and Ghosh, 2008; Ghosh and Hayden, 2012; L Espinosa et al., 2014).

Altogether, these observations set the basis for an exhaustive effort to elucidate the members of the pathway, the study of the activation processes and its complex regulation, which is a puzzle that still remains uncompleted (Zhang et al., 2017). Here I will provide an overview of the shared principles, main players and means of activation of the NF-κB pathway.

I1.2. Shared principles and main players of the NF-κB signaling

I1.2.1. Shared principles

The activation of the NF-κB pathway is governed by several regulatory elements that act positively or negatively in response to stimuli (Ghosh and Hayden, 2012).

As a simplified overview, in non-stimulating conditions, NF-κB dimers are sequestered in an inhibited state in the cytoplasm by means of their association with the IκB proteins. A wide variety of inducing stimuli that converge in triggering the activation of the IκB kinase complex (IKK) then leads to phosphorylation, ubiquitination, and proteasomal degradation of the IκB proteins. Freed NF-κB dimers translocate to the nucleus, bind specific DNA sequences, and promote

transcription of target genes (Hayden and Ghosh, 2008; Ghosh and Hayden, 2012).

Inactivation of the pathway requires de-activation of the IKK complex, the re-synthesis of the IκB proteins, and the displacement of NF-κB dimers from both DNA and transcriptional coactivators (Hayden and Ghosh, 2008; Ghosh and Hayden, 2012) (**Figure I1)**.

Thus, in order to explain these processes, we will first introduce the main players that comprise the NF-κB pathway.

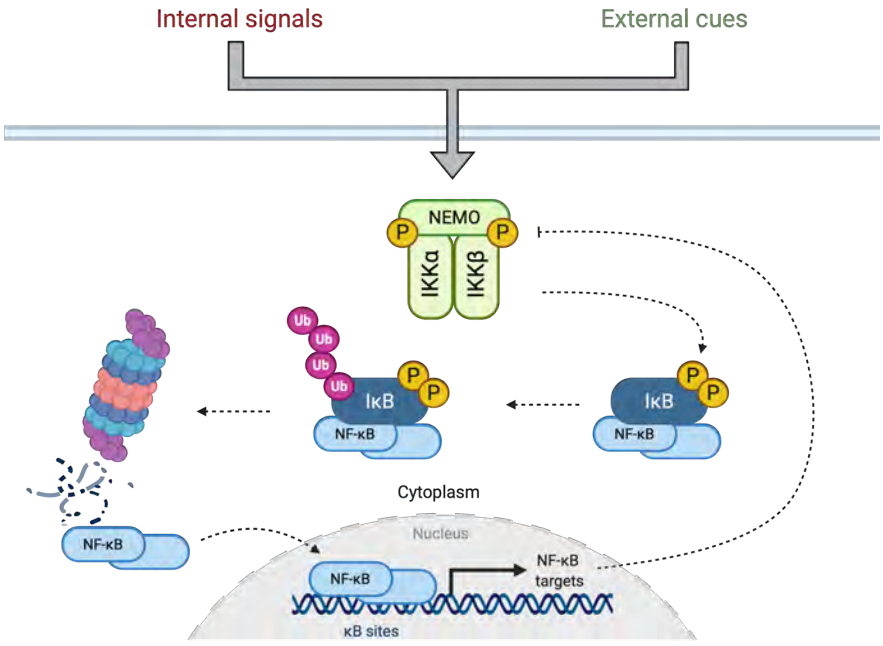

Figure I1. Simplified NF-κB pathway. A wide variety of internal signals or external cues lead to the activation of the IKK complex, phosphorylation and proteasomal degradation of IκB proteins in the cytoplasm, and the release of NF-κB dimers that allows their translocation to the nucleus, where they exert their transcriptional activity. The transcription of NF-κB

target genes promote the termination of the pathway. Created with biorender.com.

I1.2.2. Main players

The mammalian NF-κB family, also termed Rel family of transcription factors, consists of five members: p50 (NF-κB1), p52 (NF-κB2), p65 (Rel A), Rel B, and c-Rel. These subunits can form homo- and heterodimers and are classified in two classes (Siebenlist et al., 1994; Baldwin, 1996; Ghosh et al., 1998; Hayden and Ghosh, 2008; Zhang et al., 2017) (**Figure I2)**.

Class 1 subunits include p50 and p52, which are the post-translationally cleaved forms of their precursor proteins p105 and p100, respectively. Both proteins include a C-terminal region containing ankyrin repeats (AnkR). On the other hand, Rel A, Rel B and c-Rel belong to **class 2 subunits**, that are synthesized in their mature form and include a trans activation domain (TAD), which provides the ability to induce gene expression (Hayden and Ghosh, 2008; Zhang et al., 2017).

Different combinations of heterodimers that contain a TAD domain act as transcriptional activators, whereas class 1 (p50 or p52) homodimers act as repressors, unless bound to secondary proteins. This diversity of dimer combinations recognizes distinct variants of the κB site with distinctive affinities, and thus, generating several gene regulatory

patterns (Hoffmann and Leung, 2003; Saccani et al., 2003; Hayden and Ghosh, 2008; Zhang et al., 2017).

Despite their functional differences, all the NF-κB subunits have a 300 aminoacids Rel homology domain (RHD) at the N-terminus of the protein, which contains the nuclear localization signal (NLS) and has three functions: homo- and heterodimerization, sequence-specific DNA binding, and their interaction with the IκB proteins (Hayden and Ghosh, 2008; Ghosh and Hayden, 2012; Zhang et al., 2017).

The **IκB proteins**, which will be reviewed in depth in **section I1.5**, comprise IκBα, IκBβ, IκBε, IκBζ, $IκB_{NS}$, BCL-3 (B-cell lymphoma 3-encoded protein), and the precursor Rel proteins p100 (IκBδ) and p105 (IκBγ). These proteins are characterized by the presence of five to seven tandem AnkR, which mediate protein-protein interaction and the cytoplasmic retention of NF-κB (Ghosh et al., 1998; Hayden and Ghosh, 2008; Zhang et al., 2017).

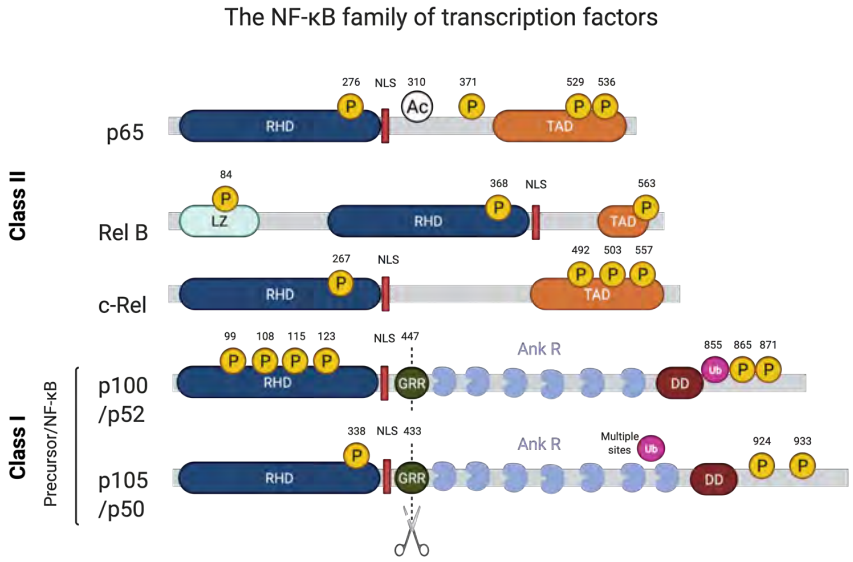

Figure I2. The NF-κB family of transcription factors. Schematic structures of the members of the family of NF-κB transcription factors, indicating domains and sites of different post-translational modifications. NLS: Nuclear localization signal; P: Phosphorylation; Ac: Acetylation; Ub: Ubiquitination; RHD: Rel Homology Domain; TAD: Trans activation domain; LZ: Leucin Zipper domain; Ank R: Ankyrin repeats domain; DD: Death Domain; GRR: Glycine-rich region, that facilitate proteasomal cleavage of the precursor. Created with biorender.com.

I1.3. Canonical NF-κB pathway

I1.3.1. General activation

The activation of NF-κB can be triggered by a variety of ligands that produce different responses that are classified as canonical or non-canonical NF-κB pathways. The canonical NF-κB pathway is illustrative of the basic scheme of NF-κB signaling (**Figure I3)**.

In the canonical pathway, inducing stimuli mainly by PAMPs (Pathogen-associated molecular patterns) and pro-inflammatory cytokines, such as TNFα, are recognized by cytokine receptors, inducing the activation of adaptor proteins that ultimately activate TAK1 (Transforming growth factor-β Activated Kinase 1), which promotes the phosphorylation and activation of the NF-κB kinase IKKβ (IκB Kinase Beta). IKKβ, IKKα, and NEMO (NF-κB essential modulator or IKKγ) are the main components of the IKK complex (Karin and Ben-neriah, 2000) and phosphorylate the IκBs proteins (bound to NF-κB dimers in the cytoplasm) on two N-terminal serines (Ser32/36 for IκBα; Ser19/23 in IκBβ and Ser18/22 for IκBε) (DiDonato et al., 1996; Shirane et al., 1999). These specific phosphorylated IκBs are then recognized by the β-TrCP F-box-containing component of a Skp1-Cullin-F-box (SCF)-type E3 ubiquitin-protein ligase complex, named SCF βTrCP, resulting in polyubiquitination and subsequent degradation of phosphorylated IκB by the 26S proteasome subunit (Baldwin, 1996; Yaron et al., 1997; Karin and Ben-neriah, 2000; Ben-Neriah, 2002; Steinbrecher et al., 2008; Zhang et al., 2017). Upon IκB degradation, the NLS of NF-κB transcription factors is exposed and NF-κB dimers are further activated through various post-translational modifications in order to translocate them to the nucleus, where they bind to specific DNA sequences and promote transcription of target genes (Zabel et al., 1993; Baeuerle and Baltimore, 1996; Zhang et al., 2017).

Importantly, different IκB proteins are degraded at different rates in response to specific stimuli and are re-synthesized following NF-κB activation (Hoffmann et al., 2002). The most common example of this is the re-synthesis of IκBα through direct binding of NF-κB transcription factors to the promoter of IκBα, which is a negative feedback loop that helps to control the strength and duration of the activation signal (Le Bail et al., 1993; Sun et al., 1993; Chiao et al., 1994; Hayden and Ghosh, 2008).

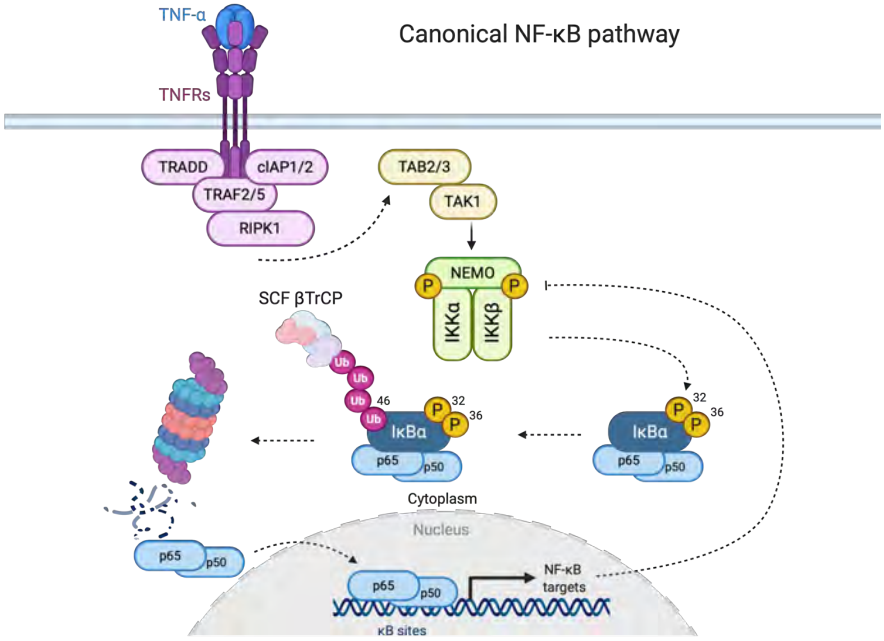

Figure I3. Canonical NF-κB pathway activated by TNFRs. Upon ligand stimuli, TNFRs recruit TRADD, cLAP1/2, TRAF2/5 and RIPK1 adaptor proteins that lead to the activation of TAB2/3 and TAK1, which phosphorylate NEMO-dependent IKK complex. The SCF βTrCP complex recognize specific phosphorylated IκBα that is degraded in the proteasome. p65/p50 dimers are translocated into the nucleus and activate transcription. Created with biorender.com.

I1.3.2. Activation through members of the IL-R and the Toll-like receptor (TLR) family

The activation of the canonical NF-κB signaling pathway can also be mediated through members of the Toll-like receptors family (TLR). These are specialized “danger-sensing” receptors that mediate a variety of transcriptional responses via various signaling pathways including NF-κB, MAP kinases and JAK, and thus coordinating different immune responses (Luo et al., 2005; Kawai and Akira, 2007).

TLRs are transmembrane proteins that include an extracellular leucine-rich repeat (LRR) domain, which is responsible for the recognition of the different ligands; a transmembrane domain (TMD) and a cytoplasmic Toll/interleukin-1 receptor (TIR) domain (Gay et al., 2014).

In mammalian systems, the activation of the TLRs is achieved by PAMPs stimuli that triggers a range of signaling that are mediated by multiple adaptors. Importantly, these adaptors are recruited to receptor complexes on the plasma membrane or endosomes, typically interacting with the TIR domain, where they act as scaffold for downstream signaling kinases (Yamamoto and Gaynor, 2004; Toshchakov et al., 2011). The specific adaptor protein provides an additional level of control

of the response, and thus different adaptors provide different signaling complexes (O'Neill and Bowie, 2007).
The most common adaptor protein is Myeloid Differentiation primary response 88 (MyD88), which recruits downstream interleukin-1 receptor-associated kinase 4 (IRAK) to ultimately activate TAK-1-mediated-phosphorylation of the IKK complex, leading to the general activation of the canonical NF-κB pathway (Loiarro et al., 2009; Gay et al., 2011) (**Figure I4A)**.

Another type of receptors that activate a different set of adaptor complexes are T-cell receptors (TCRs) and recruit the CARD protein BCL-10-MALT1 (CBM) signalosomes, which are particularly important in B an T cell development but display an ubiquitous expression. After exposure to distinct immune triggers, a caspase-recruitment domain (CARD) protein and B cell lymphoma 10 (BCL-10) form filaments with mucosa-associated lymphoid tissue lymphoma translocation protein 1 (MALT1) protease to regulate canonical NF-κB (Ruland and Hartjes, 2019) (**Figure I4B)**.

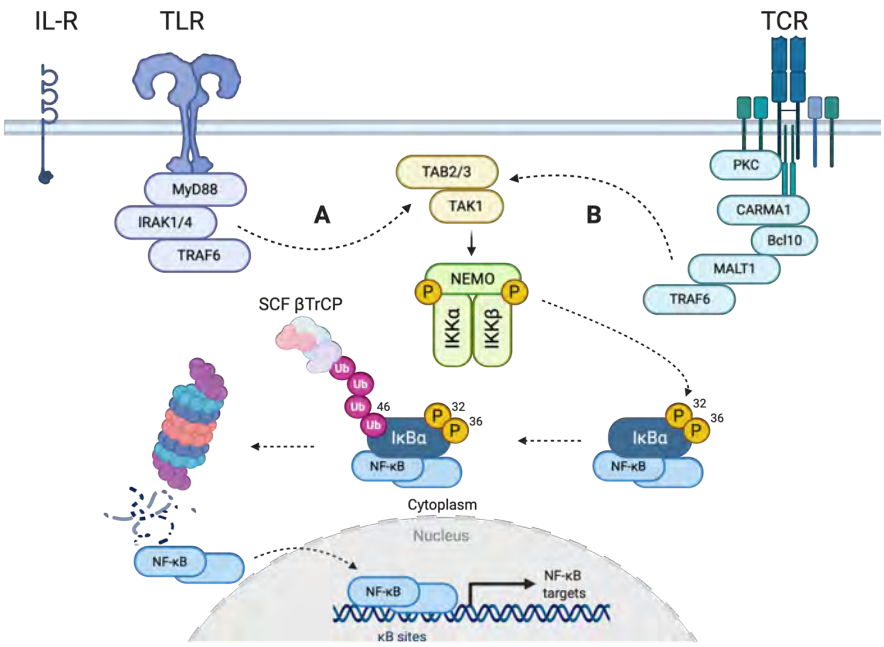

Figure I4. Activation of the NF-kB pathway through TLRs and TCRs. Stimuli that activate interleukin and Toll-like receptors **(A)** recruit MyD88, IRAK1/4 and TRAF6 adaptor proteins that ultimately lead to activation of IKK complex by TAK1. Similarly, T-cell receptors **(B)** mediate this activation using PKC, CARMA1, Bcl10, MALT1 and TRAF6 adaptor that form the CBM signalosome. Created with biorender.com.

I1.4. Non-canonical NF-κB pathway

The non-canonical NF-κB signaling have a prominent role regulating lymphoid development and does not respond to classical IKK way of NF-κB activation (Nishikori, 2005). In contrast to the canonical pathway, its induction depends on ligands such as CD40 or lymphotoxins α/β (reviewed in Cildir et al., 2016.

The activation of IKK complexes is dependent of the NF-κB inducing Kinase (NIK) instead of NEMO, which phosphorylates

and activates IKKα and then the NF-κB p100 subunit, activating its polyubiquitin-mediated partial proteolysis to p52. The p52/RelB heterodimer is the most common active transcription factor (Senftleben et al., 2001; Cildir et al., 2016) (**Figure I5)**.

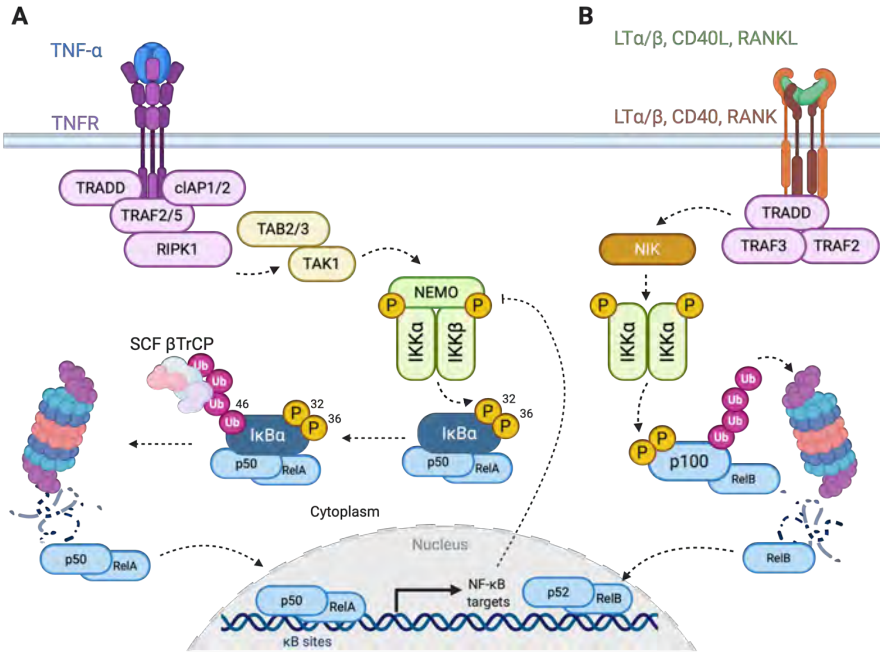

Figure I5. Non-canonical NF-kB pathway. Comparison with NF-kB canonical (A) and non-canonical (B) pathway. Created with biorender.com.

I1.5. The IκB family of proteins

I1.5.1. Prototypical IκB proteins

As previously mentioned, the IκB family of proteins are crucial regulators of NF-κB activity, mainly by their **cytoplasmic binding** to NF-κB dimers as in the case of IκBα, IκBβ and IκBε,

or by being part of the precursor Rel proteins p100 (IκBδ) and p105 (IκBγ).

This cytoplasmic role initially characterized these proteins as part of the dogmatic view of the prototypical IκBs, with the notable exception of the presence of a nuclear IκBα that is essential for the efficient post-activation termination of NF-κB signaling by facilitating the release of the dimers from chromatin (Arenzana-Seisdedos et al., 1997; Schuster et al., 2013; Zhang et al., 2017). Importantly, IκBα, IκBβ and IκBε present a common degron DGSXXS sequence, which includes two serine phosphorylation sites that are essential for the ubiquitination and ulterior proteasomal degradation of the proteins (DiDonato et al., 1996; Yaron et al., 1997; Mathes et al., 2008) (**Figure I6A)**.

Notably, all human IκB proteins show a low tissue-specificity as they are present in a wide variety of cell types, however, and in alignment with their main function as regulators of immunity, the most prominent expression is observed in bone marrow and lymphoid tissues (Uhlen et al., 2017, Human Protein Atlas available from www.proteinatlas.org).

I1.5.2. Atypical IκB proteins

In contrast, the atypical IκB proteins, as the case of BCL-3, IκBζ, $IκB_{NS}$, IκBη and IκBL (**Figure I6B)** have a **prominent**

nuclear role upon cytokine stimuli, being capable of interacting with NF-κB dimers to modulate dimer exchange and their stabilization on the DNA, as well as the recruitment of histone modifying enzymes, thus acting either as repressors or inducers of transcriptional activity (Schuster et al., 2013) (**Figure I7)**.

BCL-3 was the first identified atypical IκB protein originally classified as a proto-oncogene in B-cell chronic lymphocytic leukemia patients that presented the translocation t(14:19)(q32;q13.1) (Ohno et al., 1990). It is formed by an N-terminal TAD domain, followed by seven ankyrin repeats and a second TAD domain at the C-terminal. It is highly upregulated in different cancers, suppresses the activity of p53 and acts in an anti-apoptotic fashion (Kashatus et al., 2006; Schuster et al., 2013).

IκBζ consists of an NLS, a TAD domain, and seven ankyrin repeats, and has an important role in T helper cells development and keratinocytes homeostasis (Okamoto et al., 2010).

$I\kappa B_{NS}$ is formed by only six ankyrin repeats, and mediates both immune activation and suppression, thus being an important modulator of immune homeostasis (Hirotani et al., 2005).

IκBη and IκBL are the most recently identified members of the atypical IκBs, and although they contain ankyrin repeats, are

localized in the nucleus, and suppress NF-κB target genes, very little is known about their specific modes of action (Yamauchi et al., 2010; Chiba et al., 2011).

Remarkably, the fact that all atypical IκBs are induced via LPS stimulation and their high sequence similarities suggest that they could functionally cooperate, rather than compete during NF-κB regulation by interacting with NF-κB dimers, as well as a variety of chromatin modifiers that include but are not limited to histone deacetylases (HDACs) and histone acetyl transferases (HATs) (Schuster et al., 2013).

Hence, accumulated evidence has shown that atypical IκB proteins play an important role in regulation of inflammation by TLRs, as well as both innate and adaptive immunity (Schuster et al., 2013; Miura et al., 2016).

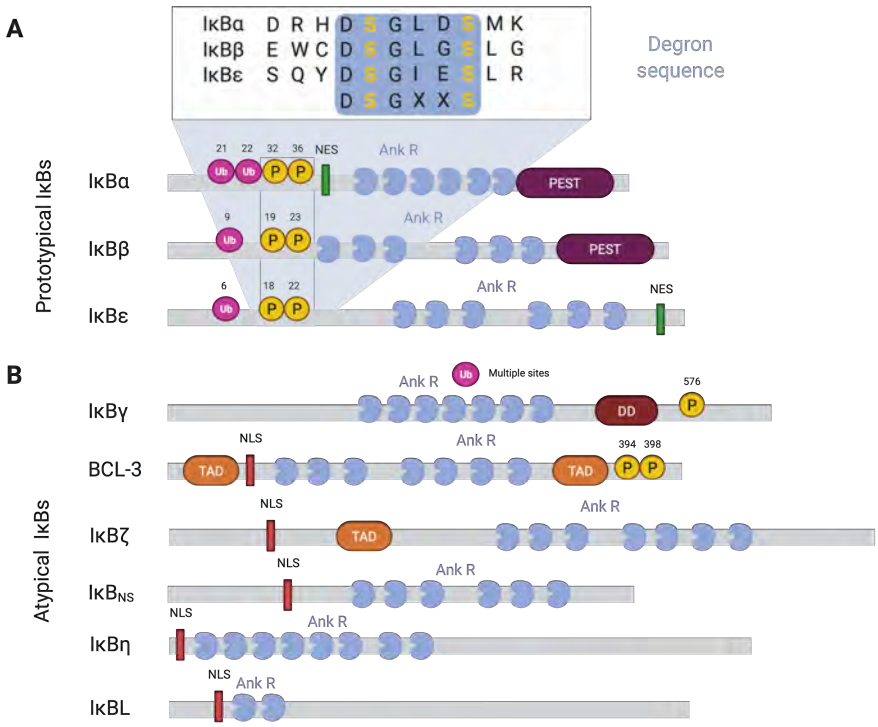

Figure I6. Structure of IκB family of proteins. All IκB proteins include Ank R domains. Atypical IκB proteins usually include an NLS. Created with biorender.com.

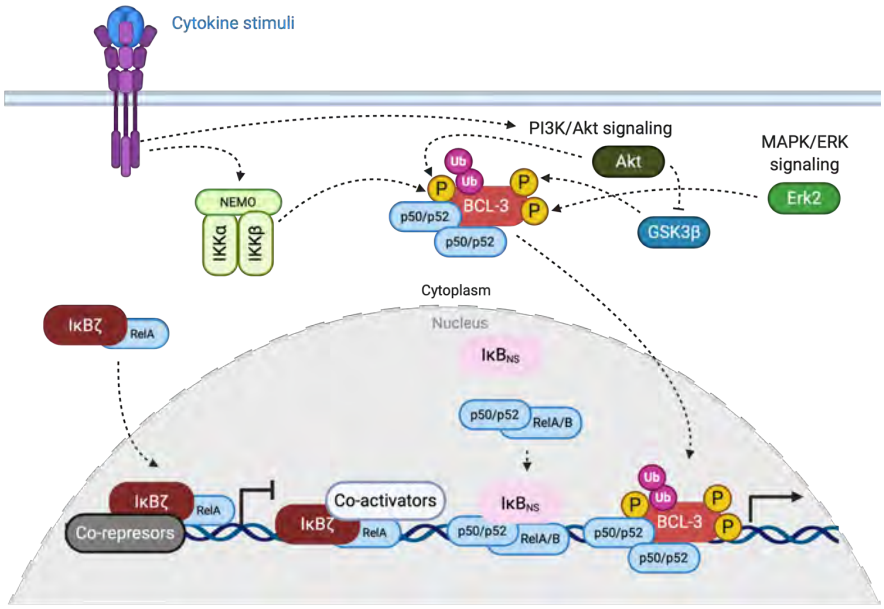

Figure I7. Roles of the atypical IκB family of proteins. Atypical IκB proteins can modulate NF-κB activity positively and negatively by associating with NF-κB dimers, by affecting their affinity to DNA or, by recruiting other co-factors. Created with biorender.com.

I1.5.3. Beyond the dogma: Alternative nuclear roles of prototypical IκB proteins

Contrary to the more than 20-year-old dogma of the prototypical IκB proteins, increased evidence indicated the existence of an NF-κB-independent role in the nucleus directly regulating gene transcription. Specifically, following LPS stimulation, an hypo-phosphorylated newly synthesized IκBβ translocates to the nucleus and binds p65 and c-Rel at the promoter region of specific genes such as TNF-α and IL1-β, and protects the NF-κB factors from its association with IκBα and chromatin release, ultimately leading to an overactivation

of transcription in macrophages (Rao et al., 2010; Scheibel et al., 2010; L. Espinosa et al., 2014) (**Figure I8A)**.

Additionally, alternative nuclear roles in different tissue contexts were described in the case of IκBα. In fibroblasts, nuclear IκBα associated directly to the promoter regions of genes that are not NF-κB targets, as *hes1* and *herp2*, regulating cell differentiation (Aguilera et al., 2004) (**Figure I8A)**.

In keratinocytes, a fraction of a phosphorylated and SUMOylated forms of IκBα (PS-IκBα) binds to chromatin associating to the N-terminal tail of histones H2A and H4 to transcriptionally regulate gene families related to development and cancer such as HOX and IRX (Mulero et al., 2013) (**Figure I8B)**.

Mechanistically, this regulation occurs in cooperation with elements of the Polycomb Repressive Complex 2 (PRC2) that impose the trimethylation of the lysine 27 of the histone H3 (H3K27me3), which has been proven essential for a proper skin differentiation and homeostasis (Ezhkova et al., 2009; Mejetta et al., 2011; Mulder et al., 2012).

Therefore, PS-IκBα-chromatin-bound regions that are targeted with PRC2 provide a new level of regulation that can be activated by specific stimuli, such as TNF-α treatment or with

factors that induce keratinocyte differentiation, like Ca^{2+}, releasing PRC2 from the chromatin and activating transcription (Mulero et al., 2013). Interestingly, a similar mechanism occurs in the intestine functioning as a chromatin sensor of inflammation by means of a nuclear phosphorylated IκBα. (Marruecos et al., 2020) (**Figure I8B)**.

Remarkably, the role of IκBα as a regulator of Polycomb function is conserved in *Drosophila* as the absence of IκBα homolog *Cactus* enhanced the homeotic phenotype displayed by Polycomb mutations (Mulero et al., 2013).

However, the involvement of the prominent role of the NF-κB transcription factors as well as other IκB regulators that could be affecting these nuclear functions has not been elucidated yet.

Notably, as numerous reports have involved the NF-κB pathway in cancer development, progression, and resistance to conventional cancer treatments, the inquiry for effective therapeutic modulators although extensive has not produced suitable results as present toxicity, low specificity and bioavailability (Eluard et al., 2020). Thus, understanding alternative roles of the main inhibitors of the pathway is of great interest to the biomedical field.

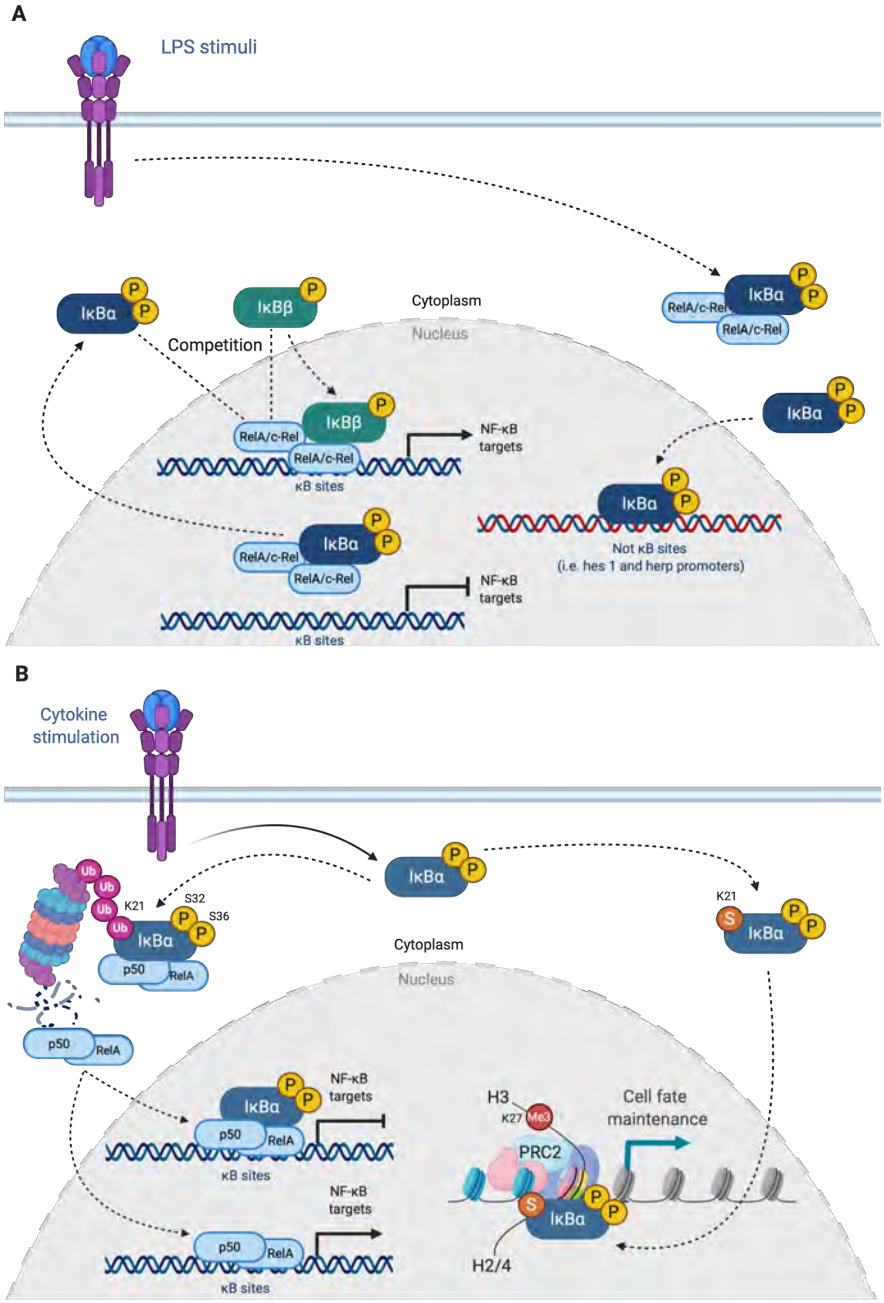

Figure I8. Alternative nuclear roles of prototypical IκB proteins. (A) In activated conditions, newly synthesized IκBβ and IκBα exert nuclear roles that affect transcriptional activity. **(B)** Phosphorylated and SUMOylated IκBα is translocated into the nucleus and in cooperation with PRC2, modulate transcriptional activity by altering H3K27me3 chromatin marks. Created with biorender.com

I2. *C. elegans* as a model system

I2.1. *C. elegans* biology

I2.1.1. *C. elegans* as a model organism

Caenorhabditis elegans is a small nematode of about one millimeter long at the adult stage. Its natural habitats are the soil and high-humidity environments where they can feed on different species of bacteria that are usually present in decomposing fruits, compost or leaves (Frézal and Félix, 2015; Schulenburg and Félix, 2017).

The most broadly wild type strain used in the laboratory is the N2, which was isolated in Bristol, United Kingdom (Brenner, 1974). *C. elegans* husbandry is maintained in agar plates seeded with the uracil auxotrophic *Escherichia coli* strain OP50 and are grown at temperatures that range from 15ºC to 25ºC, controlling in this way their developmental speed that can be as fast as 3 days at highest temperature (Stiernagle, 2006).

The use of *C. elegans* as a model organism bestow plenty advantages, including its reduced size, its fast life cycle, transparent body, and the capability to cryopreserve strains for decades in ultrafreezers (-80ºC) or in liquid nitrogen (-196ºC).

This facilites the generation of extensive stock collections of mutant strains in every *C. elegans* laboratory, as well as major *C. elegans* biobanks, such as the *Caenorhabditis* Genetics Center (University of Minnesota, USA, available at https://cgc.umn.edu), which is accessible for all the worm research community and help to standardize biological material protocols worldwide (Stiernagle, 2006).

Another major advantage of *C. elegans* is its compact and well-annotated genome, containing around 20,000 protein-coding genes. *C. elegans* was the first metazoan to have its genome completely sequenced (The *C. elegans* Sequencing Consortium, 1998) and new generation sequencing technologies have allowed the complete refinement of its sequence (Yoshimura et al., 2019).

Such high-quality genomic information is complemented with a vast catalog of annotations including gene structure information, gene expression, allelic variations, exhibited phenotypes, among many more. Additionally, the data is constantly curated and most of them are consolidated in a centralized online repository named WormBase (Harris et al., 2020, available at wormbase.org).

Importantly, a complete description of *C. elegans* anatomy, including the description of its invariable lineage and each of the cells that compose it are available online at WormAtlas

(Altun and Hall, 2020, available at wormatlas.org). Correspondingly, many relevant topics of *C. elegans* biology are extensive and constantly reviewed in the WormBook (wormbook.org), which also emphasizes the strong sense of community that distinguish the *C. elegans* researchers.

Remarkably, about 42% of genes identified in human disease have an ortholog in *C. elegans* (Markaki and Tavernarakis, 2010), which fueled up the task of modeling human disease. by identifying novel genes and pathways involved in human disease, or by mimicking human pathogenic alterations in a simplified system that can help unravel new disease modifiers (Markaki and Tavernarakis, 2010; Apfeld and Alper, 2018).

Additionally, a crescent number of genetic and genome editing tools are constantly generated, and large-scale studies using state of the art technologies such as single-cell RNA-sequencing, provide a powerful toolbox for studying a vast array of biological questions (Nance and Frøkjær-Jensen, 2019; Packer et al., 2019).

I2.1.2. Life cycle and reproduction

C. elegans has a very fast life cycle of 2-3 weeks. Starting with an embryonic stage in which fertilized eggs develop to embryos and hatch in about 12 hours, then followed by four larval stages (named L1 to L4), each of them separated by a

molting phase in which the cuticle of the worm is renewed, to ultimately become egg-laying adults in 3 days at 25ºC (**Figure I9**).

There are two sexes in *C. elegans*, hermaphrodite and male. Hermaphrodites are the most prominent sex in populations as they are able to produce sperm that can fertilize their own oocytes, normally producing around 300 isogenic animals each generation at 20ºC (Herman, 2006).

Males are present at a low frequency and display specific morphological features such as a copulatory apparatus at the end of the tail, and a slightly reduced size compared with adult hermaphrodites, among others (Emmons, 2005) (**Figure I10)**. In the laboratory routine, male populations are useful almost only for genetic crosses (reviewed in Fay, 2006).

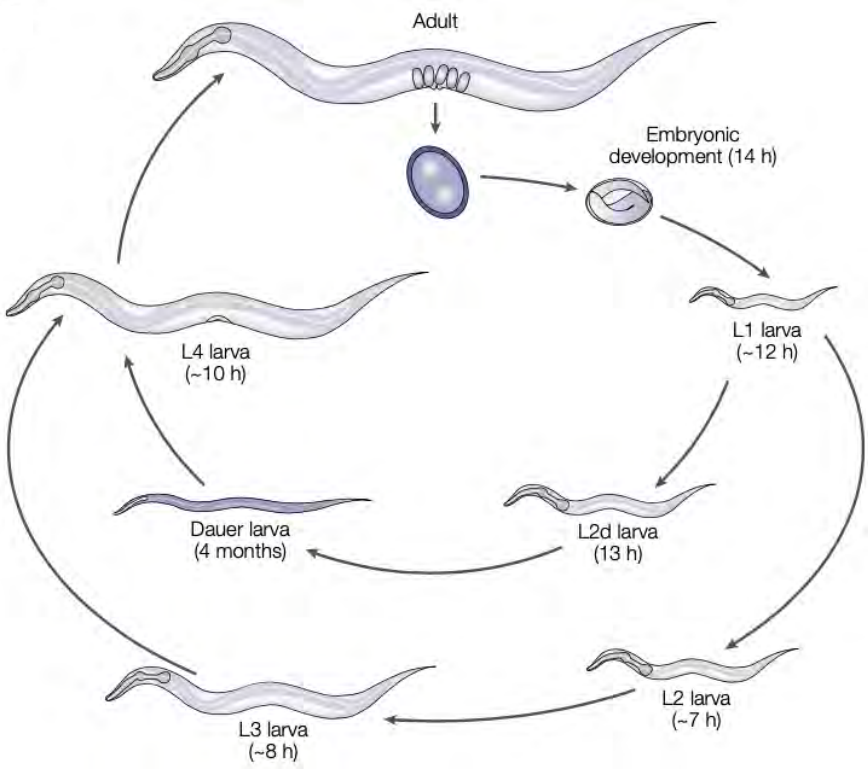

Figure I9. *C. elegans* life cycle. *C. elegans* developmental stages starting from fertilization to adulthood are presented. Duration of each phase is depicted at 25ºC. Extracted from Jorgensen and Mango, 2002.

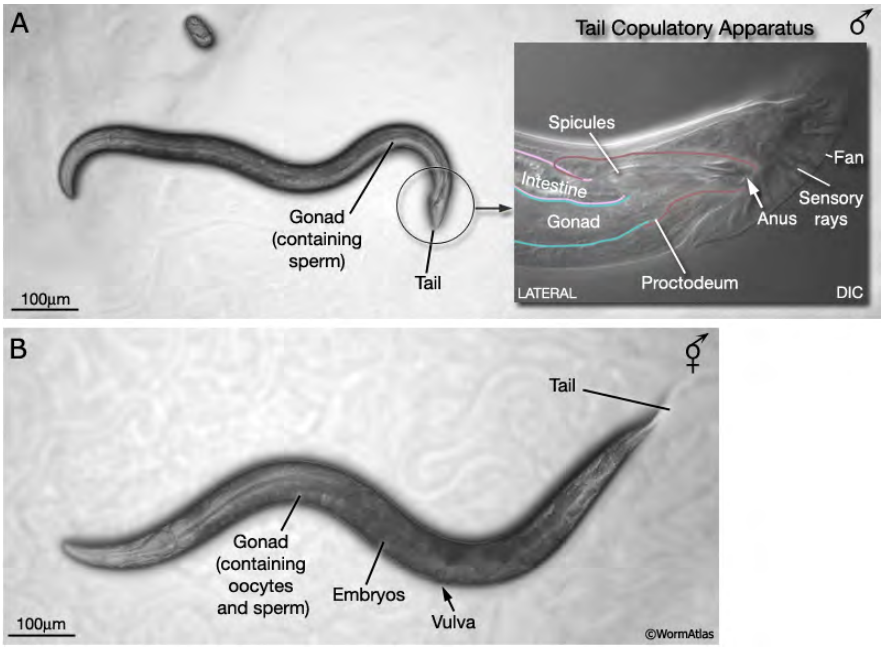

Figure I10. *C. elegans* sexual dimorphism. (A) Representative DIC image of an adult male. Male tail copulatory apparatus marked by the circled area and displayed with a higher magnification in the image at the right with its structures depicted. (B) Representative DIC image of an adult hermaphrodite. Lines point to the main anatomical differences compared to male animals. Extracted from WormAtlas (www.wormatlas.org).

I2.1.3. Embryonic development

During *C. elegans* embryonic development, embryos grow in a series of stages and cell divisions can be followed by differential interference contrast (DIC) microscopy (**Figure I11)**. The first divisions post-fertilization take place in the hermaphrodite germline and then, embryos are laid approximately at 30-cell stage. This proliferative phase produces about 300-250 cells and after the comma stage, morphogenesis begins but proliferation continues.

Gastrulation occurs between the 30 and 300 cells embryonic stage. When gastrulation is complete, embryos enter a morphogenetic phase that gives rise to different tissues and structures. Development of these layers will produce the different post-embryonic cell lineages. The ectoderm generates neurons and hypodermis; the mesoderm will form the muscles and pharyngeal tissues; and the endoderm will generate the intestine and the germline.

Next, in the elongation phase (from 400 to 671 cells), these structures are progressively folded into a thinner form inside the eggshell until the larvae is ready to hatch, reaching 671 cells. The main body plan is established during embryogenesis and does not suffer major changes during post-embryonic development (Schierenberg et al., 1980; Sulston et al., 1983; Bucher and Seydoux, 1994; Chin-Sang and Chisholm, 2000).

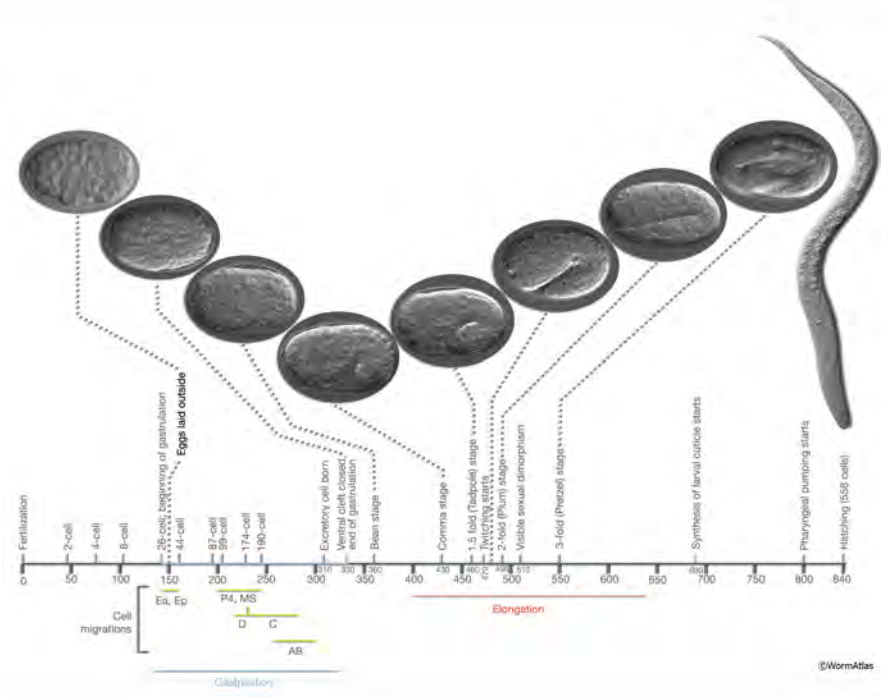

Figure I11. *C. elegans* embryogenesis. Representative DIC microscopy images of the main embryonic stages and a recently hatched larva. Time is presented in minutes after fertilization at 20-22ºC. Gastrulation period is underlined in blue. Migration of the cells to their respective lineages are depicted in yellow. Endoderm precursors (E); Mesoderm (MS); Germline precursors (P4); Hypodermis and neurons (AB). Elongation phase is depicted in red. Extracted from WormAtlas (www.wormatlas.org).

I2.1.4. Post-embryonic development

Post-embryonic development is governed by an accurate sensing of the environment, as nutrient availability, temperature, exposure to chemicals, and other similar stresses (Baugh, 2013).

When recently hatched larvae lack food, they enter into a phase called L1 arrest (also known as L1 diapause). This

arrest is especially relevant in the use of *C. elegans* in the laboratory because represents a convenient way to synchronize cultures by hypochlorite treatment. Bleaching gravid adults in a medium without food yields a sterile preparation of eggs, which will enter L1 arrest when hatched, and will resume development in a synchronous way upon feeding (Porta-de-la-Riva et al., 2012). Importantly, L1 arrested animals are resistant to different stresses, which allows long-term frozen storage (Stiernagle, 2006; Baugh, 2013).

Post-embryonic development is activated by feeding after hatching or L1 arrest, resuming cell divisions. The 51 blast cells established at the end of embryogenesis divide in almost invariant patterns along the four larval stages, thus giving rise to a constant cell number with determined fates in which the Hox genes have a crucial role determining the body pattern, resulting in 959 somatic and around 2000 germ cells in an adult hermaphrodite (Sulston and Horvitz, 1977; Herman, 2006).

Alternatively, under harsh environmental conditions, such as the absence of food, L2 larvae can enter in an alternative, energy-saving, remodeled and protective stage named the dauer stage. As a dauer larvae, worms can arrest their development up to several months and resume it when favorable conditions are reestablished (Baugh, 2013) (**Figure I9 and I12B)**.

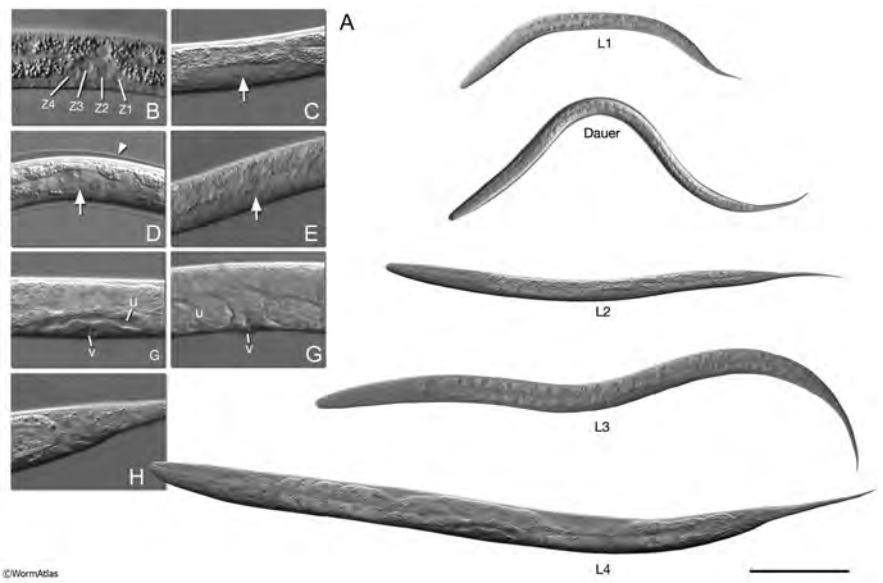

Figure I12. *C. elegans* larval stages. (A, B) Representative DIC images of *C. elegans* larval stages (A) and that can be subjected to diapause/arrest (B). (C-I) Microscopy images of different characteristic structures that arise during post-embryonic development: (C) Primordial gonadal cells arising in L1. Germline (Z2 and Z3) and somatic gonad (Z1 and Z4). (D) Germ cells increase in number in L2. (E) Dauer gonad is similar to an L2 larva. (F) Gonads extend along the ventral body at L3. (G) Tree-shaped vulva have formed by mid-L4 stage. (H) Fully developed vulva and full of fertilized eggs when reaching adulthood. (I) Ship-like morphology of the hermaphrodite tail. Adapted from WormAtlas (www.wormatlas.org).

I2.1.5. *C. elegans* body plan and tissues

As other nematodes, *C. elegans* has a cylindrical body shape, consisting of an inner and outer tubes separated by the pseudocoelomic fluid-filled space. The inner tube includes the intestine, pharynx, and gonads. The outer tube comprises the cuticle, which is secreted by the hypodermis (epidermis of the worm), excretory system, neurons and muscles (Corsi et al., 2015).

C. elegans **nervous system** is composed of 300 neurons and is divided into a large somatic nervous system that is mainly distributed in the head and tail regions (280 neurons), complemented with a small pharyngeal nervous system (20 neurons). In the somatic nervous system, neuronal cells and their connections are positioned between the body wall muscle and the hypodermis. In contrast, pharyngeal neurons are in direct contact with pharyngeal muscles (White et al., 1986; Corsi et al., 2015) (**Figure I13)**.

Despite the limited number of neuronal cells, there are approximately 118 distinct classes of neurons classified by topology and synaptic patterns, and recently the entire map of connections between all the neurons (connectome) have been elucidated (Cook et al., 2019), which makes it a suitable model to study neurobiological questions.

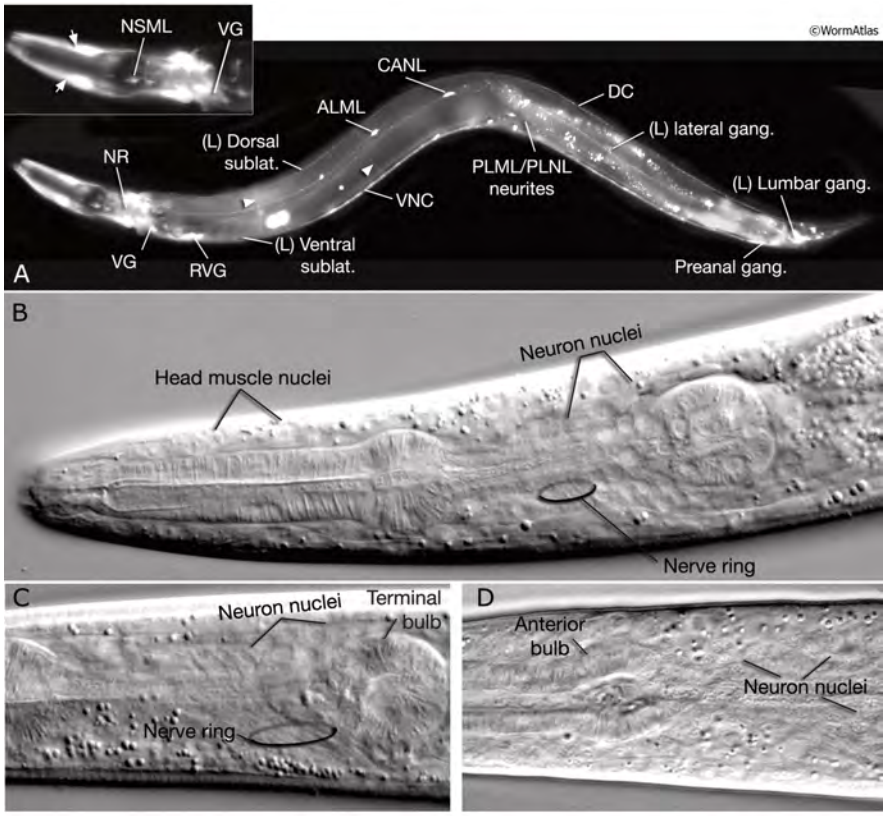

Figure I13. *C. elegans* nervous system. (A) Fluorescent microscopy image of an *unc-119::GFP* transgenic animal expressing a panneuronal reporter. Nerve ring (NR); retrovesicular ganglion (RVG); ventral ganglion (VG); ventral nerve cord (VNC); distal cord (DC). Other important individual neurons are depicted. (B-D) DIC images of the head of a young adult hermaphrodite with some neuronal structures depicted. Extracted from WormAtlas (www.wormatlas.org).

C. elegans **reproductive system** is comprised by the somatic gonad, the germline, and the egg-laying apparatus. Migration of the developing gonad is directed by the distal tip cells (DTC), which are two somatic cells located at the end of each gonad arm (Wong et al., 2012). The germline are two symmetric U-shaped gonad arms that are connected to a central uterus through the spermatheca and are enclosed in the somatic gonadal sheath. Importantly, germline cells are syncytial, thus

being nucleus surrounded by a shared cytoplasmic core (**Figure 14A and B)**. At the proximal end of the gonad arms, germ cells progressively pass through the mitotic, meiotic prophase and diakinesis stages. Once they pass through the oviduct, oocytes increase in size and detach from the syncytium, in a maturation process as they move proximally. Oocytes are fertilized by the sperm in the spermatheca. Diploid zygotes are stored in the uterus and expulsed through the vulva (Corsi et al., 2015) (**Figure I14C**).

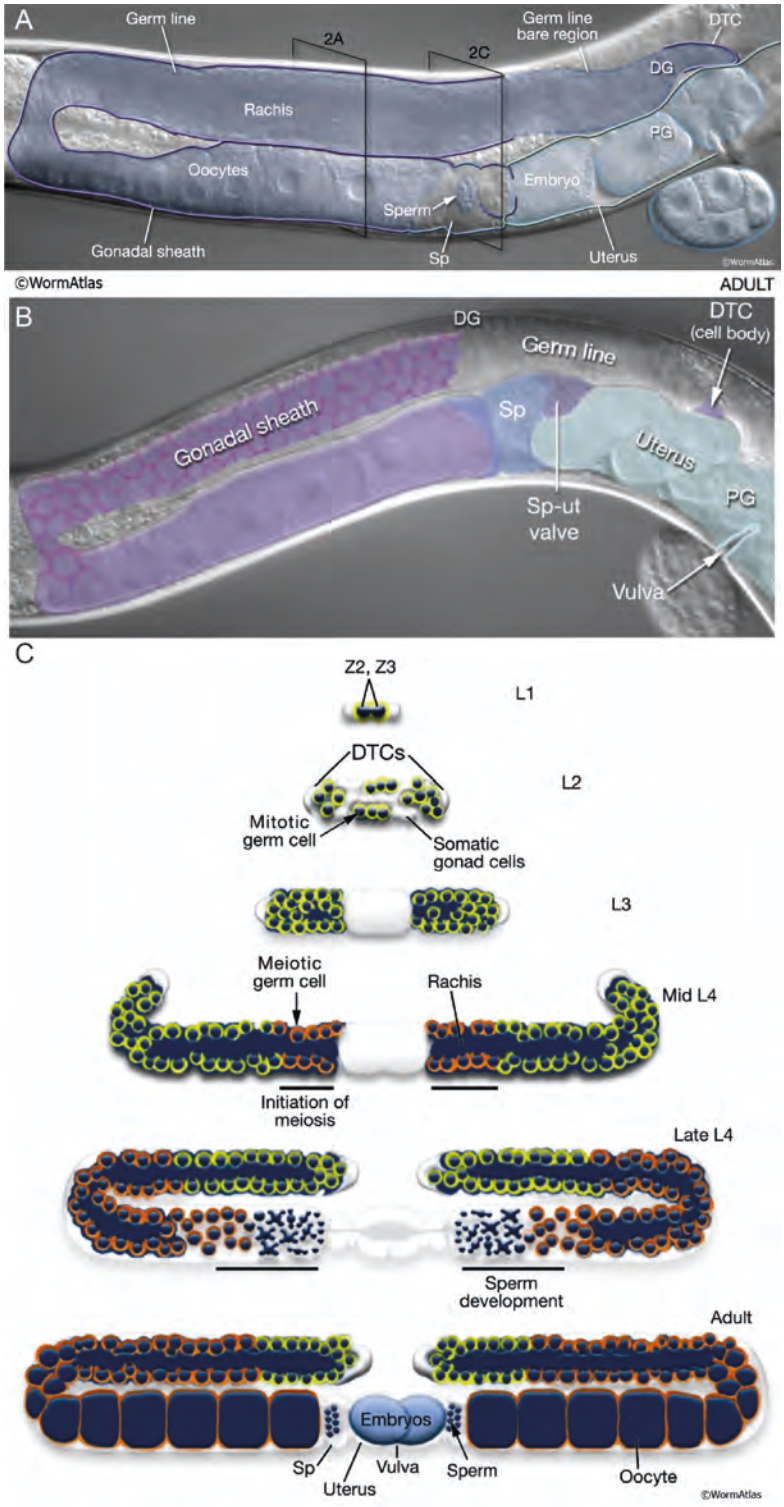
A
Germ line
2A
2C
Germ line
bare region
DTC
DG
Rachis
PG
Oocytes
Embryo
Sperm
Gonadal sheath
Sp
Uterus
©WormAtlas
ADULT
B
DG
DTC
(cell body)
Germ line
Sp
Gonadal sheath
Uterus
PG
Sp-ut
valve
Vulva
C
Z2, Z3
L1
DTCs
L2
Mitotic
germ cell
Somatic
gonad cells
L3
Meiotic
germ cell
Rachis
Mid L4
Initiation of
meiosis
Late L4
Sperm
development
Adult
Embryos
Sp
Uterus
Vulva
Sperm
Oocyte
©WormAtlas

Figure I14. *C. elegans* reproductive system. (A, B) DIC microscopy images of a hermaphrodite adult germline (enclosed in purple) (A), somatic gonad (in pink) and other components of the reproductive system (in light blue) (B). DG: Distal gonad; PG: Proximal gonad; Sp: Spermatheca. (C) Schematic representation of the development of the germline and somatic gonads. All images extracted from WormAtlas (www.wormatlas.org).

I2.2. Genetic tools in *C. elegans*

I2.2.1. Genetic manipulation in *C. elegans*

The power of a genetic model system mostly relies in the ease with which gene sequences and gene expression can be manipulated. *C. elegans* has made substantial contributions to understand different aspects of the genetic basis of the biology of multicellular systems.

Early research, like the very own Sydney Brenner's (Brenner, 1974), was mainly focused in performing forward genetic screens by means of a combinatory approach inducing chemical mutagenesis, plus genetic mapping of mutations, and a meticulous microscopy or behavioral assays looking for particular phenotypes involved with specific biological processes. Over the years, genome sequencing facilitated the identification of mutations and polymorphisms, resulting in a readily available large collection of mutant strains (Jorgensen and Mango, 2002; Barstead et al., 2012; Waterston et al., 2013).

Additionally, reverse genetics approaches have been increasingly used and were facilitated by the easy implementation of RNAi in worms and also by the constantly expanding toolbox of transgenesis (Lisa Timmons and Andrew Fire, 1998; Timmons et al., 2001; Rual et al., 2004; Ahringer, 2006; Ceron et al., 2007; Nance and Frøkjær-Jensen, 2019).

I2.2.2. RNA interference

Andrew Fire and Craig Mello discovered a highly conserved phenomenon in which double-stranded RNA (dsRNA) molecules are able to inhibit gene expression in a controlled and specific way in *C. elegans* (Fire et al., 1998). This basic discovery in biology led them to be awarded with the Nobel Prize in Physiology or Medicine in 2006.

In principle, exogenous dsRNA molecules enter the cells and act in the RNA interference (RNAi) pathway. Mechanistically, dsRNAs are recognized by RDE-4 and recruited to the Dicer complex, which is responsible to cleave dsRNAs generating small interfering RNAs (siRNAs). Then, siRNAs are recognized by RDE-1, that degrades one of the strands (sense) of the dsRNA. The remaining strand (antisense) guides RDE-1 to a portion of specific mRNA that display base-pair complementarity, and secondary siRNAs are synthesized. These new siRNAs are recruited by other argonautes to exert gene silencing (Kim et al., 2001; Braukmann et al., 2017) (**Figure I15A)**.

There are three methodologies for delivering dsRNA and induce silencing by RNAi. The first one is by microinjecting it directly into the animal gonad to generated gene silencing effect in the next generation (Fire et al., 1998). The second consists in soaking animals in a liquid solution containing dsRNAs (Tabara et al., 1998). The third, and the most commonly used due to its convenience, consists in feeding artificially engineered bacteria that produce specific dsRNAs, and it is known as “RNA by feeding” (Lisa Timmons and Andrew Fire, 1998). Importantly, the silencing effect of any of the three methods spreads thorough nearly every tissue (with the notable exception of some neuronal cells because of the lack of a dsRNA transporter in their cell membrane) in the animal, thus causing a systemic effect (Timmons et al., 2001) (**Figure I15B)**.

The ease of performing RNAi experiments fueled up the generation of two genome-wide RNAi feeding libraries, that consist of thousands of bacterial clones that produce specific dsRNAs against up to 94% of *C. elegans* genes (Kamath et al., 2003; Rual et al., 2004). The difference between both libraries is that one of them includes genomic DNA fragments containing exons and introns (Kamath et al., 2003), while the other was generated containing only the open reading frames (ORFs) from cDNA libraries (Rual et al., 2004).

For both libraries, sequences were cloned into ampicillin resistant L4440 plasmids between two T7 promoter sites, allowing bidirectional transcription. Then, plasmids were transformed into the IPTG-inducible *E. coli* HT115 (DE3) strain, which induce a T7 polymerase and carries a tetracycline-resistance cassette inserted in the bacterial genome that disrupts the RNAse III enzyme, preventing degradation of dsRNA (Timmons et al., 2001).

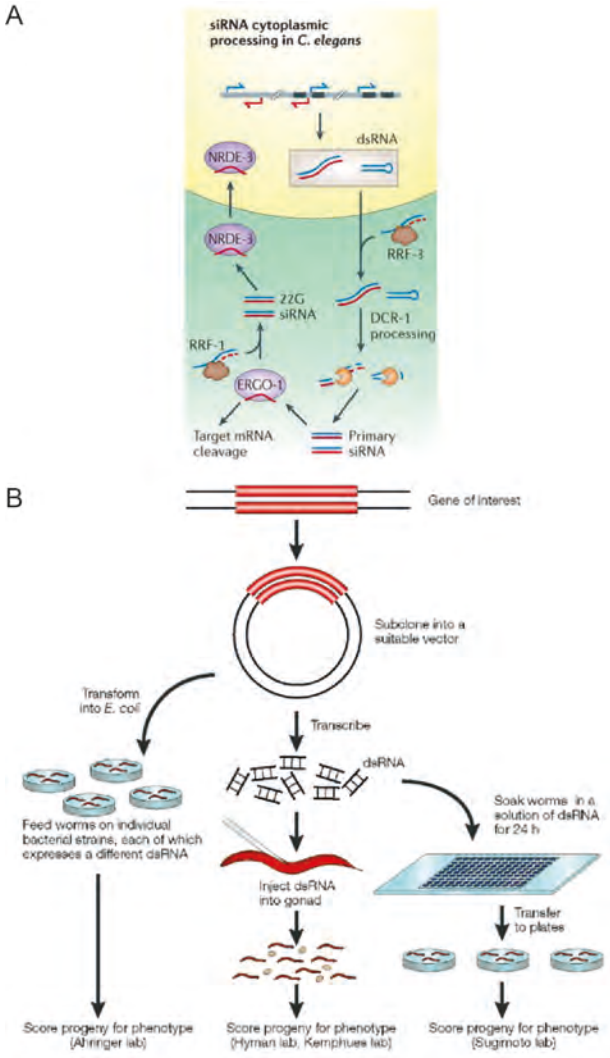

Figure I15. RNAi in *C. elegans*. (A) Molecular mechanism of RNAi machinery in *C. elegans*. NRDE: Nuclear RNAi defective. RRF: RNA-dependent RNA polymerase Family. DCR: Dicer related. (B) RNAi methodologies in *C. elegans.* Adapted from Kim et al., 2001.

I2.2.3. RNAi and CRISPR as tools for studying gene functions

Since RNAi discovery, RNAi by feeding in *C. elegans* has been the most commonly used method for gene inactivation. However, in the last decade the implementation of CRISPR-Cas as a genome editing tool is transforming biological experimentation since can produce stable and precise mutations that facilitate functional analyses (Lander, 2016; Mojica and Montoliu, 2016).

Clustered regularly-interspaced short palindromic repeats (CRISPR) are repetitive elements discovered in bacterial and archaeal genomes (Mojica et al., 1993) that form part of an ancient adaptive immune system against viruses and plasmids (Mojica et al., 2005). This evolutionarily creative mechanism was then applied by researchers to edit the genome of eukaryotic systems, including *C. elegans* (Friedland et al., 2013).

In this thesis, the use of CRISPR-Cas9 genome editing is of special interest, since it allows us not only to easily generate multiple deletion alleles to study gene functions, but also

facilitate the study of the localization of the protein under endogenous or physiological conditions by inserting in-frame the coding-sequence of a fluorescent protein (FP) (Nance and Frøkjær-Jensen, 2019).

CRISPR-Cas genome editing technology consists of three basic components: a CRISPR RNA (crRNA), a trans-activating RNA (tracrRNA), and a CRISPR-associated nuclease (Cas). The most commonly used is Cas9, however the vast variety of naturally occurring Cas proteins and rational molecular engineering are constantly expanding the CRISPR toolbox (Vicencio and Cerón, 2021). The crRNA for Cas9 includes a 20-nucleotides long protospacer sequence that is complementary to a spacer sequence in the region of interest to be edited, and complementarity to the tracrRNA. The crRNA and tracrRNA are usually combined into a chimeric single guide RNA (sgRNA) molecule (Jinek et al., 2012).

Thus, Cas9 endonucleases along with a sgRNA can scan the genome for the protospacer adjacent motifs (PAMs). Once the PAM is recognized by the Cas9 and sgRNA complex, it hybridizes to the specific RNA sequence and the Cas9 perform a double-strand break (DSB) 3 base pairs (bp) upstream of the PAM site. Finally, the DSB will be repaired mainly by non-homologous end joining (NHEJ) (imprecise repair) or homology directed repair (HDR) (precise repair using a repair template) (Sternberg et al., 2014) (**Figure I16)**.

The method for delivery of CRISPR reagents in *C. elegans* is by microinjection into the gonad of young adult hermaphrodites, which thank to its syncytial nature (germ cells share a common cytoplasm) allows the editing of multiple progeny from a single injected animal (Nance and Frøkjær-Jensen, 2019).

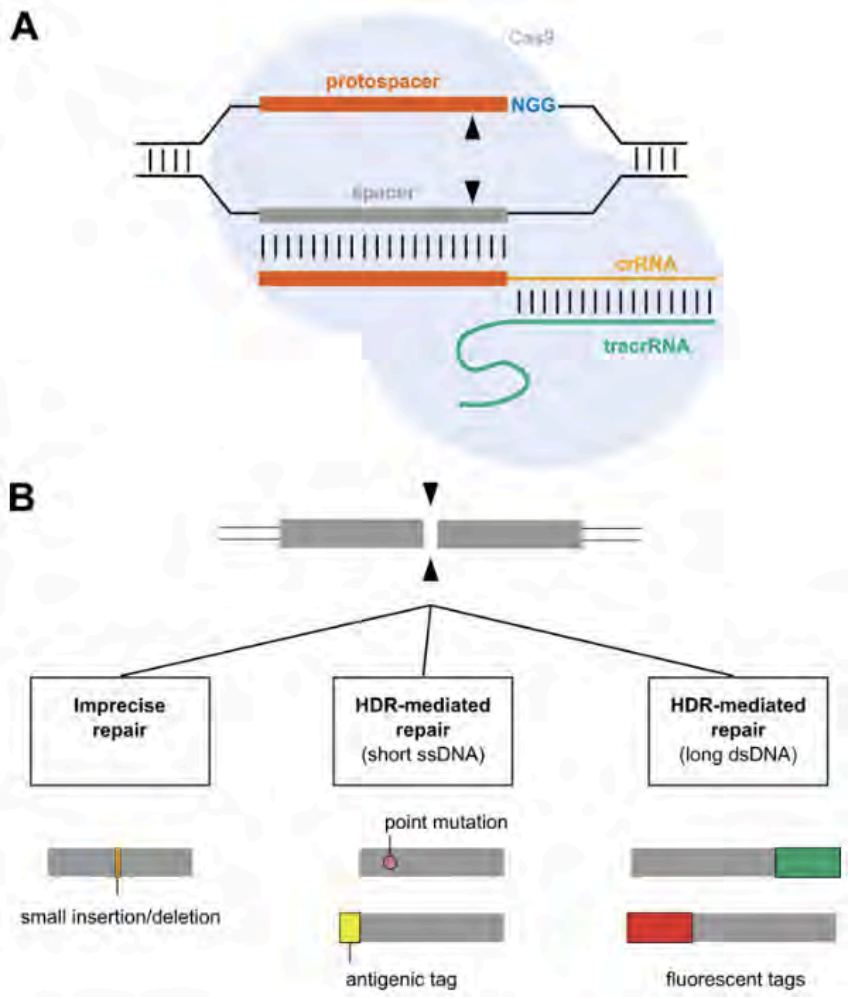

Figure I16. CRISPR reagents and mechanisms of DSB repair. (A) Schematic representation of Cas9-crRNA-tracrRNA complex bound to a target gene. Vertical black lines represent base pairs. Black triangles show Cas9 cut sites. The PAM sequence (NGG) is depicted in blue. **(B)** Imprecise repair occurs if no repair template is supplied, resulting in small insertions or deletions that often change the reading frame. Short ssDNA repair templates can be used to introduce point mutations or short antigenic tags. On the other hand, long dsDNA molecules can be employed to introduce fluorescent tags at the 5' or the 3' end of a gene. Reproduced from Serrat, 2019.

I3. *C. elegans* chromatin

I3.1. *C. elegans* genome organization

C. elegans genome is 97 megabases (Mb), and is distributed on six chromosomes: five autosomes, numbered I-V, and X chromosome. As a diploid animal, each somatic cell contains a pair of autosomes and either two X chromosomes, in the case of hermaphrodites, or a single X chromosome in the case of males (Cohen-Fix and Askjaer, 2017).

C. elegans chromosomes are holocentric, which means that they have centromeres along their full length instead of a single centromere, like mammalian cells (Maddox et al., 2004).

Active genes are distributed in autosomes in a non-random manner, as the density of active genes is higher in the center than at the chromosome arms. This pattern correlates with the presence of repressing and activating chromatin marks. On the

other hand, the X chromosome display a more uniform pattern of chromatin marks (Gerstein et al., 2010) (**Figure I17**).

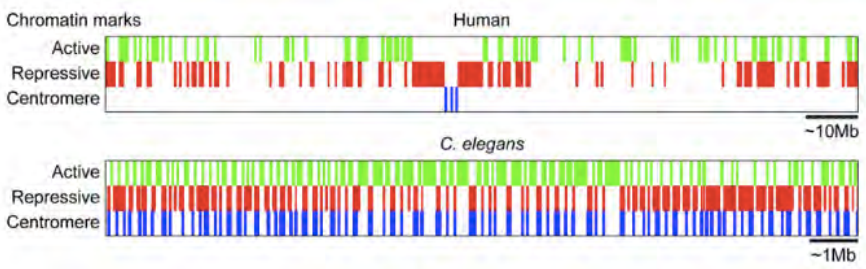

Figure I17. Comparison of global chromosome patterning in humans and *C. elegans*. Centromeres are depicted in blue. Active chromatin marks are represented in green, and repressive in red. Reproduced from Cohen-Fix and Askjaer, 2017.

I3.2. *C. elegans* general chromatin organization

Eukaryotic DNA is organized and compacted in the nucleus by means of the association of histones and other proteins that collectively constitute a complex named chromatin that controls genomic activity. The building blocks of chromatin are the nucleosomes, which comprise 145-147 bp of DNA wrapped 1.8 times around an octamer of four evolutionarily conserved core histone proteins: H2A, H2B, H3, and H4. In turn, nucleosomes are separated by DNA spacers of approximately 10-90 bp in length (Cohen-Fix and Askjaer, 2017).

Chromatin is usually classified as two major types: euchromatin, representing the portions that have transcriptional activity, and heterochromatin, which

encompasses a repressed state (Ahringer and Gasser, 2018) (**Figure I18**).

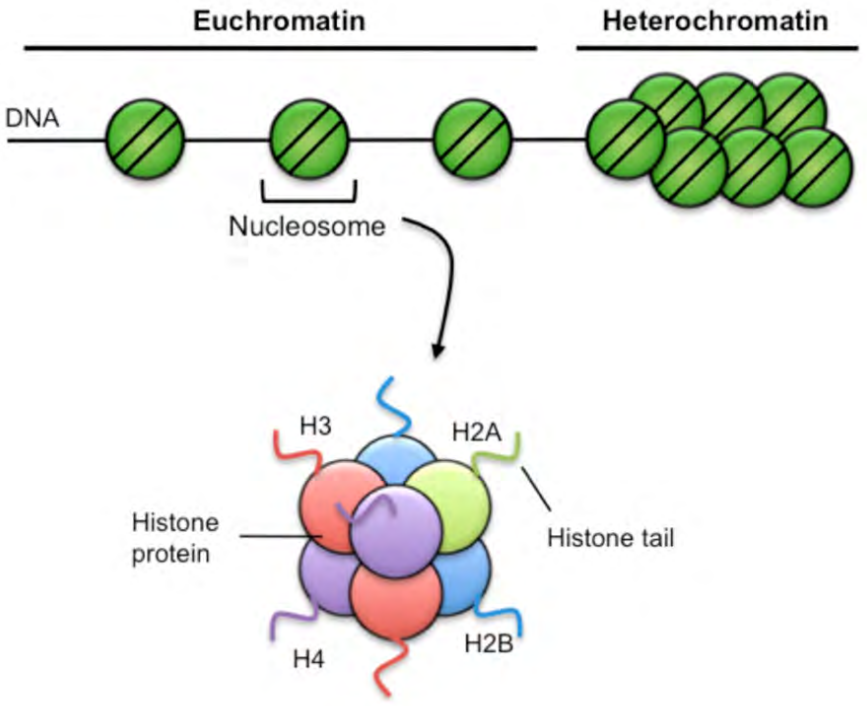

Figure I18. Chromatin structure. Nucleosomes are shown in green. Histones H3 (red), H4 (purple), H2B (blue) and H2A (green) are also shown. Reproduced from Russ et al., 2012.

I3.3. Histone post-translational modifications

The N-terminal tail of all histones, and the C-terminal of histones H2A and H2B is subjected to a diverse set of post-translational modifications (PTMs) that have different impacts in chromatin conformation. Euchromatin and heterochromatin

are distinguished by the composition and location of these different PTMs (Ahringer and Gasser, 2018).

Euchromatin can be potentially active or actively transcribed and is characterized by its enrichment in RNA polymerase, histone tail acetylation, and trimethylation on histone H3 lysines 4 and 36 (H3K4me3 and H3K36me3). Conversely, heterochromatin is linked to transcriptional repression and present histone methylations such as H3K9me3 or the Polycomb-deposited modification H3K27me3 (Ahringer and Gasser, 2018) (**Figure I19**).

Notably, repressive chromatin modifications are heritable and have a crucial role in the establishment and maintenance of developmental epigenetic programs of differentiation, but can also be dynamically modified in response to environmental stresses (Fabrizio et al., 2019).

Heterochromatin can be classified in constitutive, which refers to the repetitive-rich genomic regions; and facultative, which comprises genes that are potentially active in a spatiotemporal or other context-specific expression and is marked by the H3K27me3, which is deposited by the PRC2 (Wiles and Selker, 2017).

Although each of these chromatin marks are hallmark of each type of heterochromatin, a degree of overlap between both

marks have been found in some genetic regions, and are very conserved from *C. elegans* to mammals (Liu et al., 2011; Vandamme et al., 2015). Moreover, epigenetic-mediated gene silencing in *C. elegans* depends almost entirely of modification of chromatin marks, since it lacks 5-methyl cytosine marking on DNA (CpG DNA methylation), which makes it a good model organism to study histone-dependent repressive chromatin (Tursun, 2017).

The enzymes responsible for histone lysine methylation are named histone methyltransferases (HMTs). Despite most of the specific substrates of the HMTs have not yet been uncovered in *C. elegans*, the ones for H3K27 (MES-2) (Bender et al., 2004), and H3K36 (MET-1 and MES-4) (Bender et al., 2006; Furuhashi et al., 2010; Rechtsteiner et al., 2010) have been characterized.

Mechanistically, histone modifications can directly change nucleasome-nucleasome and/or nucleasome-DNA interactions by altering the charge of the histone tail, disrupting the contact with DNA and the nucleosomal core, or by creating new binding areas that can be specifically recognized by other proteins.

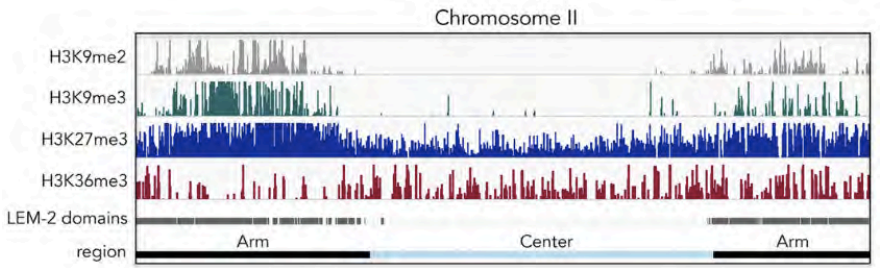

Figure I19. Histone modifications associated with heterochromatin and genome domains in *C. elegans*. Pattern of histone modifications associated with heterochromatin (H3K9me2, H3K9me3, and H3K27me3), H3K36me3, and LEM-2 domains (indicating nuclear lamina association) in embryos across *C. elegans* chromosome II. The majority of H3K9me marks and LEM-2 domains are found on the chromosome arms. H3K27me3 levels are higher on arm regions compared to the center. H3K36me3 shows a more uniform pattern, with a slight enrichment in the central region. Reproduced from Ahringer and Gasser, 2018.

I3.4. PRC2 and H3K27me3 in *C. elegans*

The H3K27me3 is the most abundant histone methylation mark in *C. elegans*, is found in nearly 70% of histones in embryos, and is imposed by the PRC2 (Vandamme et al., 2015). The *C. elegans* PRC2 complex is composed of MES-2, ortholog of mammalian Enhancer of Zeste Homolog 2 (EZH2) that imposes methylation activity, MES-6 ortholog of mammalian Embryonic Ectoderm Development (EED) that propagates the mark to adjacent histone tails, and MES-3, which is a novel Polycomb protein with no identified ortholog and it is thought to act as scaffold of the complex (Bender et al., 2004).

The MES complex was identified in a forward genetic screen for genes required for germline development. Mutations in these genes caused a maternal-effect sterile (Mes) phenotype

in grandchildrens. That means that homozygous mutants (F_1) derived from heterozygous mothers (P_0) are viable and fertile, but their progeny (F_2) is sterile due to germ cell death (Capowski et al., 1991) (**Figure I20**). Therefore, *mes* genes encode factors that are maternally supplied and required for germline development in the offspring.

Interestingly, *C. elegans* PRC2 mutants do not show major somatic defects in development, in contrast with mammals in which it leads to several defects including cancer (Gaydos et al., 2014; Pasini and Di Croce, 2016), but only display low-penetrance malformations associated to a deregulation of Hox genes expression (Capowski et al., 1991; Ross and Zarkower, 2003).

The MES-2/MES-3/MES-6 complex also plays an important role in the silencing of the X chromosome and the repression of autosomal somatic genes in the germline (Gaydos et al., 2014). Consequently, loss of PRC2 allows germ cells reprogramming into somatic cells such as neurons or muscles by ectopically expressing high levels of cell-type-specific transcription factors in the germline (Patel et al., 2012).

Another relevant role of PRC2 safeguarding cell fate occurs in embryonic cells, as loss of *mes-2* increases plasticity of somatic cell lineages. This increase in plasticity affects the time window during which the embryonic cells could be

reprogrammed to other lineage identities, normally only achievable during early embryogenesis and extended to late embryogenesis under that conditions, but still impossible during post-embryonic development (Yuzyuk et al., 2009).

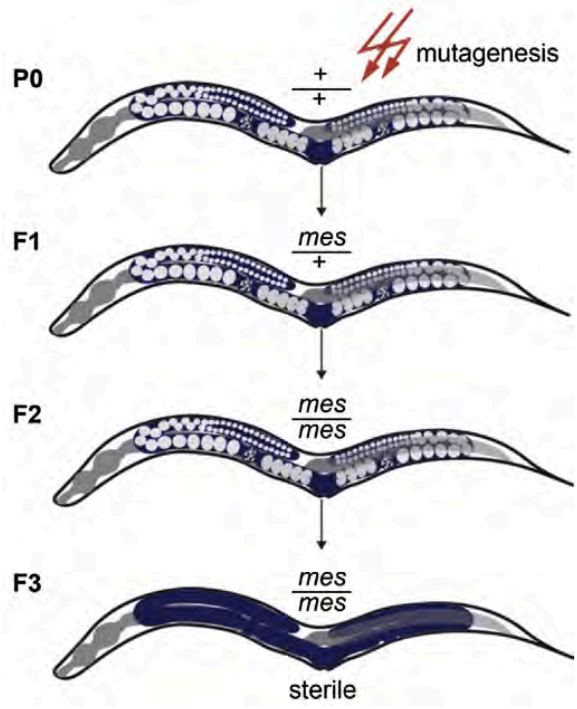

Figure I20. Identification of PRC2 elements encoded by the *mes* genes. *mes-2, mes-3, and mes-6* mutants were identified in a mutagenesis screen that looked for animals that fail to have grandchildren because of germline defects. P_0 homozygous wild-type animals (+/+) were mutagenized and producing F1 progeny that are heterozygous for a *mes* mutation (*mes*/+). These F_1s' produce homozygous *mes* F_2 progeny with a healthy germline because they inherit the maternal product of their parents, which is not the case in the F_3 progeny, as they lack of any *mes* transcripts dose and develop a sterile germline. Other *mes* genes have been identified in a similar basis. Reproduced from Tursun, 2017.

I3.5. Antagonism between H3K27me3 and H3K36me3 in *C. elegans*

In addition to the components of PRC2 in *C. elegans*, another MES protein was identified termed MES-4, which is homolog of mammalian HMT NSD1 and has been shown to deposit the H3K36me3 histone mark, which is linked with transcriptionally active chromatin loci (Rechtsteiner et al., 2010). Prominently, MES-4 excludes PRC2 from autosomal genes, leading to concentrated PRC2 activity on specific chromatin loci. This focusing of PRC2 is important in order to prevent the incorrect spread of H3K27me3 on autosomes that would silence genes that do not need to be silenced (Gaydos et al., 2012) (**Figure I21A)**.

Accordingly, *mes-4* mutants present an “unfocused” PRC2 activity which ubiquitously spreads on chromosomes, thus lowering the levels of repression of the normal H3K27me3-marked loci and ectopically activating genes, creating a “dilution effect” of H3K27me3 (**Figure I21B**). This antagonistic role between H3K27me3 and H3K36me3 is a general phenomenon in other organisms and explain the fact that PRC2 and MES-4 mutants display the same Mes phenotype in the germline (Tursun, 2017).

It is worth noting that the levels of histone methylations are controlled by the balance between HMTs and histone demethylases (HDMs) activities (Martin and Zhang, 2005; Shi

and Whetstine, 2007). *C. elegans* UTX-1, homolog of UTX/KDM6A and JMJD-3.1, JMJD-3.2 and JMJD-3.3 that are closely related to JMJD3/KDM6B, are responsible of removing the H3K27me3 mark. Hence, antagonizing PRC2 activity and thus acting as critical regulators of development in response to external or internal cues (De Santa et al., 2007; Swigut and Wysocka, 2007).

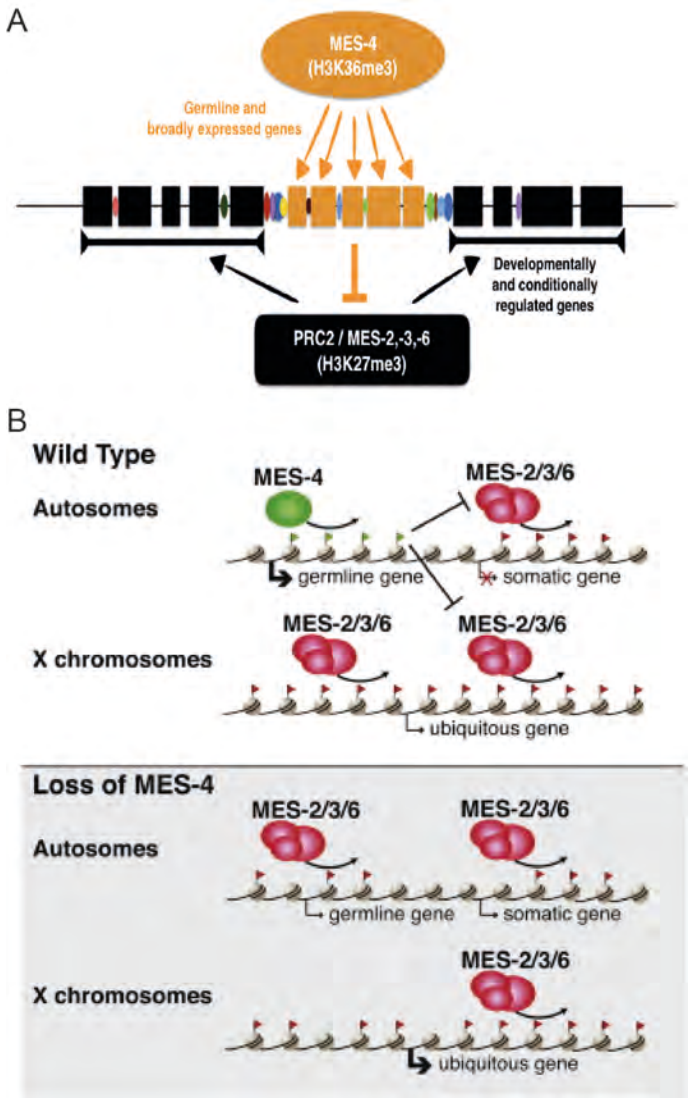

Figure I21. Antagonism of H3K27me3 and H3K36me3 marks in *C. elegans.* (A) Model for regulation of chromatin domains by MES-4, PRC2, and transcription regulatory regions. The genome is subdivided into domains of germline and broadly expressed genes (orange), and domains of genes with developmentally or conditionally regulated expression (in black boxes). MES-4 marks germline-expressed genes with H3K36me3, which inhibits deposition of H3K27me3 by PRC2, leading to demarcation of chromatin domains. Borders separating domains contain long intergenic regions enriched for TF binding (colored ovals); these regulatory regions may play a role in domain separation. Adapted from Evans et al., 2016. (B) Schematic representation of the model of antagonism produced by MES-4 and PRC2. Adapted from (Gaydos et al., 2012).

I4. Immunity in *C. elegans*

I4.1. Evolution of immune systems

Beutler and Wagner, commented about a generalized misconception of the innate immune system, as it is referred as a “primitive” immune system. However, despite its phylogenetic origins are indeed ancient, “there is nothing crude, nothing unsophisticated, and nothing inferior about innate immunity. On the contrary, innate immune systems has had time to achieve a level of refinement that is nothing short of dazzling, and a modicum of respect is at long last due”. Fundamentally, any immune system has two prime requirements: *(i)* to eliminate a broad range of pathogens and *(ii)* to not cause damage to the host in the process.

Vertebrates possess two types of immune systems: innate and adaptive. The innate immune system is considered the first line of defense against the entry of pathogens and is in charge of the rapid elimination of those that penetrated the organism before they cause infection. Importantly, the caused response is not very specific as it is based on the recognition of evolutionarily preserved structures found in pathogens (PAMPs), that act as ligands of pattern recognition receptors that are expressed by the cells of the innate immune system. Moreover, these specialized cells have the ability to act as antigen-presenting cells such as macrophages and dendritic

cells, that present microbial peptides to the adaptive immune system, providing antigen-specific protection against reinfection that represents an important evolutionarily advantage for survival (Domínguez-Andrés et al., 2020).

On the other hand, invertebrates' immunity only depends on innate mechanisms, usually entailing Toll-like receptors and downstream signaling pathways, including the NF-κB pathway (Wani et al., 2020). Because infection can reduce fecundity or cause death, these immune systems are under strong selective pressure from co-evolving microorganisms and although they present shared elements, it is common that different species present lineage-specific innovations and losses in their mechanisms of innate immunity (Kim, 2018).

I4.2. Innate immunity in *C. elegans*

In their natural habitat, free-living nematodes as *C. elegans* routinely experience fluctuations in temperature, food availability, and encounter to physical obstacles of diverse compositions. Also, their habitat is shared by other nematodes, by beneficial and harmful bacteria, and nematode-trapping fungi. Therefore, these animals have co-evolved to be able to detect and discriminate between diverse environmental cues in order to perform basic life processes as mating, finding food, avoid danger, and other activities to ensure surviving (Goodman and Sengupta, 2019; Wani et al., 2019).

As an invertebrate, *C. elegans* only comprise an innate immune system that is able to recognize and respond to viral, bacterial, and fungal infections (Ermolaeva and Schumacher, 2014). Notably, *C. elegans* do not have specialized immune cells, but infection and immune response can occur via several routes and tissues, for example through the cuticle and hypodermis, by other external organs such as the uterus and rectum, or following colonization of the intestine having passed through the pharynx (Engelmann and Pujol, 2010; Kim, 2018).

These different cells elicit distinctive transcriptional programs, which include genes that encode for antimicrobial peptides and enzymes, enhancing survival upon infection (Irazoqui et al., 2010). Outstandingly, most of these genes have human correlates, if not direct homologs (Wani et al., 2019).

Apart from the inducible mechanisms of the innate immune system, *C. elegans* count with at least other two main defense mechanisms against microbial attacks. The first one is an avoidance behavior, by which worms are able to distinguish between and even “remember” pathogenic or not pathogenic agents using their olfactory and chemosensory neurons to move towards or away from them. This behavior relies in proper and specific neuronal activity to act effectively (reviewed in Schulenburg and Ewbank, 2007.

A second axis of protection is portraited by *C. elegans* strong collagen and chitin-composed extracellular cuticle, that acts as

a physical barrier. Complementarily, the pharyngeal grinder destroys great part of the live pathogens that are ingested during feeding, preventing their infection in the intestine (Labrousse et al., 2000; Engelmann and Pujol, 2010).

I4.3. *C. elegans*: A gift from biology to study IκB alternative functions

Remarkably, *C. elegans* and other similar nematodes do not possess any homologs of NF-κB transcription factors as well as various key components of the TLR to NF-κB pathway, such as the TLR adaptor MyD88, NEMO and the IKKs (Irazoqui et al., 2010).

However, interestingly, it does include other important components that have been characterized in immune and developmental contexts, such as a single TLR named TOL-1; a TIR-only protein named TIR-1 that is closely related to SARM, another member of TLR protein adaptors; PIK-1 which is homolog of IRAK; TRF-1 which is homolog of TRAF; MOM-4 which is homolog of TAK1; and PMK-3 which is homolog of the p38 MAPK (Brandt and Ringstad, 2015; Brennan and Gilmore, 2018).

Nevertheless, perhaps the most striking evolutionary detail in this matter is that even lacking the most prominent upstream (IKKs) and downstream (NF-κBs) components of the pathway,

increased evidence reports the existence of two homologs of the IκB family of proteins: NFKI-1 and IKB-1 (Pujol et al., 2001; Ludewig et al., 2014; Chen et al., 2017; Flynn et al., 2020).

Finally, since even more evolutionarily ancient organisms, such as the members of *Porifera* and *Cnidaria*, do encompass a functional NF-κB pathway, it is probable that nematodes used to have it but lost it across evolution in favor of alternative mechanisms of regulation, yet it is still a matter of debate (Brennan and Gilmore, 2018) (**Figure I22**).

Taken together, and in addition to all the remarkable advantages of using *C. elegans* as a model system, the ground-breaking nature of this project is paved in the highly conserved chromatin organization and PRC2 regulation, along with innate immune pathways that include components of the NF-κB pathway without any of the prominent transcriptional activity that the NF-κB transcription factors cause, entailing a suitable scenario to study alternative roles of the IκB proteins.

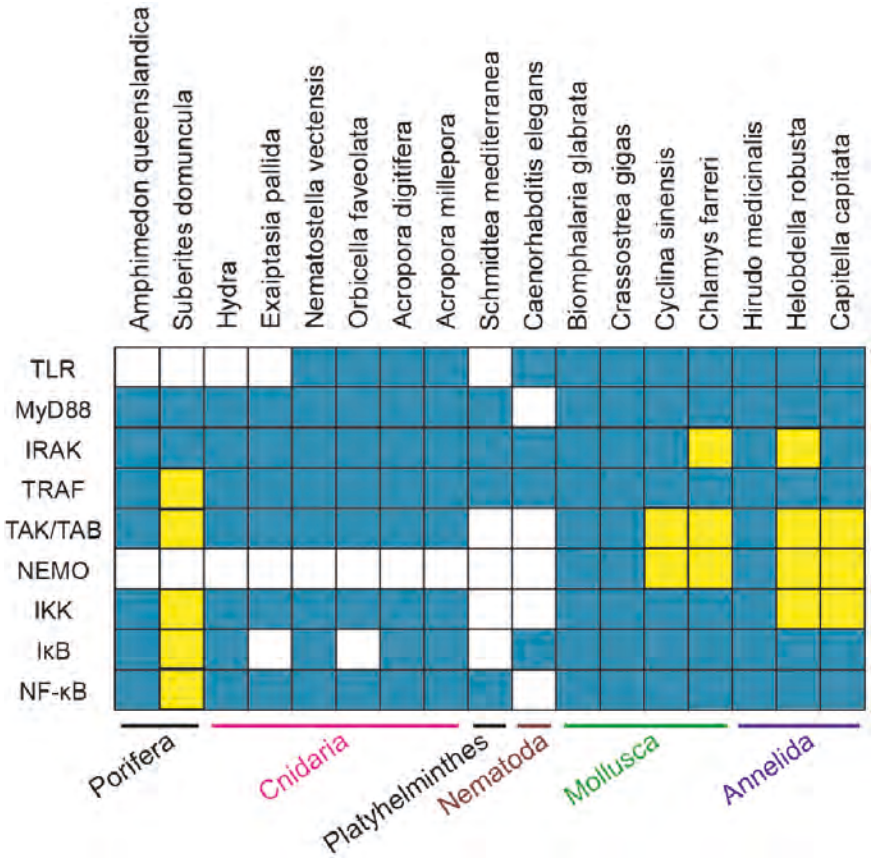

Figure I22. TLR-to-NF-κB pathway components expressed in organisms in phyla Porifera through Annelida. Members of the conserved TLR-to-NF-κB pathway found in the indicated organisms ordered from ancient (left) to most recently branched (right). Blue boxes depict the presence of a component of the pathway. White boxes indicate absence. Yellow boxes depict components that have not yet been identified in literature, but it is hypothesized to be present based on the completeness of the other components in other organisms of the same phylum. Reproduced from Brennan and Gilmore, 2018.

AIMS

AIMS

1. To determine the cellular and subcellular location of NFKI-1 and IKB-1.

2. To characterize phenotypically *nfki-1* and *ikb-1* mutants.

3. To study NFKI-1 and IKB-1 role in the nucleus.

RESULTS

R1. *nfki-1* and *ikb-1* are the *C. elegans* homologs of mammalian IκB family members

R1.1. Phylogenetic analyses identify NFKI-1 and IKB-1 as the *C. elegans* homologs of human IκB proteins

In order to spot IκB counterparts in *C. elegans*, we retrieved phylogenetic trees from the TreeFam project (Schreiber et al., 2014) and the BlastP program (Camacho et al., 2009). Both analyses locate NFKI-1 (**Figures R1A and R2A**) and IKB-1 (**Figures R1B and R2B)** in the branch of the IκB proteins. Next, according to OrthoList 2 (Kim, Underwood, Greenwald, & Shaye, 2018, http://ortholist.shaye-lab.org), we identified NFKI-1 as the most likely ortholog for human IκBα, IκBβ and IκBδ, and IKB-1 for human BCL3.

Supporting a functional conservation, the region with the highest sequence similarity between NFKI-1 and IKB-1 includes a series of ankyrin repeats (**Figure R3, Figure I6**), which are known to mediate the interaction between human IκBs and other proteins (Jacobs and Harrison, 1998; Zhang et al., 2017).

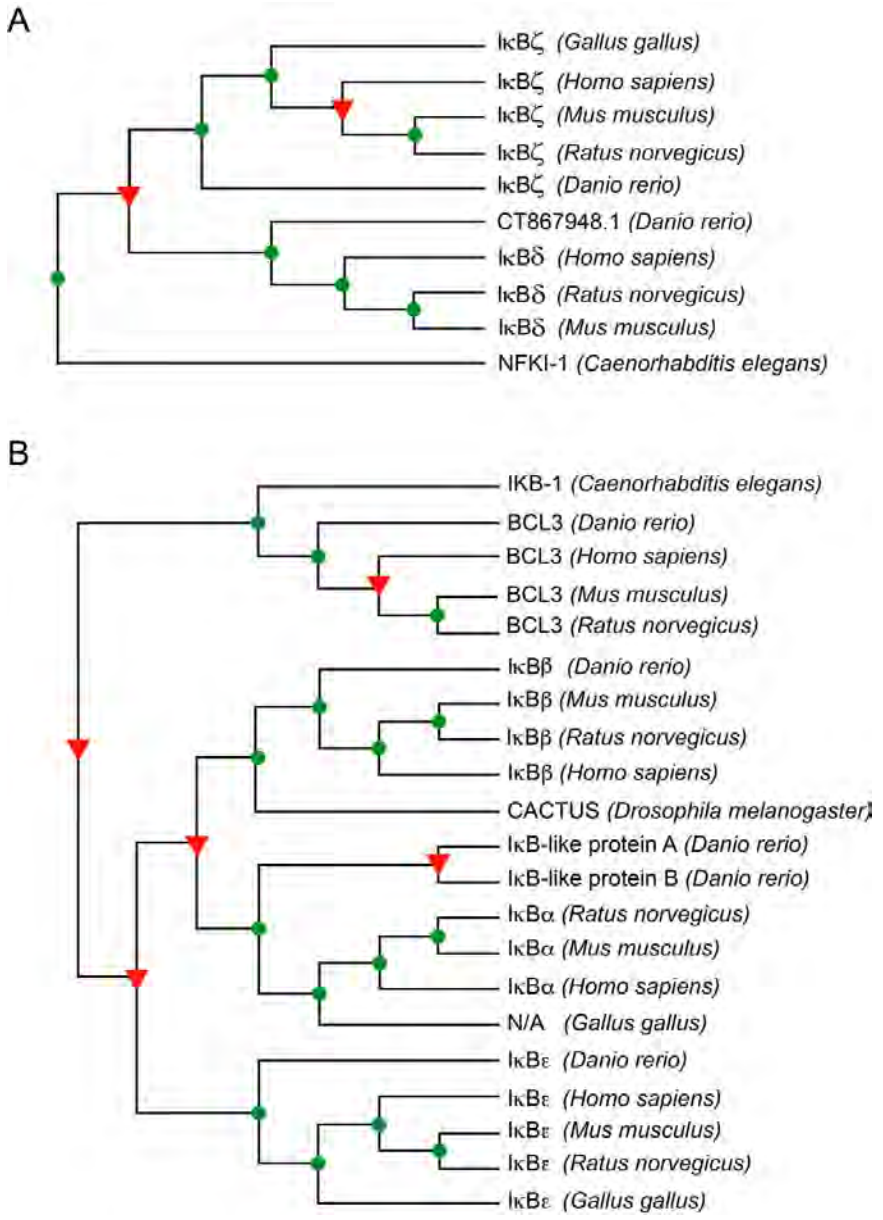

Figure R1. Phylogenetic trees from the TreeFam project associate NFKI-1 and IKB-1 with IκB family members. Phylogenetic trees for NFKI-1 **(A)** and IKB-1 **(B)** (Ruan et al., 2008; Schreiber et al., 2014).

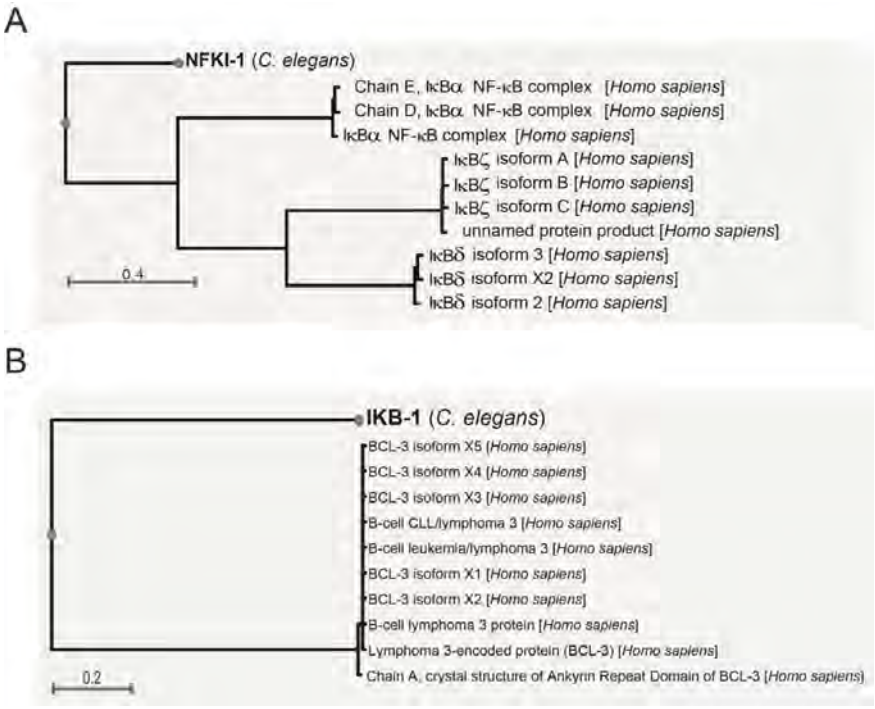

Figure R2. BlastP protein alignment of NFKI-1 and IKB-1. Protein sequence similarity analysis with BlastP program (Camacho et al., 2009) locates NFKI-1 **(A)** as homolog of IκBα, IκBζ and IκBδ, while IKB-1 **(B)** is closer to BCL3. See also best BlastP matches at www.wormbase.org.

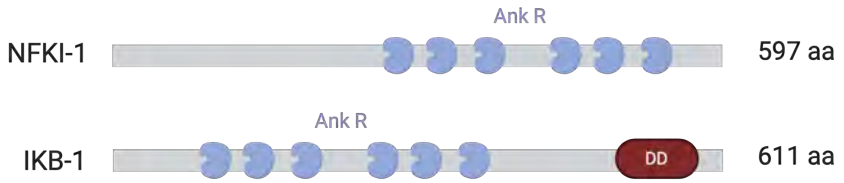

Figure R3. NFKI-1 and IKB-1 protein domains. Both proteins present ankyrin-repeat domains (Ank R), which commonly mediate protein interaction in IκB-related proteins (Jacobs and Harrison, 1998). In addition, IKB-1 contains a death domain (DD), which is associated to Toll-like receptor signaling (Chen et al., 2017). Importantly, neither NFKI-1 nor IKB-1 preserves the PEST domain present in IκBα and IκBβ and that is necessary for the regulation of NF-κB (Wang et al., 2020) (**Figure I6**).

R1.2. Key residues of IκB proteins are conserved in NFKI-1

Interestingly, NFKI-1, but not IKB-1, contains the IKK phosphorylation consensus site (DSGXXS) as well as the lysine (K) 21, localized 12 amino acids upstream of such phosphorylation domain (**Figure I6)**. These residues are hallmarks of the IκB family of proteins (Culver et al., 2010) and are highly conserved among the mammalian IκBα, IκBβ and IκBε homologues, including the *Drosophila melanogaster* protein Cactus (**Figure R4A**), which is the ortholog of human IκBα (Mulero et al., 2013). Importantly, our collaborators confirmed the presence of phosphorylated NFKI-1 at the IKK consensus site by performing Western blot experiments on L4 worms expressing endogenous EGFP::NFKI-1 using a monoclonal antibody against the phosphorylated serine at the position 32 (p-S32) of human IκBα (Brena et al., 2020)(**Annex R1**). Interestingly, this phosphorylation was not observed using two additional antibodies that recognize both p-S32 and p-S36, and only p-S36 of human IκBα (data not shown).

As mentioned in the introduction, SUMOylation is a post-translational modification that occurs in mammalian IκBs (Desterro et al., 1998; Mulero et al., 2013; Perkins, 2013). By using the GPS-SUMO tool (Ren et al., 2009; Zhao et al., 2014) we identified additional SUMOylation consensus sites (lysines, K) at the amino-terminal half of both NFKI-1 **(Figure R4B)** and IKB-1 (**Figure R4C**), as well as putative SUMO-interaction regions.

Altogether, these results determine that NFKI-1 and IKB-1 are the homologs of the mammalian IκB family of proteins in *C. elegans*.

A

KEESIRGRPPSADSGVSSPM	NFKI-1 (*Caenorhabditis elegans*)
LKKERLLDDRHDSGLDSMK	IκBα (*Homo sapiens*)
GKAADADEWCDSGLGSLG	IκBβ (*Homo sapiens*)
RKGPDEAEESQYDSGIESLR	IκBε (*Homo sapiens*)
KQKEFAVPNETSDSGFISGP	Cactus (*Drosophila melanogaster*)

B

NFKI-1

```
  1 MATVAPKGNC LVARAIPSDS HADQLTDLLC KLSVNGDANQ KSVNKFESQH GVTPSDFRDI
 61 QNIRSSALAK KTKTSKFQLD GVTLFADLTP NSKSKKKTEN QETKEKDEEA EEKKDGPPKD
121 DKELKMKKEK EQEDENAELD EQKKDGDLLG RGPVHNVRVA TGGSHPYHRA QIPYGCAAQT
181 PITDISAYTG YGSGYECGST WSLSPDTTIG SISASTTPDT VLSSDGYGSA SPPQHSPKES
241 LQSPFSDISS ADTSRVLTPE NNELPESLQD FILQYSNQYT KEESIRGRPP SADSGVSSPM
301 SARSAPYASP HVPQGTCSGP TTPSFNQTRL SPRTSENGIT AKQRLNAIIP ESDLATGFHW
361 ACTTWKNVLT NRDADGDTPL HIVAAHNDLG KIYALCETLR KTMNENDDNV FNVSNNFGET
421 PLYVAVLQRS IEVVEYLLEL GASPNSRSSR AVGDSPLHFA TARGMNNMVE ALLSKREIRV
481 NETNDDGQTS LLCAVKMHGM MDEQTQHKID NKSIIEMLIK AGADPTIAET STGKTIVHHA
541 VDKMDVELLD FLKTVVNEDT FTELANLSDF HGDTAVDLLC SSTQNEDTNN VRENLYIRLL
601 TSGAVPNKSR A
```

C

IKB-1

```
  1 MSKADENDAN LTENGVHKSR SDSEINSHTS SIHKSSSQHR RLFIDDISTI EASAGDRVWA
 61 TCSGAGDATE LITIHFLGDQ FEESAIDVVR KHSLVMFTVP SLKVDSELEV ELRFSTSNDN
121 VTTISFKYLP RKIQRSHTQE ISLFDNLLEF ATNGDTISLL QPFVAQISKQ DIEGNTVFHV
181 AAKNGQSFSL KLLLSVIPPD IKNEVINVQN THGLTALHVA IRTGDPDAVH YLMNHGAKID
241 ISDNHGSTAL HYLGDAYNES IFKEILEPSR GQRFDVNQLN SEGFAPIHVA VRRLKLSLIE
301 MLIEAGALID FLDTEKKRNA LMHAIEMNDF ETIQLLVERG SGTNIEDESG ETALSLAVKN
361 VNYPVIGLLL DNGADPNRQN SKGICLADSE DSVIQNIING DRPELPKKEA FGVPNDLAIS
421 RSPLFGRSHP DQAPGEESGR HRVVKRSREE ILNDAQTLLA ETDSMAPRVS RISTSESEDE
481 QQPGPSTSSG TRRRRSEWDR NPKLSDSVCN LDYLTRIRVA KIFDDQCKWQ RLAQQLNCDH
541 MVELISICSS GDDSSPTMIL LDQFEQLEDS SISRLRDAMN QMAEDDAVKL IDSRYVY
```

Figure R4. NFKI-1 and IKB-1 display putative post-translational modification sites. (A) Alignment of NFKI-1 with human IκBα, IκBβ and IκBε, centered on the region containing the consensus phosphorylation sites (residues 32 and 36 in IκBα, in red) for IKKβ kinase. Note the

conservation of the upstream lysine residue that is either ubiquitinated or SUMOylated (in green) in IκBα. (B, C) Potential SUMOylated lysines (K, highlighted in green) and SUMO-interaction sites (in red) in the NFKI-1 (B) and IKB-1 (C) proteins, as predicted using the GPS-SUMO tool (Zhao et al., 2014).

R2. Cellular and subcellular distribution during development

R2.1 *nfki-1* and *ikb-1* expression patterns retrieved from transcriptomic databases

To get insights into *nfki-1* and *ikb-1* functions during *C. elegans* development, we explored their expression patterns in public transcriptomic datasets in different cell types and developmental stages. Temporal series of RNA-sequencing (RNA-seq) of the modENCODE project during embryonic and post-embryonic development showed the onset of *nfki-1* and *ikb-1* expression at late embryo, coinciding with morphogenesis and final differentiation of embryonic cells. Then, expression is maintained through all post-embryonic stages (**Figure R5A)** (Gerstein et al., 2010; Boeck et al., 2016; Hutter and Suh, 2016). Interestingly, *nfki-1* and *ikb-1* present an elevated expression in L1 and in dauer larvae, which are observed under starving conditions (Hu, 2007).

Further examining this dataset, *nfki-1* expression seems to be rather ubiquitous but enriched in neuronal cells, whereas *ikb-1*

is mostly restricted to muscle cells (**Figure R5B**).

Remarkably, both genes seem to be completely excluded from the germline. There are tissues and cell types that display co-expression to some extent, as is the case of the pharynx, body wall muscle or the DTCs. This is further supported by single-cell transcriptomic time courses during embryonic development that suggest that *nfki-1* and *ikb-1* are expressed in distinct cell types, overlapping only in a few cells (**Figure R5C**) (Packer et al., 2019).

Overall, *nfki-1* and *ikb-1* expression seems to be associated to differentiated somatic cells, being *nfki-1* rather ubiquitous and *ikb-1* mostly confined to muscle-related cell lineages.

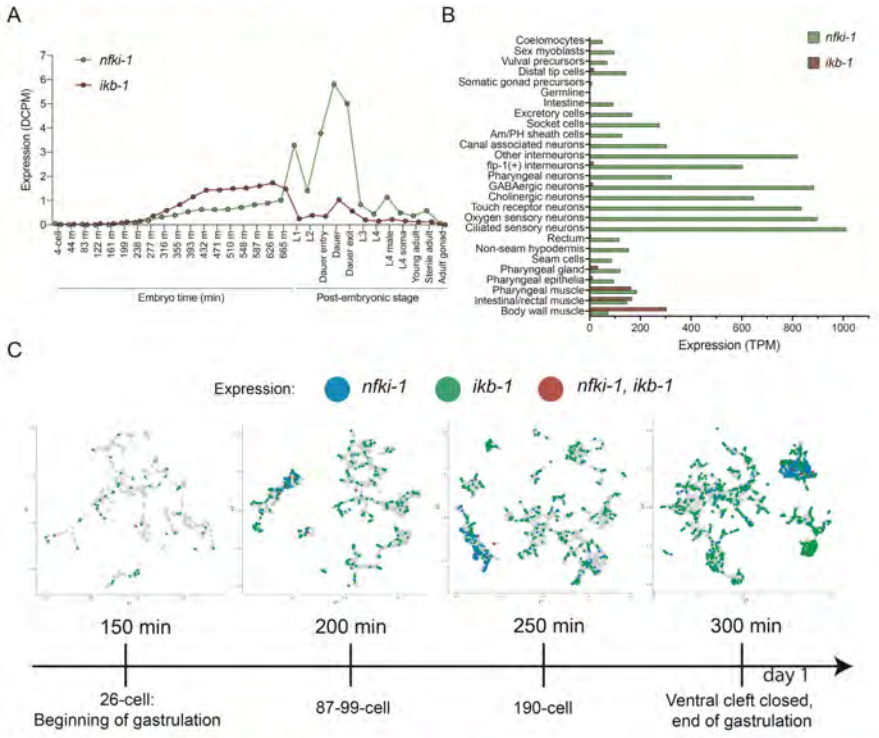

Figure R5. Expression profiles of *nfki-1* and *ikb-1*. (A) RNA-seq time series (Gerstein et al., 2010) showing *nfki-1* (green) and *ikb-1* (red) stage-specific expression profiles during embryonic development and all post-embryonic stages. Expression data is presented as the average depth of coverage per million mapped reads (DCPM). (B) Tissue-specific expression profiles of L2 animals (Cao et al., 2017). *nfki-1* (green) is mainly expressed in the nervous system and *ikb-1* (red) in the muscular system. Expression data is presented as transcripts per million reads (TPM). Data for (A) and (B) were retrieved from GExplore 1.4 (www.genome.sfu.ca/gexplore) (Hutter and Suh, 2016). (C) Time courses of single-cell transcriptomics during embryogenesis. t-distributed Stochastic Neighbor Embedding (t-SNE) representations of the single-cell expression profiles at four different time points during embryonic development, clustered according to its tissue-specific lineage (Packer et al., 2019). Expression of *nfki-1* is denoted in blue, *ikb-1* in green, and co-expression in red. Note that both *nfki-1* and *ikb-1* show a complementary expression pattern, with co-expression in a few cells. t-SNE representations were retrieved from https://cello.shinyapps.io/celegans/

R2.2. Generation of NFKI-1 and IKB-1 endogenous reporter strains

In order to study the expression patterns of NFKI-1 and IKB-1 *in vivo*, we generated endogenous fluorescent reporters using CRISPR-Cas9 genome editing.

Specifically, we created two tagged strains for *nfki-1*: one with a 3xFLAG epitope tag (CER424: *nfki-1(cer102[3xFLAG::nfki-1)*]) X) (**Figure R6A**) and another with an EGFP fused to *nfki-1* (CER461: *nfki-1(cer116[EGFP::nfki-1]*) X) (**Figure R6B**).
Importantly, both fusion tags were inserted at the 5' end of the gene to minimally interfere with protein function since the ankyrin repeat domains are located closer to the C-terminal part of the protein. We designed a crRNA to generate a DSB near the start codon and used an ssDNA donor containing the 3xFLAG sequence (66 nt) in order to add the antigenic tag in frame. In an independent experiment, we used the same crRNA to insert the gene encoding the sequence of EGFP (855 bp) using the Nested CRISPR methodology (Vicencio et al., 2019). In the case of *ikb-1,* an mCherry was inserted at the C-terminal part of the protein (PHX267: *ikb-1(syb267[ikb-1::mCherry])* I), as the Ank R domains are closer to the N-terminal end (**Figure R6C**).

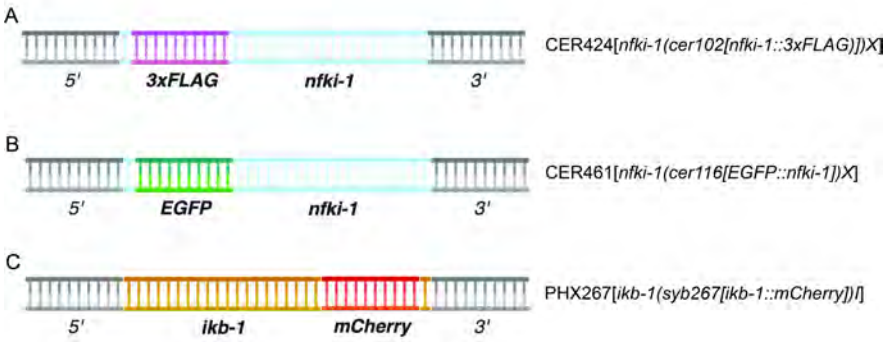

Figure R6. *nfki-1* and *ikb-1* endogenous tags design. (A, B) Schematic representation of the CRISPR-Cas9-generated *nfki-1* endogenous fusion tags and the upstream (5') and downstream (3') regions to *3xFLAG::nfki-1* (A) and *EGFP::nfki-1* (B). (C) *ikb-1::mCherry* endogenous reporter.

R2.3. Analysis of NFKI-1 and IKB-1 endogenous fluorescent reporters

We used CRISPR-engineered endogenous fluorescent reporters to study the expression patterns of *nfki-1* and *ikb-1 in vivo*. At the L1 stage, when *nfki-1* expression was higher according to databases (**Figure R5A**), we observed a lack of overlap between *nfki-1* and *ikb-1* expression (**Figure R7A**), as predicted by previous transcriptomic studies (**Figure R5B-C**). Of note, *EGFP*::*nfki-1* expression was evident in neuronal cells of the head but low in other cell types, and such feature was maintained during post-embryonic development (L1-L4 stages). In the case of *ikb-1::mCherry*, expression was observed at the pharynx and muscle cells scattered through the body at L1. The expression at the pharynx was clearly detectable at later developmental stages (**Figure R7B-D)**.

Such observation matches with the lower transcript abundance from L3 onwards detected by the modENCODE datasets (Gerstein et al., 2010). It is worth noting that IKB-1::mCHERRY displayed a characteristic dot-like signal that has previously been reported for mammalian BCL3 (Zhang et al., 1994; Schuster et al., 2013).

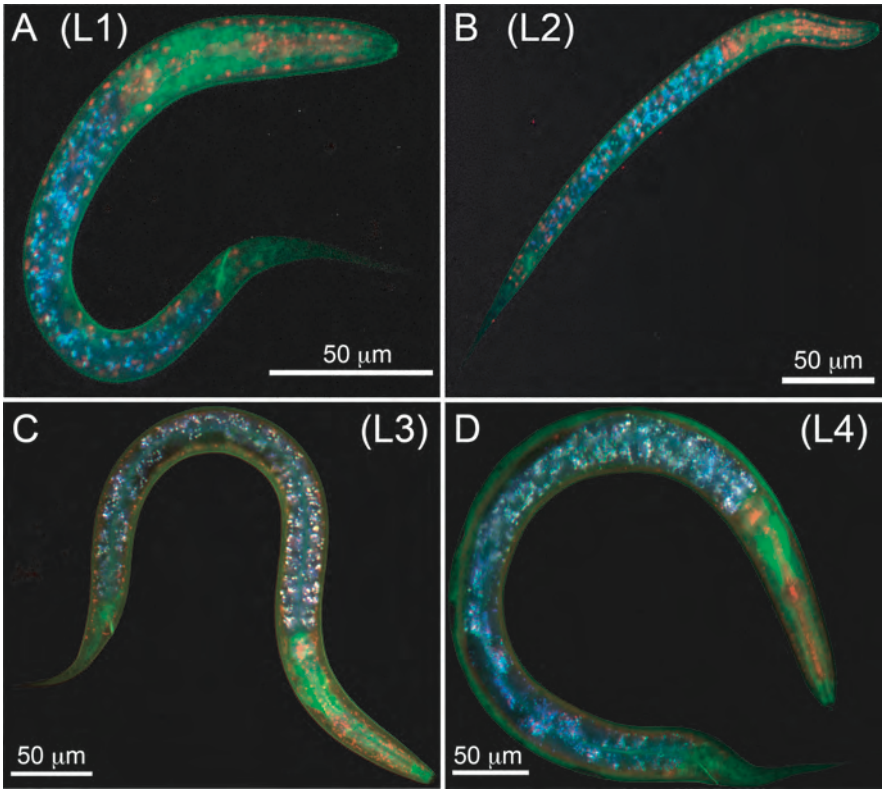

Figure R7. NFKI-1 and IKB-1 endogenous fluorescent reporters at postembryonic stages. (A-D) Microscopy images of animals carrying both IKB-1::MCHERRY and EGFP::NFKI-1 reporters at the indicated developmental stages. DAPI channel is merged to indicate gut autofluorescence. Scale bars: 50 μm.

R2.4. A low proportion of NFKI-1 and IKB-1 is present in the nucleus

In silico NLS analyses of NFKI-1 and IKB-1 suggested that both proteins would predominantly present a cytoplasmic localization (green) but also indicated nuclear and cytoplasmic localization peptides (yellow) based on NLS-associated peptides scores (**Figure R8**). These scores or levels of NLS activities are calculated by using the positive or negative contribution of each amino acid residue within an NLS profile (Kosugi et al., 2009). We included DAF-16/FOXO, a well-known nuclear and cytoplasmic highly dynamic protein, which displays a profile with exclusively nuclear and cytoplasmic (yellow) predicted NLS activities.

Given the presence of multiple predictions for both NFKI-1 and IKB-1 and the absence of the sequence of the two characterized NES of IκBα (Lin et al., 1996; Arenzana-Seisdedos et al., 1997; Johnson, 1999; Truhlar et al., 2008; Yazdi et al., 2015, 2017; Wang et al., 2020) in NFKI-1 and IKB-1, we did not consider convenient to generate mutants that disrupt the predicted NLSs or NESs as a way to modulate the nuclear localization of NFKI-1 and IKB-1. Instead, we decided to validate a possible nuclear localization at physiological levels.

For that, we created a strain combining the endogenous EGFP::NFKI-1 reporter with a reporter for a nuclear protein (the splicing factor SFTB-1 (SF3B1 in humans)) (Serrat et al., 2019). Indeed, by using confocal microscopy, we confirmed that NFKI-1 was predominantly in the cytoplasm, but a low percentage could be present in the nucleus (**Figure R9**). We also generated a strain that included an endogenous nuclear envelope reporter *GFP::mel-28* and *ikb-1::mCherry* and observed that IKB-1::mCHERRY present a similar subcellular distribution (**Figure R10**). Thus, only a small percentage of IκB homologs would be present in the nucleus.

These results fit with the predominant cytoplasmic distribution of IκBs in most mammalian cells (see Human Protein Atlas at www.proteinatlas.org; Uhlen et al., 2010) and the reported function of NFKI-1 (Chen et al., 2017) and IKB-1 (Pujol et al., 2001) associated to cytoplasmic signaling pathways, but are also compatible with *C. elegans* IκBs playing specific nuclear functions.

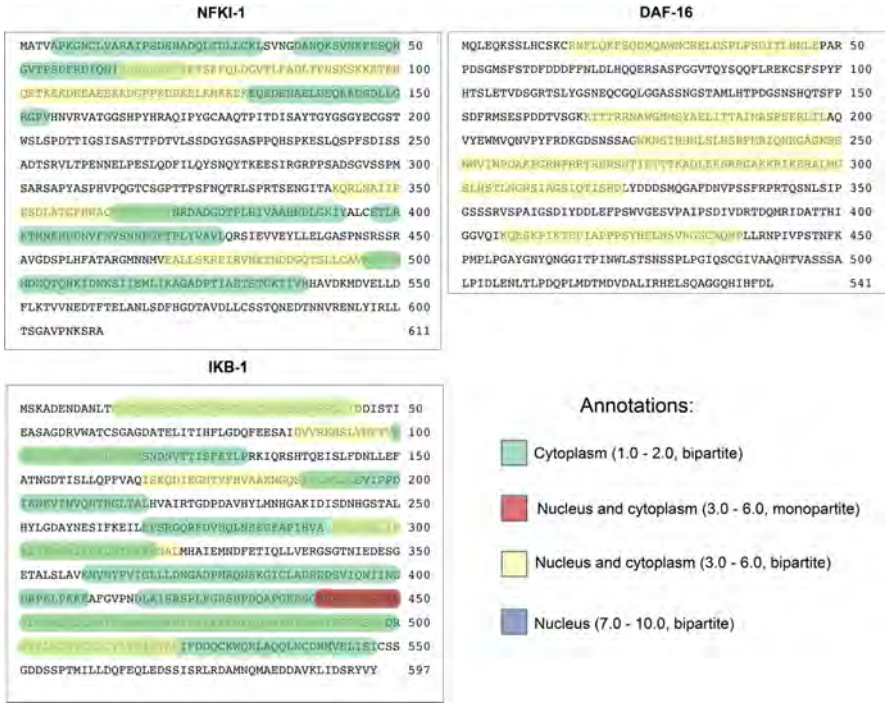

Figure R8. *In silico* NLS analysis of NFKI-1 and IKB-1. Predicted NLS-associated peptides are highlighted according to its score with cNLS Mapper. Higher scores indicate stronger NLS activities (Kosugi et al., 2009).

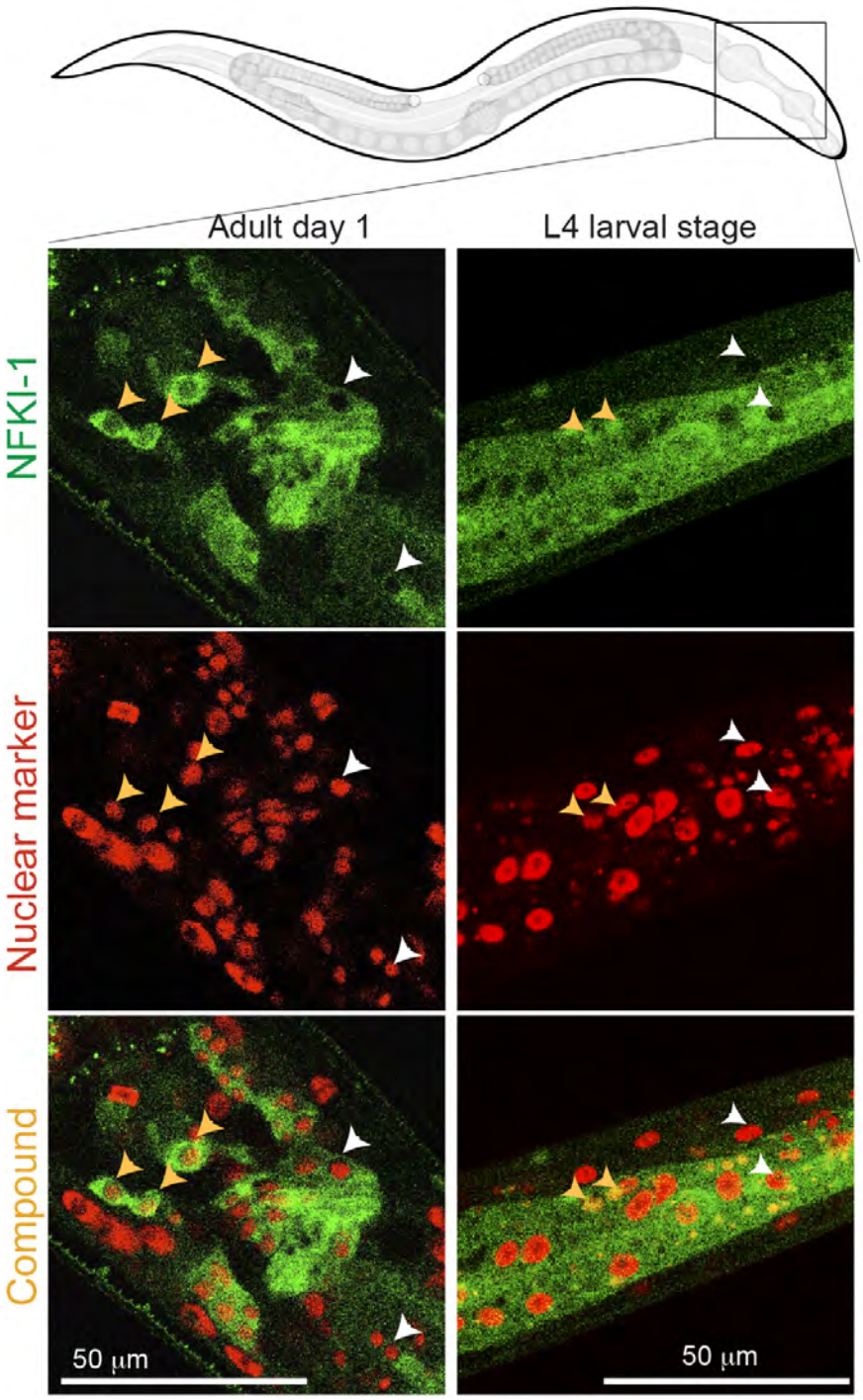

Figure R9. A low proportion of NFKI-1 is in the nucleus. Confocal microscopy images of endogenous reporters showing the expression

pattern of EGFP::NFKI-1 at the indicated developmental stages. mCHERRY::SFTB-1 is used as the nuclear marker. Yellow arrowheads denote cells that show a nuclear and cytoplasmic EGFP::NFKI-1 signal. White arrowheads point cells that display only cytoplasmic localization at the same plane. Scale bars: 50 μm. Imaging was done with 63X magnification in Z-stacks with 0.25 μm of distance between planes. Images represent a single plane.

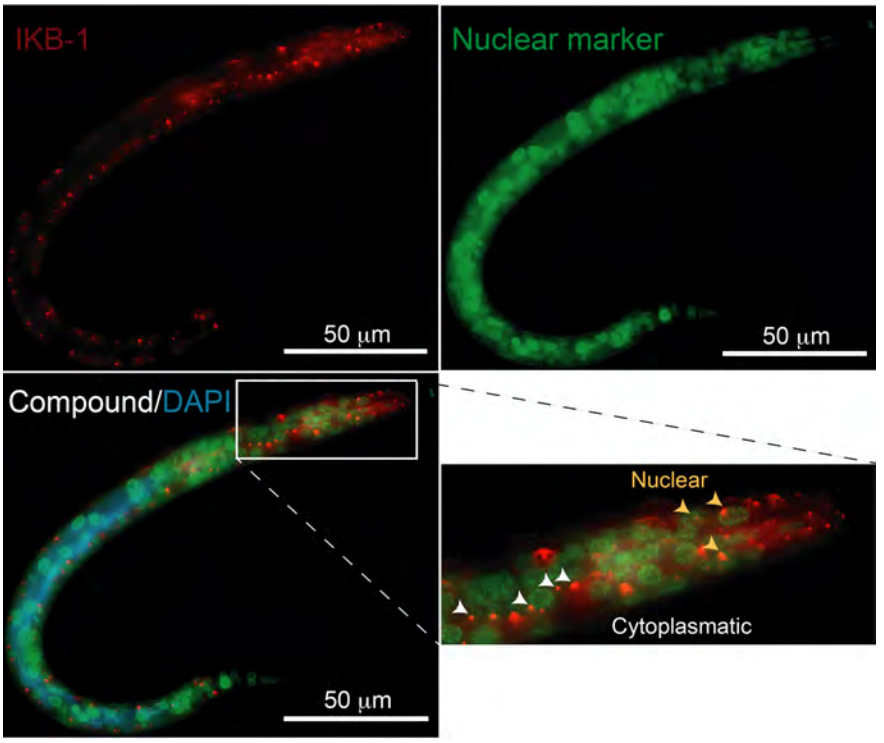

Figure R10. IKB-1 subcellular location is mainly cytoplasmatic. Representative fluorescence microscopy images of CER509: *ikb-1(syb267[ikb-1::mCherry]*) I; *mel-28(bq5[GFP::mel-28])* III] at the L2 larval stage. IKB-1::mCHERRY display dot-like structure signals in the body wall muscle and pharynx tissues. GFP::MEL-28 endogenous reporter was used as a nuclear envelope marker. Expression is mainly cytoplasmatic, but it is also present in the nucleus of a few cells. DAPI channel was added to show gut autofluorescence. Scale bars: 50 μm. Arrowheads denote cells that show IKB-1::mCHERRY signal inside the nuclear membrane (yellow) or in the cytoplasm (white).

R2.5. NFKI-1 over-expression induces nuclear accumulation

To explore the possibility of *nfki-1* being expressed in other cell types that could be overlooked because of the low levels of endogenous expression in some cells, we produced a multicopy transgene that over-expressed *nfki-1* under the control of its own promoter (several strains with extrachromosomal or integrated as low copy after gene bombardment) using expression vectors from the TransgeneOme project (Sarov et al., 2012). These transgenic animals exhibited a ubiquitous *nfki-1::TY1::EGFP::3xFLAG* expression, concurring with transcriptomic tissue-specific datasets, including its restriction to somatic cells (Cao et al., 2017). Interestingly, we clearly observed the presence of NFKI-1 in both cytoplasm and nucleus (**Figure R11A-E**).

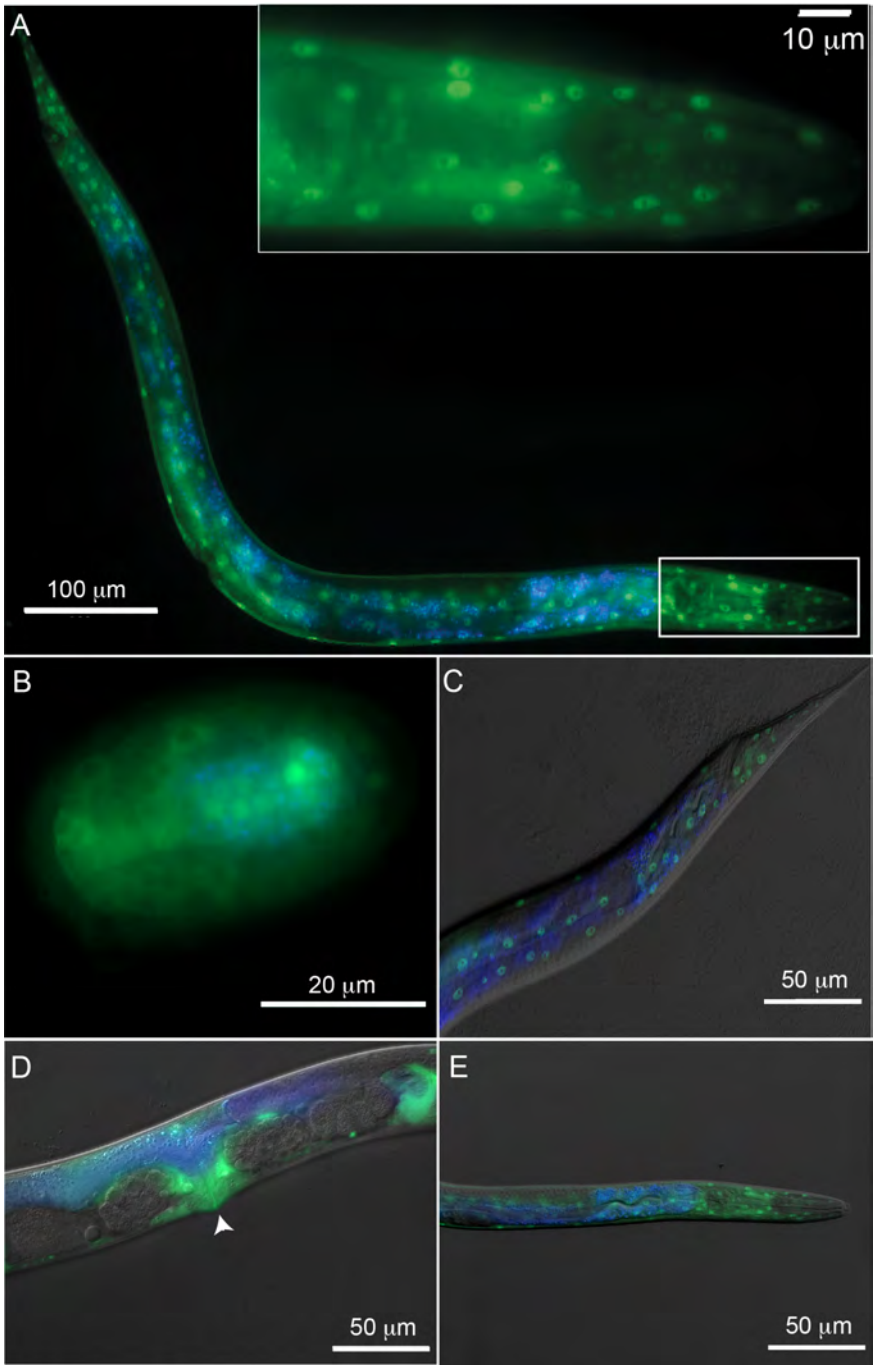

Figure R11. NFKI-1::TY1::EGFP::3xFLAG over-expression shows a nuclear and cytoplasmic subcellular localization in somatic cells.

(A) Microscopy image of one representative CER147: *cerEx35[nfki-1::TY1::EGFP::3xFLAG+unc- 119(+)*] over-expression strain at L4 larval stage. Scale bar: 100 µm. The inset shows the boxed area at higher magnification. Inset scale bar: 10 µm (B) NFKI-1:TY1::EGFP::3xFLAG is expressed during embryogenesis in the nucleus and cytoplasm. Scale bar: 20 µm (C-E) Representative images of the tail (C) vulva (D, depicted by the white arrowhead) and head (E). DIC and DAPI channels were merged to simplify anatomical location and gut autofluorescence, respectively.

R3. Phenotypes produced by IκB mutants

R3.1. Generation of *nfki-1* and *ikb-1* deletion mutants

Mutants for *nfki-1* and *ikb-1* were previously characterized, however the studies were focused on their role in innate immunity and environmental sensing, rather than in their role in development, thus no obvious developmental phenotypes were reported (Pujol et al., 2001; Chen et al., 2017).

In order to characterize the function of *nfki-1* and *ikb-1*, we produced by CRISPR-Cas9 new mutant alleles, as well as a strain with both genes mutated. Thus, we compiled several alleles and avoided the possibility of the existence of side and off-target mutations by outcrossing at least 3 times the existing mutant strains (produced by mutagenesis). For *nfki-1*, we generated two loss-of-function alleles by performing deletions near the 5' end of the gene of 368 bp (*cer1*), and a 438 bp deletion + 50 bp insertion (*cer2*), both producing a premature stop codon (**Figure R12A**). In the case of *ikb-1* we generated the loss-of-function allele *cer9* by deleting 462 bp at the beginning of the coding sequence of the gene, including the start codon, so that no transcript would be synthetized. We also characterized the *ikb-1(nr2027)* allele, which was provided by

the CGC (**Figure R12B**). The lack of transcripts was confirmed by semiquantitative RT-PCR (**Figure R13**).

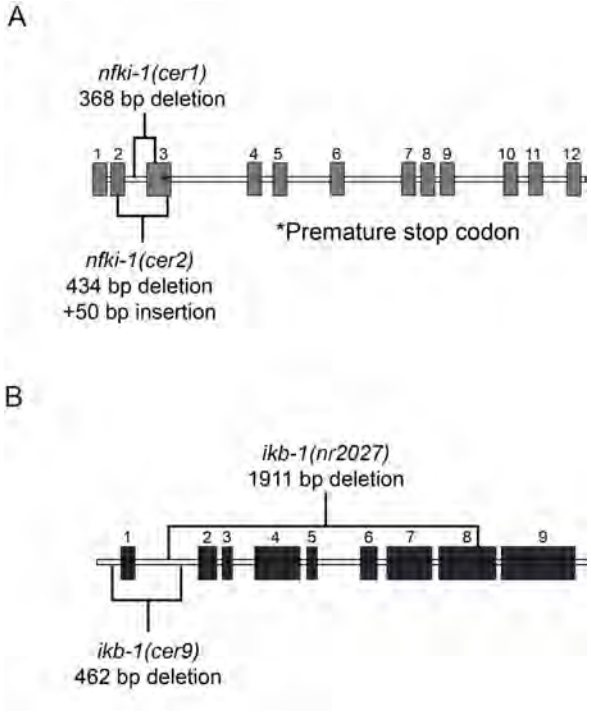

Figure R12. Graphical representation of the *nfki-1* (A) and *ikb-1* (B) mutant alleles used in the study. Filled boxes are exons, empty horizontal lines represent introns.

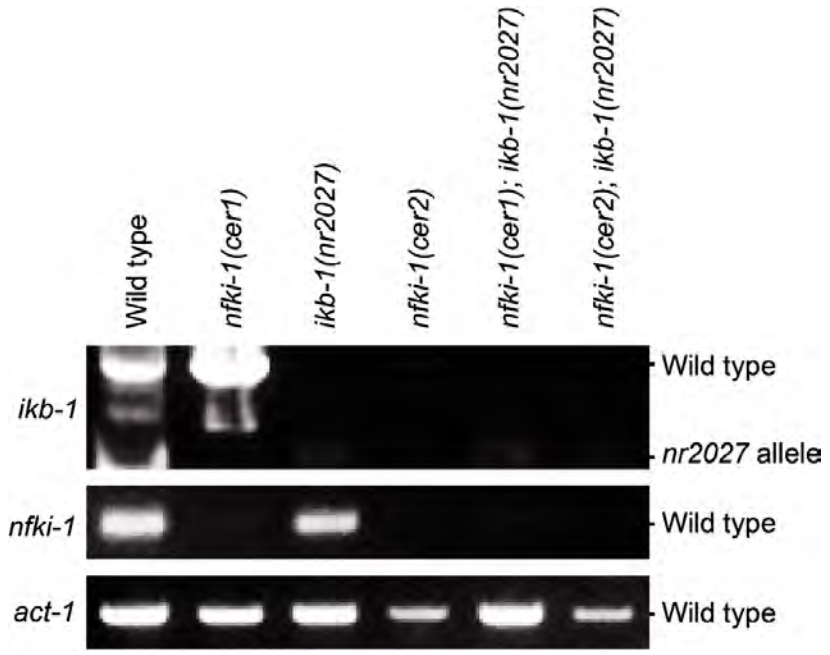

Figure R13. RT-PCRs of IκB mutants show effective gene product depletion. *cer9* allele was not included as by design lacks the start codon. Actin (*act-1*) was included as an internal control.

R3.2. *nfki-1* and *ikb-1* display impaired stress responses probably due to their cytoplasmic role

Since *nfki-1* and *ikb-1* are both upregulated in dauer stage (Ludewig et al., 2014), which is induced by harsh environmental conditions during early post-embryonic development (Hu, 2007), we conducted a survival assay with starved L1 *nfki-1* and *ikb-1* mutants. Interestingly, *nfki-1* and *ikb-1* mutants survived longer in the absence of food (**Figure R14**). We wondered if dauer or starved L1 animals would present a higher proportion of nuclear NFKI-1 and IKB-1, but it was not the case (**Figure R15**). We also found that *nfki-1* and *ikb-1* mutant animals are resistant to the stress imposed by

high temperatures (36ºC) during day 1 adulthood (**Figure R16**), but this stress also did not favor the nuclear localization at least at clearly observable levels (data not shown).

To confirm that the observed resistance to starvation and high temperature stress was due to a loss-of-function of NFKI-1, we crossed our *nfki-1(cer2)* mutants with the *nfki-1::TY1::EGFP::3xFLAG* extrachromosomal over-expression strain and repeated these assays including the new strain. Indeed, we observed a rescue for both starving and high temperature stress resistance phenotypes (**Figure R17A-C)**.

Since NFKI-1 (Chen et al., 2017) and IKB-1 (Pujol et al., 2001) have been associated to cytoplasmic signaling pathways regulating oxygen sensing and in response to pathogens, maybe functions that are related to responses to environmental sensing are linked to their cytoplasmic functions. These results are interesting, since would mean that the IκB proteins were involved in innate-immunity and stress responses even without the existence of NF-κB.

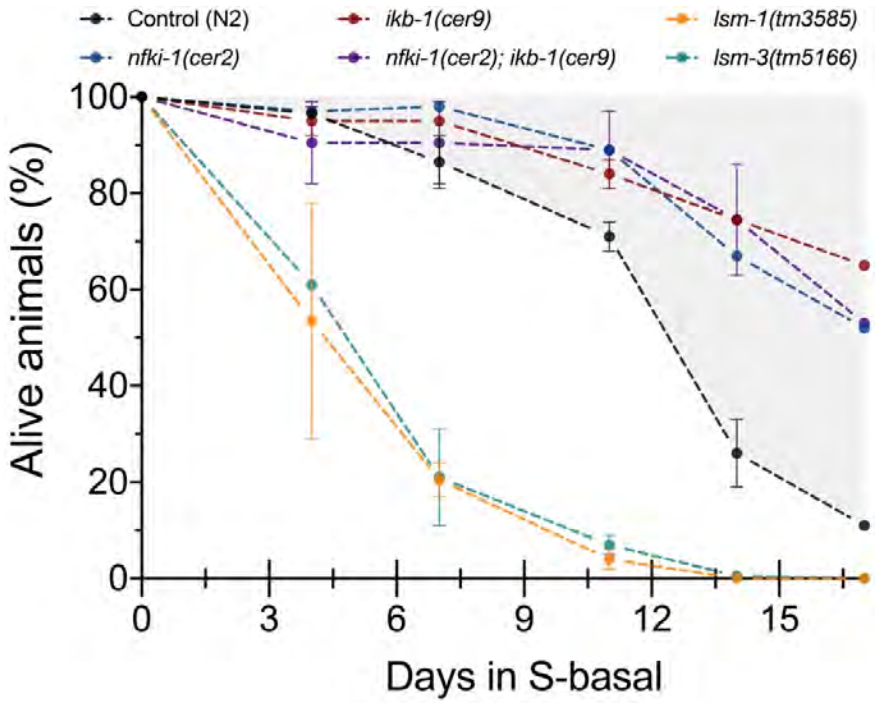

Figure R14. *nfki-1* and *ikb-1* mutants present resistance to L1 starvation. Survival curves of the indicated nematode genotypes grown under nutrient restriction. Mutants for the stress proteins LSM-1 and LSM-3, sensitive to L1 starvation, were used as controls (Cornes et al., 2015). n=100 animals per timepoint. N=2. Error bars and points show the mean of 2 experiments. Statistically significant differences between control and *nfki-1* and *ikb-1* mutants were calculated using two-tailed Spearman correlation test (CI: 95%).

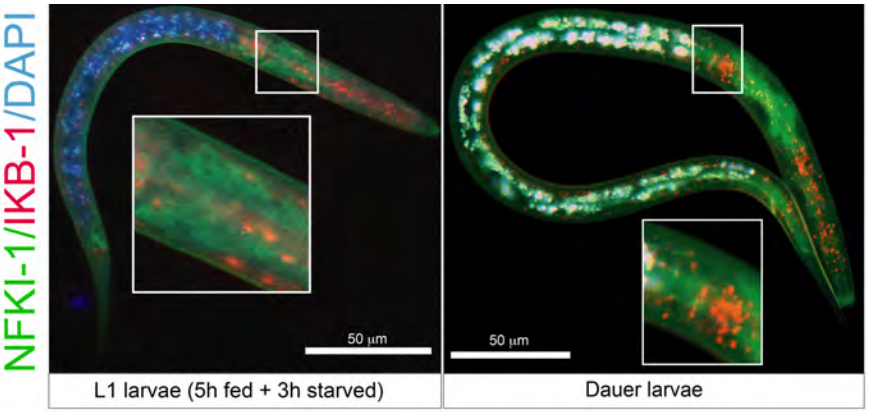

Figure R15. Starving conditions do not alter expression patterns of NFKI-1 or IKB-1. Microscopy images of animals carrying both

EGFP::NFKI-1 and IKB-1::MCHERRY endogenous reporters at the indicated developmental stages. DAPI channel is merged to indicate gut autofluorescence. Scale bars: 50 µm.

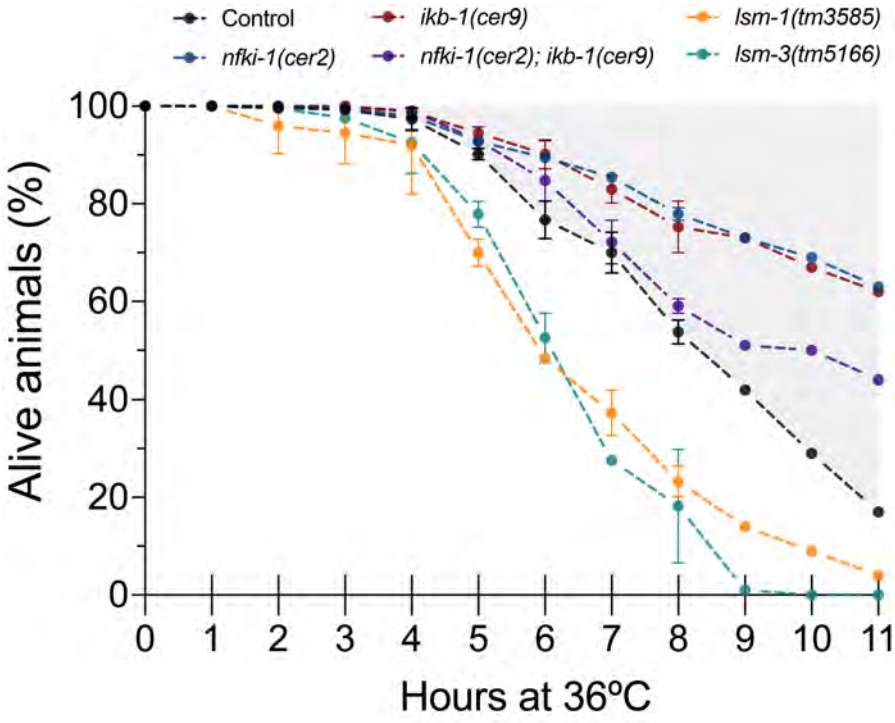

Figure R16. *nfki-1* and *ikb-1* mutants are resistant to thermal stress. Survival curves of the indicated nematode genotypes growing under high temperature (36ºC) stress. Mutants for the stress proteins LSM-1 and LSM-3, sensitive to thermal stress, were used controls (Cornes et al., 2015). N>100 animals per timepoint. N=2. Error bars and points show the mean of 2 experiments. Statistically significant differences between control and *nfki-1* and *ikb-1* mutants were calculated using two-tailed Spearman correlation test (CI: 95%).

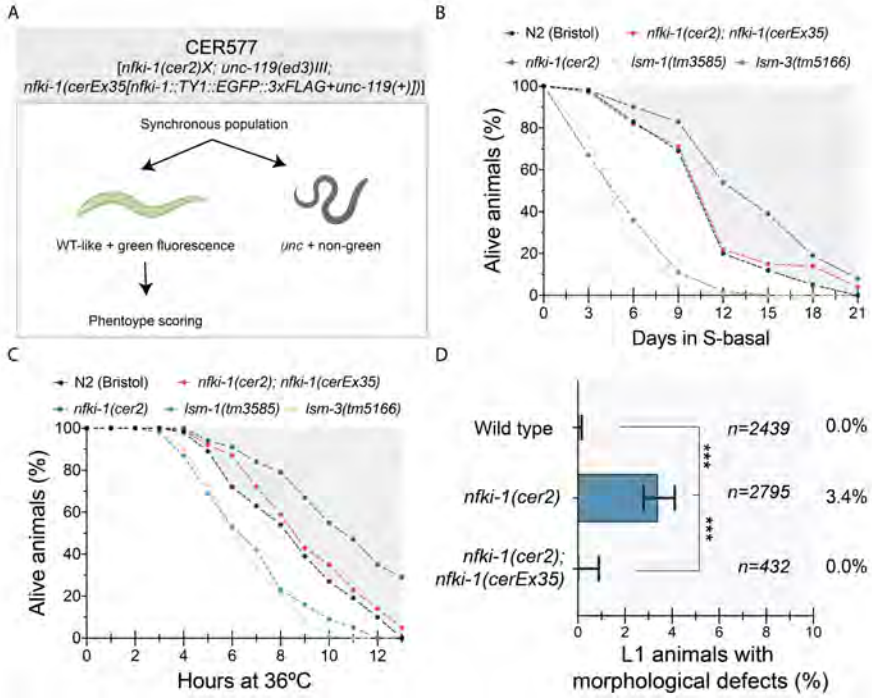

Figure R17. Over-expression of *nfki-1* rescues *nfki-1(cer2)* mutant phenotypes. (A) Experimental design of the phenotype scoring using the CER577 strain. We manually selected the green fluorescent, wild type-like (WT-like) animals and discarded the ones that presented a detectable uncoordinated (Unc) phenotype, when possible. (B) Survival curves of the indicated nematode genotypes growing under nutrient restriction. n>20 animals per timepoint. N=1. Statistically significant differences between control and *nfki-1* and *ikb-1* mutants were calculated using two-tailed Spearman correlation test (CI: 95%). (C) Survival curves of the indicated nematode genotypes growing under high temperature (36ºC) stress. n>20 animals per timepoint. N=1. Statistically significant differences between control and *nfki-1* and *ikb-1* mutants were calculated using two-tailed Spearman correlation test (CI: 95%). (D) Graph indicates the percent of larvae with aberrant morphology, which is rescued with the extrachromosomal over-expression line in *nfki-1* mutant background. *n>400.* N=1. Error bars show upper and lower limits of 95% confidence intervals (CI) calculated by Wilson/Brown method of 1 experiment. Statistically significant differences were calculated using two-sided Chi-square test (CI: 95%).

R3.3. *nfki-1* and *ikb-1* mutants phenocopy the developmental defects of Polycomb and Hox mutants

Since we were primarily interested in exploring nuclear and NF-κB-independent functions of IκB proteins, particularly in the regulation of PRC2, we looked further for phenotypes associated with alterations in Polycomb function. Remarkably, by a careful microscopic examination, we found that a low but significant percentage of *nfki-1(cer2)* and *ikb-1(cer9)* mutants displayed severe morphological defects that were initially overlooked with the stereomicroscope (**Figure R18**). To confirm that the low penetrance defects were caused by IκB mutants, we performed three additional experiments: *(i)* we rescued the *nfki-1(cer2)* phenotype with a single copy of *nfki-1* inserted into another chromosome (Chen et al., 2017) (**Figure R18**, MosSCI rescue), *(ii)* we evaluated the over-expression extrachromosomal line in an *nfki-1(cer2)* mutant background (**Figure R17D**), and *(iii)* we produced another *nfki-1* allele (*cer163)*, removing the whole *nfki-1* coding sequence (**Figure R19A**), observing similar morphological defects (**Figure R19B**). Importantly, these defects are similar to those observed in mutants of Hox genes (Van Auken et al., 2000, 2002; Zhao et al., 2010) or in Polycomb mutants (Capowski et al., 1991).

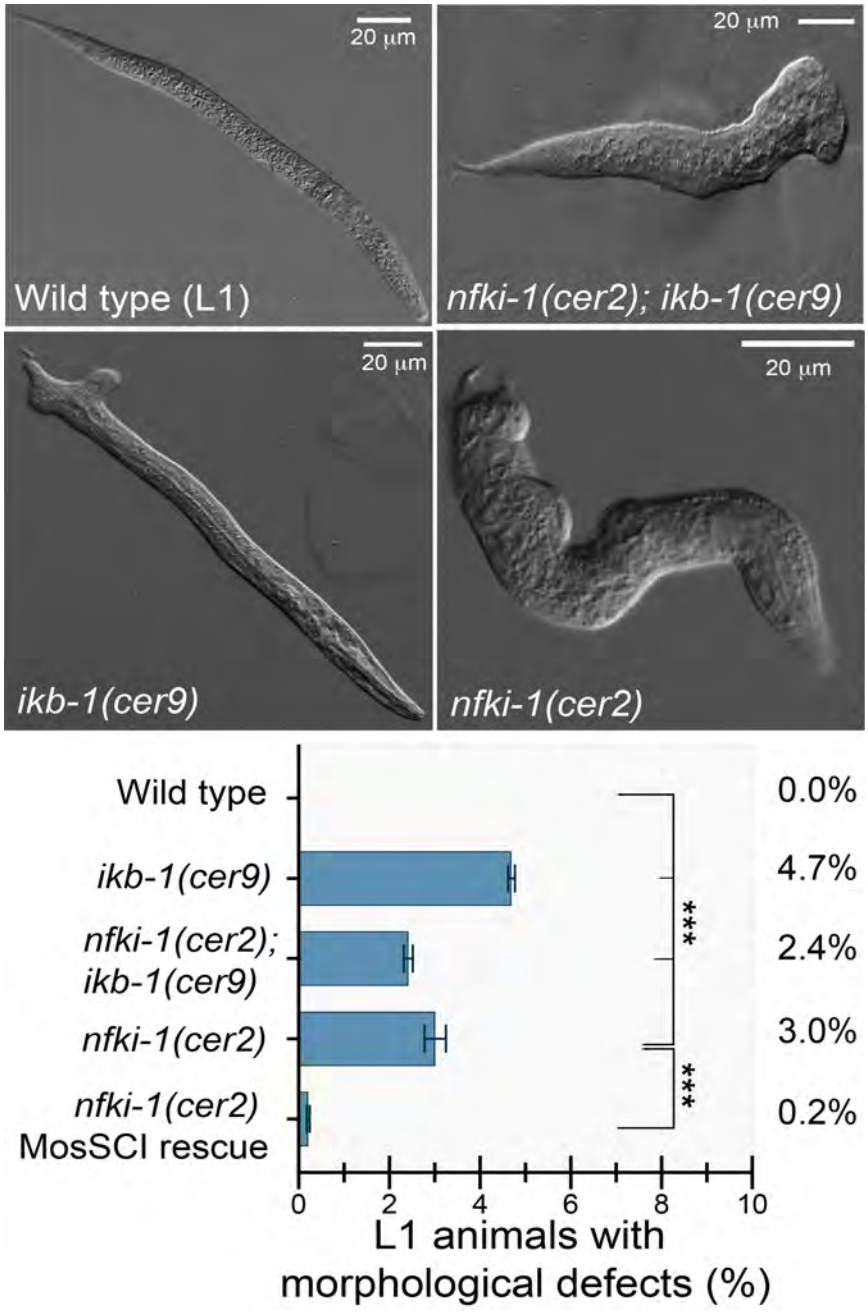

Figure R18. Morphological defects. DIC images showing the different morphological defects observed in *nfki-1* mutant animals. Scale bars: 20 µm. The graph indicates the percentage of larvae with an aberrant morphology, which is rescued after *nfki-1* wild-type copy insertion by

MosSCI in chromosome II (Chen et al., 2017) (MosSCI[*unc-119*(+); *nfki-1p::nfki-1::unc-54* 3'UTR]). *n>3000.* N=2. Error bars show SD of 2 experiments. Statistically significant differences were calculated using two-sided Chi-square test (CI: 95%).

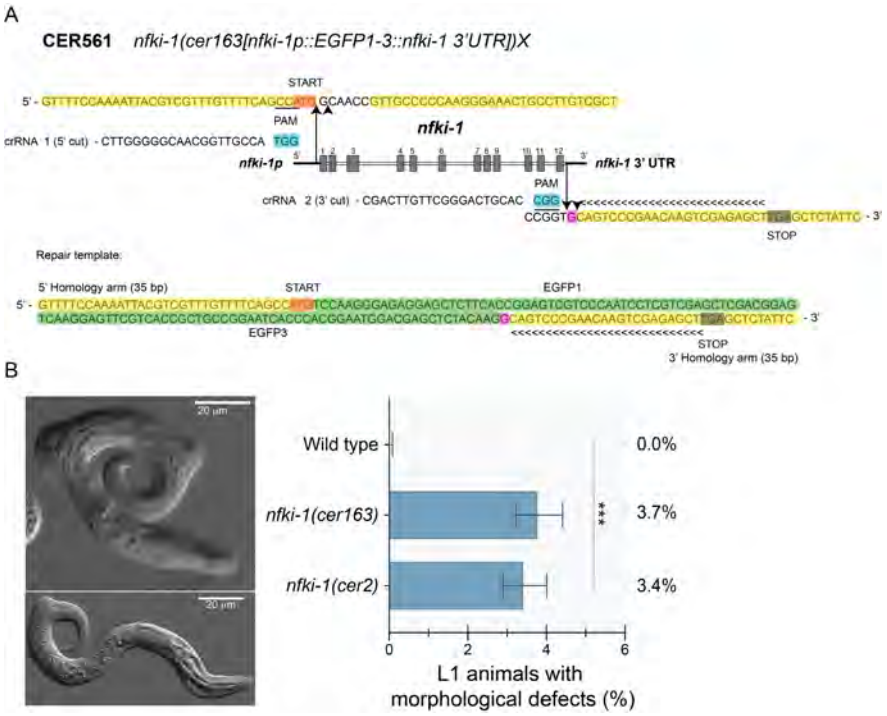

Figure R19. nfki-1 whole coding sequence deletion allele present morphological defects. (A) Schematic representation of whole gene deletion mutant strain CER561: *nfki-1(cer163[nfki-1p::EGFP1-3::nfki-1 3'UTR])* X by CRISPR-Cas9. Generation included the use of 2 crRNAs, one near the start codon (in orange) and the other near the stop codon (in brown). Protospacer adjacent motif (PAM) sequences are depicted in blue and underlined in the sequences. 35 nt-homology arms are highlighted in yellow. Chevron signs indicate *nfki-1*'s CDS last 23 nucleotides, we inserted an additional nucleotide to ensure the preservation of the frame (highlighted in pink). Black arrowheads depict the Cas9 cut site and black arrows show the insertion/deletion site. Full sequence of the repair template is displayed at the bottom. We included the flanking regions of an EGFP in the repair template (termed EGFP1 and EGFP3, respectively, highlighted in green), to facilitate a subsequent generation of a transcriptional reporter by Nested CRISPR methodology (Vicencio et al., 2019). (B) Representative DIC images showing morphological defects observed in *nfki-1(cer163)* mutant animals. Scale bars: 20 µm. The graph indicates the percent of larvae with aberrant morphology, which is similar to the percentage observed with *nfki-*

1(cer2) allele. *n>3500.* N=1. Error bars show upper and lower limits of 95% confidence intervals (CI) calculated by Wilson/Brown method of 1 experiment. Statistically significant differences were calculated using two-sided Chi-square test (CI: 95%).

We also observed consistent defects in gonad migration of *nfki-1(cer2)* and *ikb-1(cer9)* mutant animals, which are analogous to those found upon RNAi depletion of the H3K27 demethylase gene *utx-1* (**Figure R20**) (Vandamme et al., 2012), which has been reported to antagonize Polycomb function (Siebold et al., 2010). An aberrant gonad migration could be the consequence of a defect in the cell fate specification of the DTC, which is a somatic cell that controls the migration of the gonad (Wong and Schwarzbauer, 2012). Since single cell transcriptomics of *C. elegans* larvae indicate the expression of *nfki-1* and *ikb-1* in DTCs, we studied the cellular differentiation of DTCs by using the marker LAG-2::GFP and found that a small percentage of animals displayed an aberrant number of DTCs (mostly one DTC instead of two) (**Figure R21**). This result suggests that the aberrant gonad migration phenotype observed in *nfki-1* and *ikb-1* mutants could be due to defects in specification or differentiation of the DTCs. Of note, a double mutant strain for *nfki-1* and *ikb-1* did not increase the phenotype, suggesting that these genes may act in the same genetic pathway.

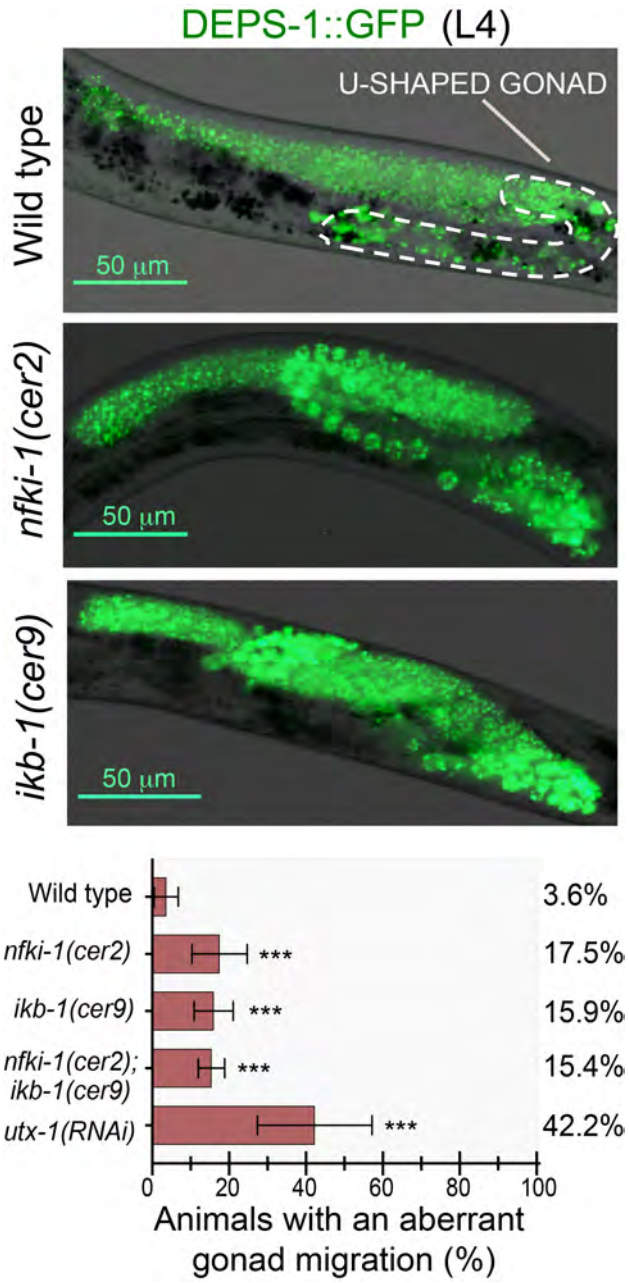

Figure R20. *nfki-1* and *ikb-1* mutants present an aberrant gonad migration. Representative microscopy images of wild type and *nfki-1(cer2)* displaying gonad migration defects by using the germline endogenous marker DEPS-1::GFP in L4 stage. The dashed white line depicts the distinctive U-shaped normal gonad morphology, which is disrupted by an aberrant migration in mutants. Scale bar: 50 μm. Graph shows the percentage of animals with an aberrant gonad migration phenotype. n>60.

N=3. Error bars show SD of 3 experiments. Statistically significant differences compared to wild type were calculated using two-sided Chi-square test (CI: 95%).

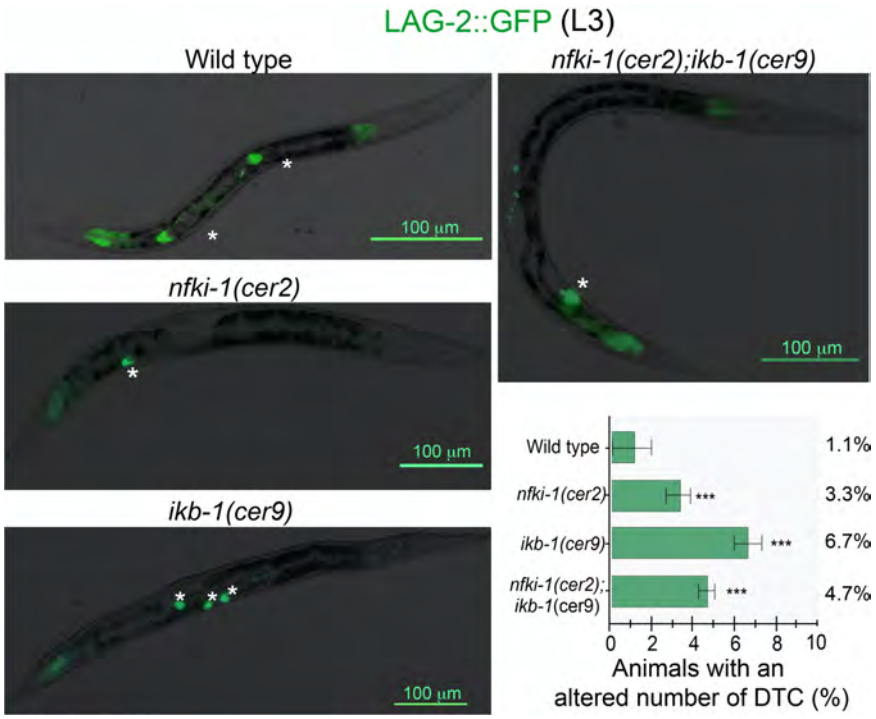

Figure R21. *nfki-1* and *ikb-1* mutants display an abnormal number of distal tip cells. Alterations in distal tip cells (DTCs) were visualized using the LAG-2::GFP reporter line in L3 stage. Note the presence of two DTCs in the WT and a variable number of DTCs in the mutants (white asterisks). Scale bars: 100 µm. Graph displays the percentage of animals with an abnormal DTC number. n>1000. N=3. Error bars show SD of 3 experiments. Statistically significant differences compared to wild type were calculated using two-sided Chi-square test (CI: 95%).

R3.4. *nfki-1 and ikb-1* mutants act independently of H3K27 remodelers *utx-1, jmjd.3,1 and cbp-1*

To test if *nfki-1* or *ikb-1* genetically interact with *utx-1*, we performed *utx-1(RNAi)* in wild type and IκB mutants. We included *jmjd-3.1(RNAi)* as it is another H3K27 demethylase,

which mutants are also associated to an aberrant gonad migration (Agger et al., 2007; Vandamme et al., 2012). We found that *utx-1* and *jmjd-3.1* show an additive effect on IκB single and double mutants, suggesting that they act in a different genetic pathway (**Figure R22**). We also tested for genetic interaction with *cbp-1*/P300, which encodes a conserved histone acetyltransferase that antagonizes Polycomb activity in *Drosophila* (Tie et al., 2016), and was found as a physical interactor of NFKI-1 in a nuclear fractionation experiment of *C. elegans* cells (Flynn et al., 2019). *cbp-1(RNAi)* produced a low percentage of embryonic lethality that did not significantly vary on *nfki-1(cer2)* and *ikb-1(cer9)* backgrounds (**Figure R23**).

Altogether, our results suggest an ancestral role for IκB proteins regulating *C. elegans* development, probably through modulation of Polycomb activity, that impacts on the differentiation state of specific cells during development. To study such function from a molecular mechanistic approach would be challenging since the nuclear proportion of IκB homologs at physiological levels is low and the observed phenotypes occur in a single pair of cells (DTCs) or at very low penetrance (L1 morphological defects). Nevertheless, we performed additional experiments to investigate their general role in the nucleus.

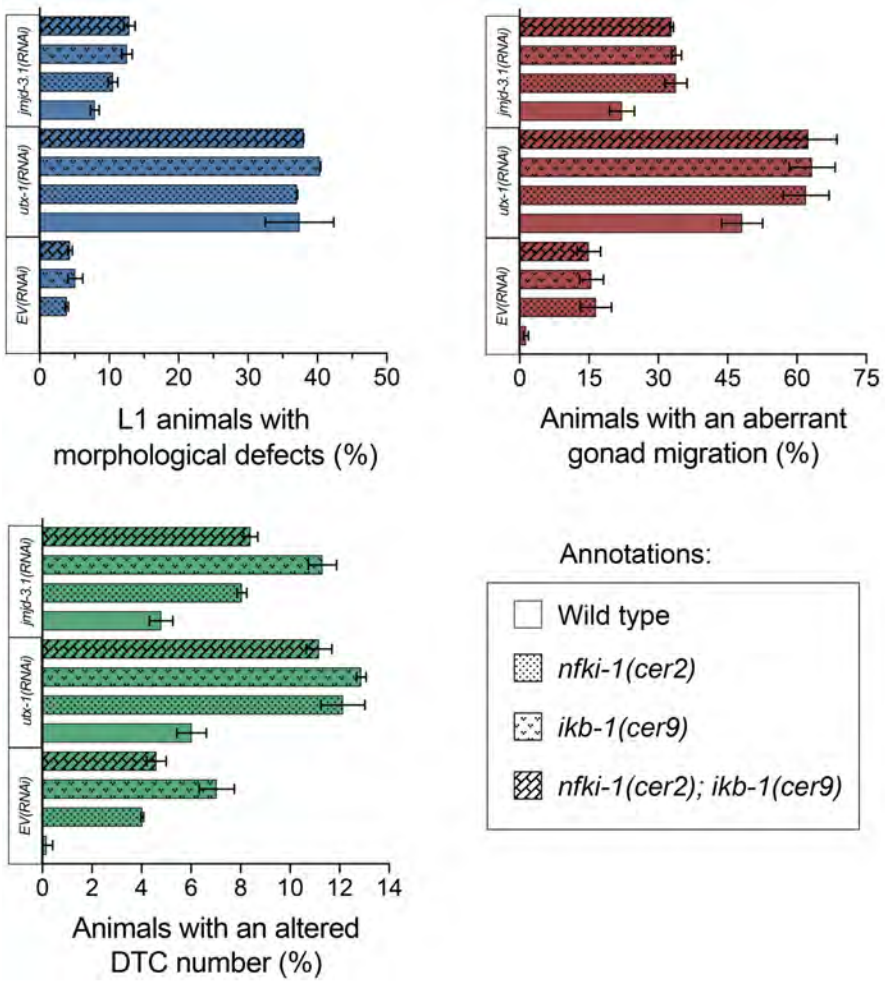

Figure R22. *nfki-1(cer2)* and *ikb-1(cer9)* are not epistatic with *utx-1(RNAi)* and *jmjd-3.1(RNAi).* The graphs depict the percentage of animals presenting the described phenotypes upon RNAi depletion of empty vector *EV(RNAi), utx-1(RNAi)* and *jmjd-3.1(RNAi)* in wild-type and IκB-deficient genetic backgrounds. n>400 for morphological defects assay. n>70 for gonad migration assay. n>100 for DTC number assay. N=2 for the three different experiments. Error bars show SD of 2 experiments.

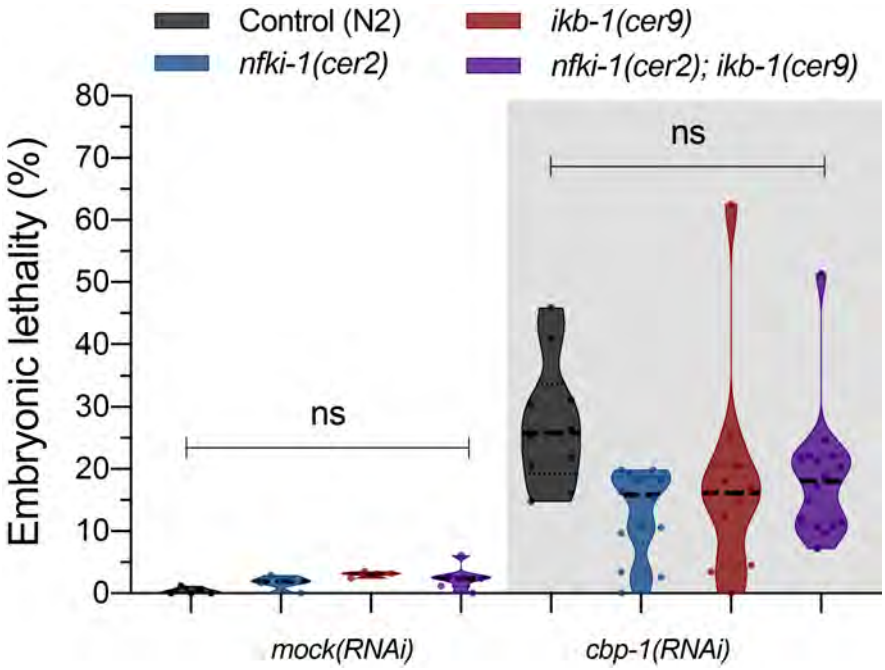

Figure R23. *nfki-1* and *ikb-1* do not genetically interact with *cbp-1(RNAi)* regulating embryonic lethality. Violin plots depicting the percentage of embryonic lethality upon RNAi depletion of *cbp-1* in a wild-type or IκB-deficient genetic background. Each point represents a single animal. Black dashed lines indicate the median and colored dashed lines show the interquartiles. n>4. N=1.

R4. NFKI-1 and IKB-1 role in the nucleus

R4.1. Endogenous NFKI-1 and IKB-1 bind chromatin *in vivo*

In mammalian cells, the association of IκBα to chromatin have been proved crucial to describe its nuclear functions (Mulero et al., 2013). Our collaborators found a physical interaction of NFKI-1 and IKB-1 with histones and the elements of the PRC2, MES-2, MES-3 and MES-6 *in vitro* (**Annex R2**).

In order to identify if NFKI-1 and IKB-1 interact with chromatin *in vivo* under physiological conditions, we performed chromatin immunoprecipitation followed by sequencing (ChIP-seq) in a strain containing 3xFLAG::NFKI-1 and IKB-1::mCHERRY endogenous tags at L1 stage. As a result, we detected NFKI-1 ChIP peaks linked to 127 genes, and 208 genes in the case of IKB-1. Interestingly, both proteins shared ChIP peaks in 39 genes (13.18%) (**Figure R24A**). Targets primarily localized in the promoter regions of genes and were similarly distributed among chromosomes (**Figure R24B and R24C**). Altogether, we demonstrated that NFKI-1 and IKB-1 have the capacity to bind chromatin *in vivo*.

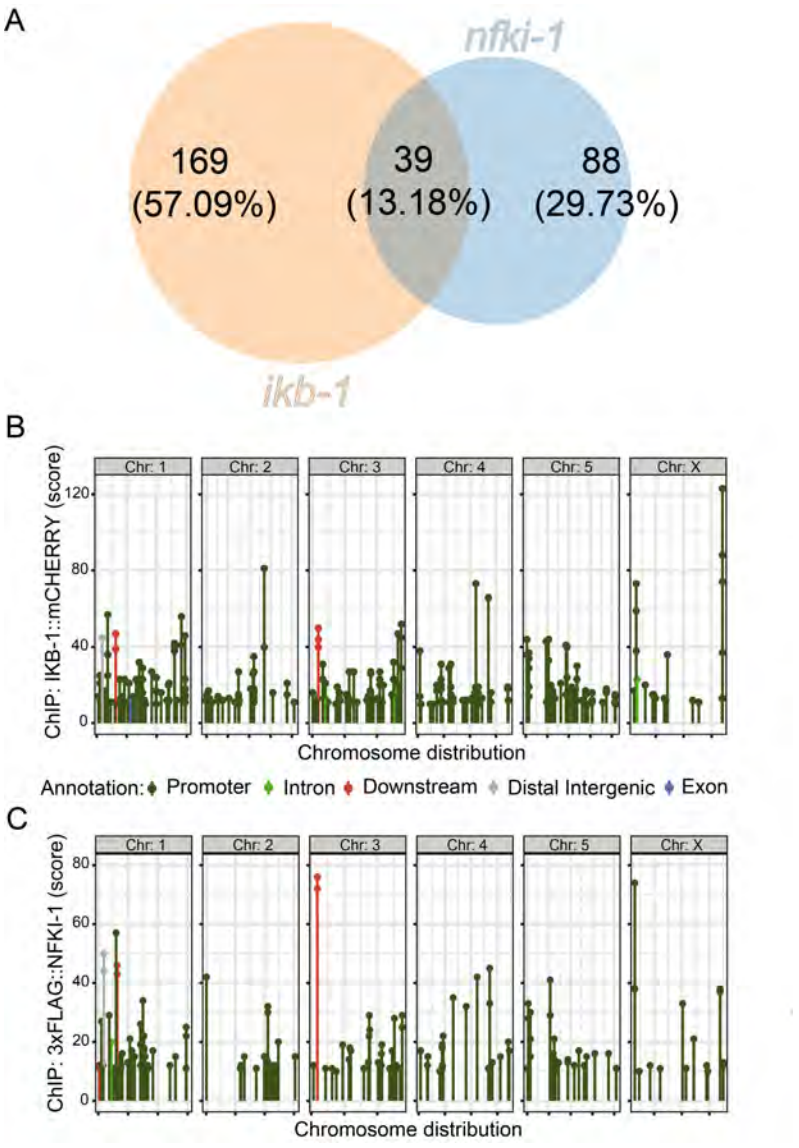

Figure R24. ChIP-seq of endogenous NFKI-1 and IKB-1. (A) Venn diagram showing the peaks overlap from 3xFLAG::NFKI-1 and IKB-1::mCHERRY ChIP-seq. (B-C) Distribution of peaks from IKB-1 (B) and NFKI-1 (C) ChIP-seq across *C. elegans* chromosomes, indicating the localization of the peaks relative to the closest annotated gene. Data are presented relative to input. ChIP-seqs were performed at L1 larval stage in the CER425: *ikb-1(syb267[ikb-1::mCherry])* I;*nfki-1(cer102[nfki-1::3xFLAG])]* X strain and N2 as wild type control.

R4.2. A common subset of genes is deregulated in *nfki-1* and *ikb-1* mutant transcriptomes

To investigate the function of *nfki-1* and *ikb-1* at the transcriptomic level, we performed RNA-seq of synchronized single and double mutant animals at L4 larval stage. *nfki-1(cer1)* and *ikb-1(nr2027)* mutant animals showed 2534 (1777 upregulated and 757 downregulated) and 2090 (1590 upregulated and 500 downregulated) differentially expressed genes (DEGs) compared to wild-type transcriptomes (considering about 16,000 coding sequences detected), respectively (adjusted p-value < 0.01, $\log_2$ fold-change ≥ 2). Interestingly, 1899 genes (69.69%) were common for both datasets (**Figure R25A**) and their fold-change expression values were highly correlated (**Figure R25B**) (R=0.947, p-value < 2.2e-16, Spearman test). This result strongly suggests that *nfki-1* and *ikb-1* could have similar functions regulating gene expression.

We also compared the single mutant datasets with the double mutants and found that 758 genes (25.86%) were common for all datasets (**Figure R26A**). By a tridimensional representation of the expression values of the differentially expressed genes, we found that *nfki-1* and *ikb-1* mutants also correlate (**Figure R26B**).

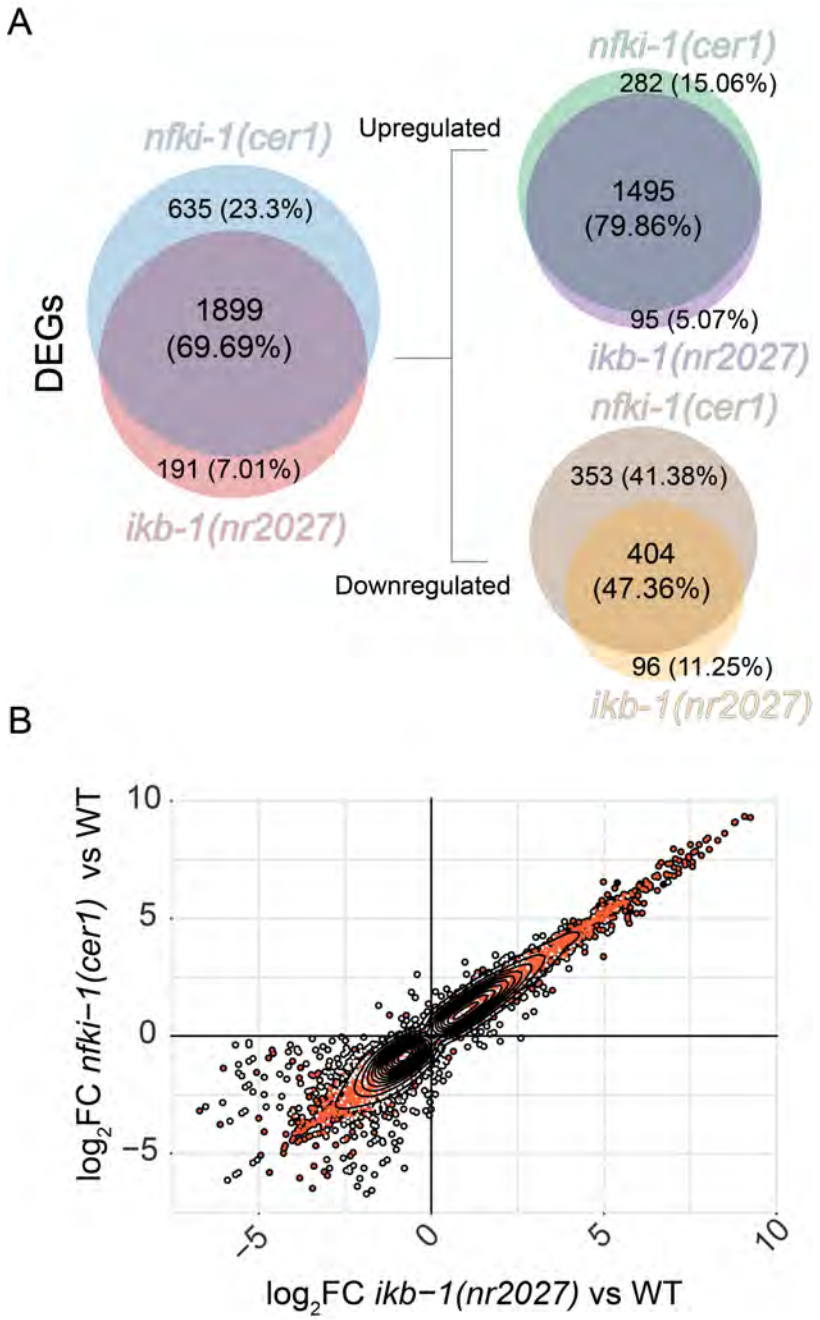

Figure R25. *nfki-1* and *ikb-1* mutants deregulate a common subset of genes. (A) Venn diagrams showing the overlap between *nfki-1(cer1)* and *ikb-1(nr2027)* datasets. Results are displayed for DEGs as for upregulated and downregulated genes independently. Upregulated genes show the

most prominent overlap with 1495 genes (79.86%). (B) 2D plot illustrating the correlation between log_2 fold change of differentially expressed genes in *ikb-1* and *nfki-1* deficient animals. RNA-seqs were performed in L4 synchronous populations of the strains CER178: *nfki-1(cer1)* X and CER185: *ikb-1(nr2027)* I.

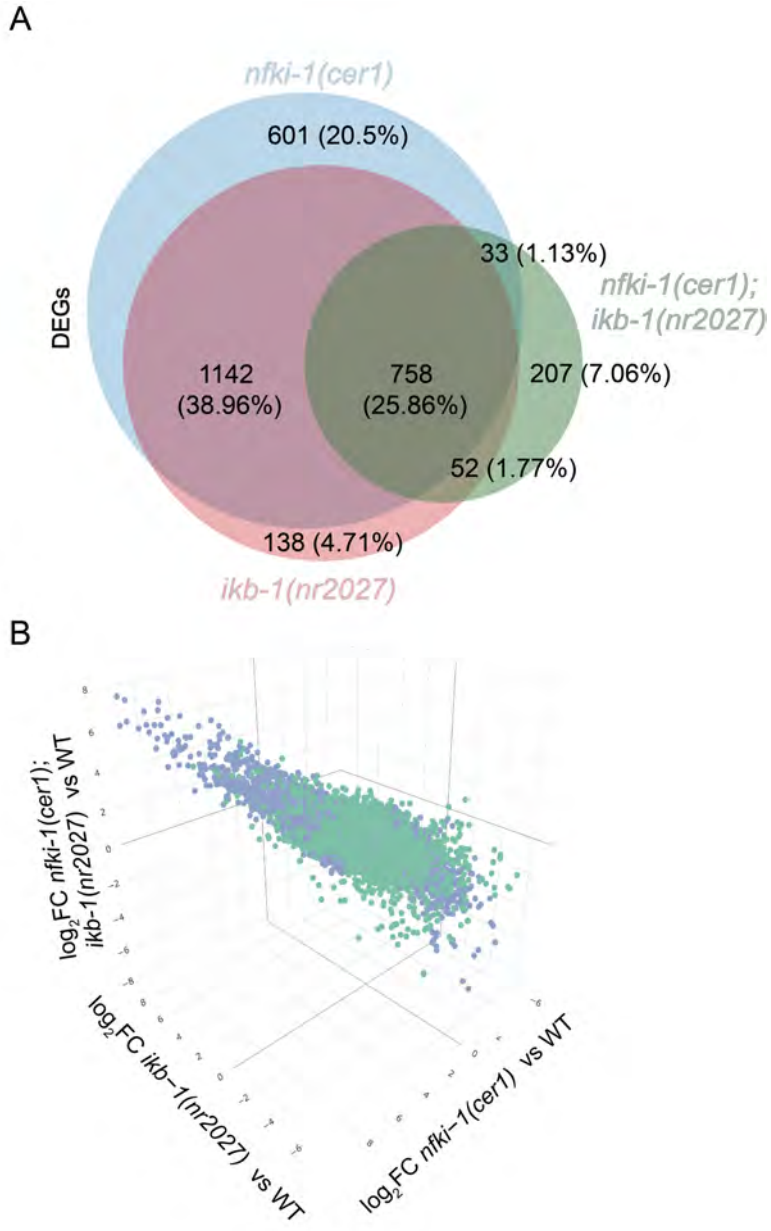

Figure R26. Common deregulation of genes in single and double *nfki-1* and *ikb-1* mutants. (A) Venn diagrams showing the overlap between *nfki-1(cer1)*, *ikb-1(nr2027)* and double mutant datasets. (B) 3D plot illustrating the correlation between genes differentially expressed in the three datasets. DEGs for individual *nfki-1(cer1)* and *ikb-1(nr2027)* are represented in blue, and green for the double mutants. RNA-seqs were performed in L4 synchronous populations of the strains CER178: *nfki-1(cer1)* X, CER185: *ikb-1(nr2027)* I and CER188: *ikb-1(nr2027) I; nfki-1(cer1)* X.

R4.3. *nfki-1* and *ikb-1* mutant transcriptomes display an enrichment in upregulated germline genes at L4 stage but not a repression in germline-specific genes

Exploring further the transcriptomic changes detected in the RNA-seq analyses at L4 stage, we noted a remarkable presence of several canonical germline genes among the upregulated genes, considering that *nfki-1* and *ikb-1* are not expressed in the germline. To study this observation, we classified DEGs according to their expression as ubiquitous, germline-specific, germline-enriched, soma-specific, or unclassified (list of genes retrieved from Gaydos *et al*., 2012). We confirmed a clear enrichment in germline genes among upregulated genes in both *nfki-1(cer1)* and *ikb-1(nr2027)* mutants (**Figure R27**). This result could mean that NFKI-1 and IKB-1 repress these germline genes in somatic cells, and thus have a role in soma *vs* germline cell fate regulation. To further explore that possibility, we built strains containing *nfki-1(cer2)* or *ikb-1(cer9)*, and endogenous fluorescent reporters of germline genes that appeared upregulated in our datasets.

However, none of the examined *pgl-1::mCherry* reporters presented an ectopic expression specific to a IκB-deficient background (**Figure R28**). This result is comparable to the other endogenous germline markers that we observed: *deps-1::gfp* and *mex-6::gfp* (data not shown). Unexpectedly, endogenous PGL-1::mCHERRY reporter displayed an ubiquitous expression at L1 developmental stage rather than being restricted to the two primordial germ cells (PGCs). However, that expression pattern was independent of the IκB-deficient genetic background as it did not vary compared to wild type, even in low penetrance morphologically defective animals (**Figure R28**).

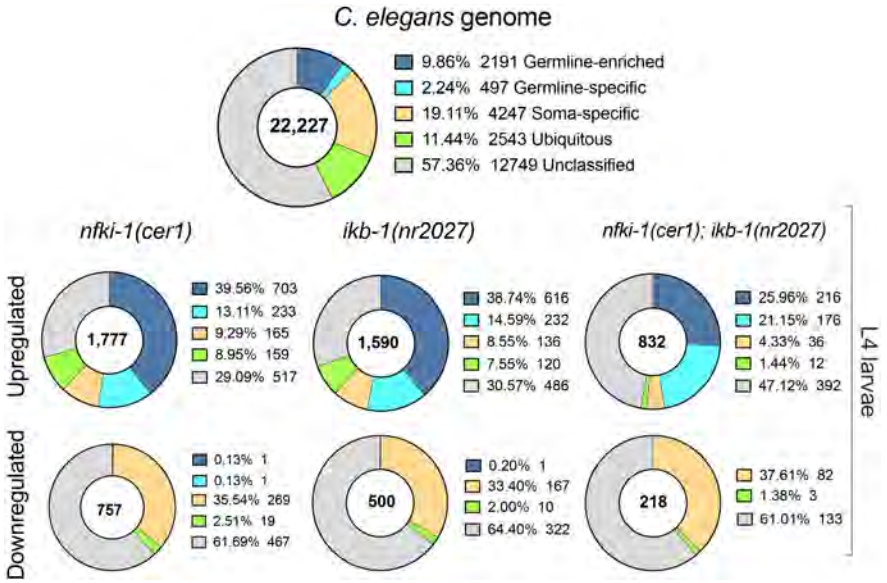

Figure R27. Upregulated genes for *nfki-1* and *ikb-1* mutants show an enrichment in germline genes. Doughnut charts showing the distribution of genes according to whether their expression is germline-enriched (dark blue), germline-specific (light blue), soma-specific (yellow), ubiquitous (green), or unclassified (gray) for differentially expressed genes at L4.

Number in the center of circles indicates the number of genes for each dataset. Categories dataset was extracted from Gaydos *et al.*, 2012. Statistically significant differences between expected and observed distribution was calculated using Chi-square test for goodness of fit ($p<0.05$).

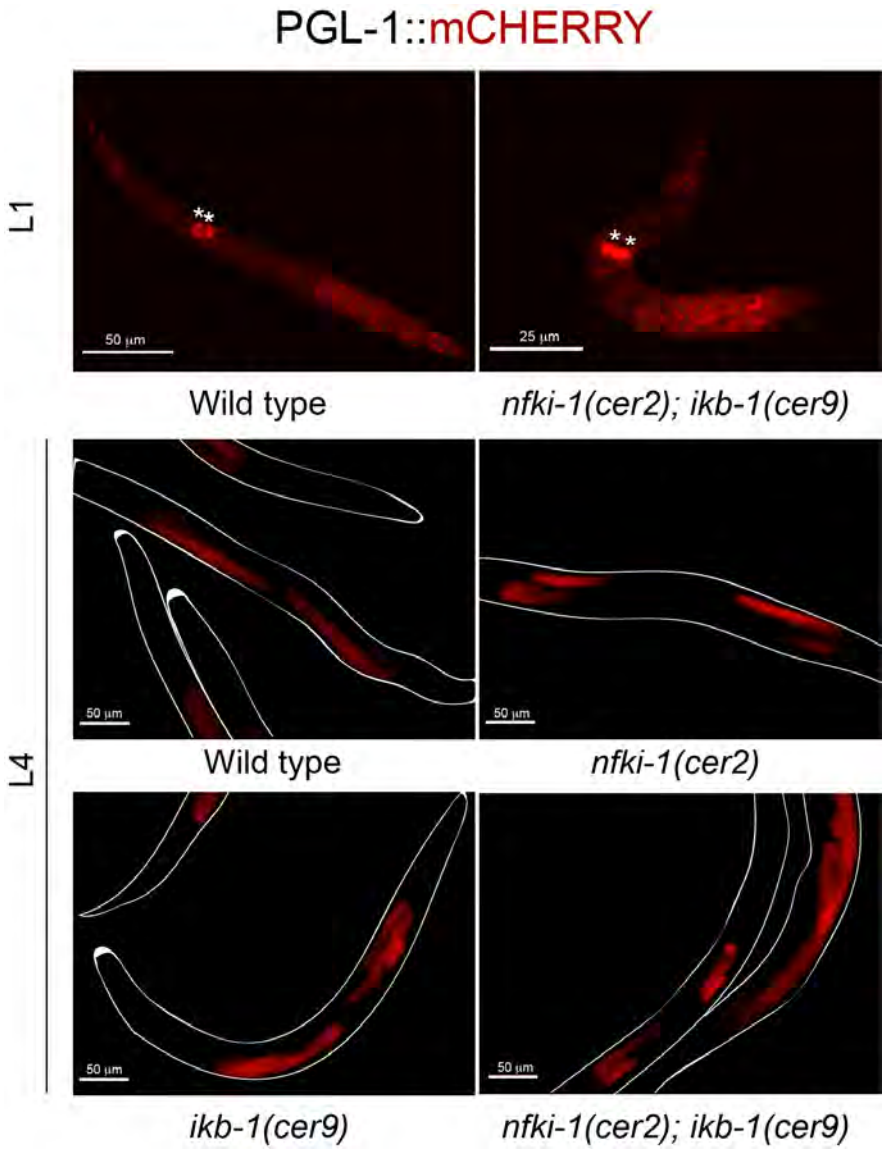

Figure R28. IκB-deficiency does not provoke ectopic expression of germline reporter. Fluorescence microscopy images of either a wild type or an animal with morphological defects in an IκB-deficient genetic

background of an endogenous *pgl-1::mCherry* reporter strain: CER415: *pgl-1(cer71[pgl-1::mCherry])* IV. Expression of PGL-1::mCHERRY is higher at PGCs (indicated by white asterisks) but also present in several somatic cells. Expression is constantly restricted during development and at L4 is clearly located only in germline cells. We observed no ectopic expression in any of the IκB mutants.

R4.4. Transcriptional regulation imposed by *nfki-1* and *ikb-1* mutants during post-embryonic development is higher at L4 stage

As ectopic expression of endogenous germline reporters was not observed in IκB mutants, we reasoned that such a prominent presence of germline-related genes could be due to an indirect effect of the absence of *nfki-1* and/or *ikb-1* and not because of a germline *vs* soma cell fate deregulation.

To shed light on this, we decided to perform an additional RNA-seq experiment at L1 developmental stage, since at that timing the germline is not fully developed and would be easier to distinguish somatic associated changes or confirm that there is a germline signature at different times of development. Additionally, we observed the morphological and starvation resistance phenotypes at that developmental stage, which would be indicative of activity of the proteins at that timing.

However, we found no significant enrichment in germline genes at L1 stage (**Figure R29A**), strengthening the hypothesis that the upregulation of germline genes identified at

L4 could be caused by indirect effects. Still, we were able to detect a correlation, albeit minor, between *nfki-1(cer2)* and *ikb-1(cer9)* DEGs at L1 (**Figure R29B-C**), supporting that both proteins play similar functions during post-embryonic development.

To compare our datasets at the two developmental stages, we performed Principal component analysis (PCA) of RNA-seq data, which clustered together L1 WT and IκB mutants, in contrast with L4 WT samples that were separated from *nfki-1* and *ikb-1* mutants, indicating that the influence of IκBs in the transcriptome is higher in L4 than in L1 stage (**Figure R30**).

The fact that we could only detect a germline signature at L4 stage and not earlier in development at L1 undermines the hypothesis that IκB homologs repress the expression of germline genes in somatic cells. However, considering that the DTCs and aberrant gonad migration defects are acquired between those time points, it is possible that such upregulation of germline genes would be associated to an imbalance in developmental timings. Specifically, we speculate about the possibility of *nfki-1* and *ikb-1* mutants having a more developed germline, compared with their somatic development since we did not observe a downregulation in *msp* (major sperm proteins) genes, which are a hallmark of the initiation of the L4 stage (L'Herault, 2007). However, this must be formally addressed in future experiments.

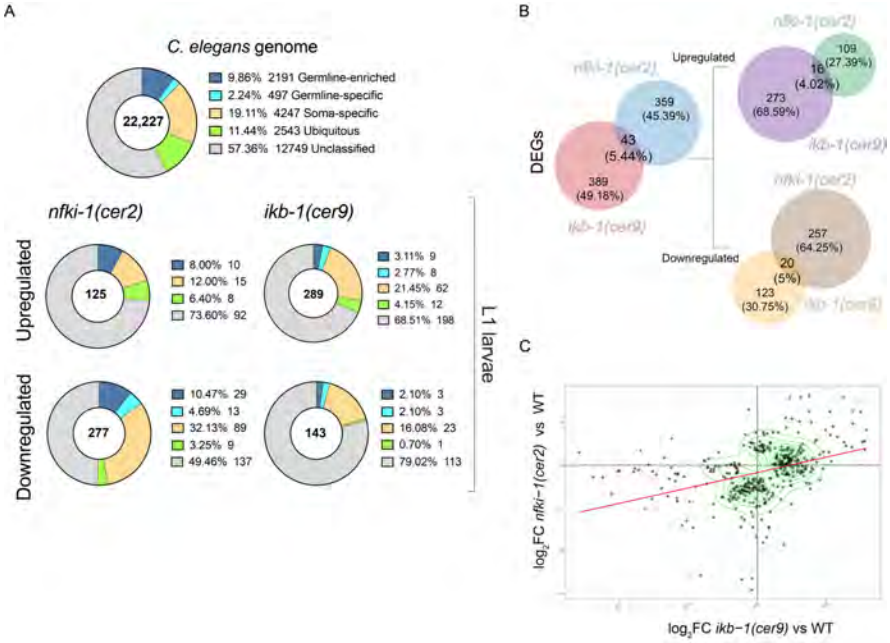

Figure R29. RNA-seq at L1 shows mild correlation between deregulated transcripts in nfki-1 and ikb-1 mutants. (A) Doughnut charts showing the distribution of differentially expressed genes at L1, as shown in Figure R27. Categories dataset was extracted from (Gaydos et al., 2012). Statistically significant differences between expected and observed distribution was calculated using Chi-square test for goodness of fit ($p<0.05$). (B) Venn diagrams showing the overlap between *nfki-1(cer2)* and *ikb-1(cer9)* datasets. (C) 2D plot illustrating the correlation between genes differentially expressed in *nfki-1* or *ikb-1* deficient animals and wild type animals. RNA-seqs were performed in L1 synchronous populations of the strains CER187: *nfki-1(cer2)* X, CER244: *ikb-1(cer9)* I, and N2 (wild type).

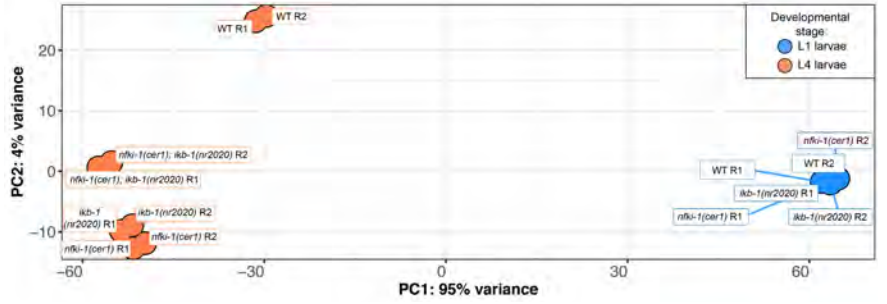

Figure R30. The influence of IκBs in the transcriptome seems to be higher in L4 than in L1. PCA analysis of RNA-seq samples at L4 (orange) and L1 (blue) for wild type (WT) and *nfki-1* and *ikb-1* mutants. 'R' denotes each replicate.

R4.5. Transcriptomic signature comparison with IL-17 mutants revealed non-overlapping functions that are relevant for development

NFKI-1 and IKB-1 functions have been associated to cytokine signaling pathways as the IL-17 signaling pathway in the case of *nfki-1* (Chen et al., 2017), and the Toll-like signaling pathway mediated by TOL-1, which is the only homolog of Toll in *C. elegans*, in the case of *ikb-1* (Pujol et al., 2001). Importantly, a recent report confirmed that NFKI-1 acts as part of a cytoplasmic complex composed by MALT-1/MALT1, ACTL-1/Act1 and PIK-1/IRAK, and acts downstream of the ILC-17.1 receptor (Flynn et al., 2020). This study generated RNA-seq profiles of mutants of *malt-1(db1194), ilc-17.1(tm5218)* and *nfki-1(db1198)* performed at late L4 stage (Flynn et al., 2020).

We compared our RNA-seq datasets at L4 stage with IL-17 mutants from Flynn *et al.*, 2020 and we found that all datasets shared gene subsets for upregulated and downregulated genes (**Figure R31A and B**). Since we wanted to discern between nuclear and cytoplasmatic roles, we focused on the subset of genes that were shared between *nfki-1(cer1), ikb-1(nr2027),* and *nfki-1(db1198)*, and were not in common with deregulated genes from *malt-1(db1194)* and *ilc-17.1(tm5218)*

(bolded in Venn diagrams of **Figure R31A and B**). To adjust the comparison, we excluded genes that display an oscillatory expression pattern (Hendriks et al., 2014), which was also performed in Flynn *et al.*, 2020 datasets, and found 201 upregulated genes and 101 downregulated genes meeting these criteria.

Next, an exploratory GO-term analysis using WormEnrichr (Kuleshov et al., 2019) suggested that upregulated genes were associated to categories that are relevant to neuronal functions and signal transduction pathways, such as different types of ion transport, and categories associated with protein phosphorylation and cell proliferation (**Figure R31C**). Interestingly, downregulated genes were enriched in categories that included regulation of DTC migration, cell fate specification and metabolic-related features (**Figure R31D**).

These results, even if exploratory, suggest that at least NFKI-1, but not excluding IKB-1, could have similar functions that are independent of their reported cytoplasmic interactors and that are relevant to different processes, including development and cell fate, particularly fitting with the DTC/gonad migration phenotype. Whether these functions occur in the cytoplasm as part of other signaling pathways or are associated to nuclear functions remains to be specifically addressed.

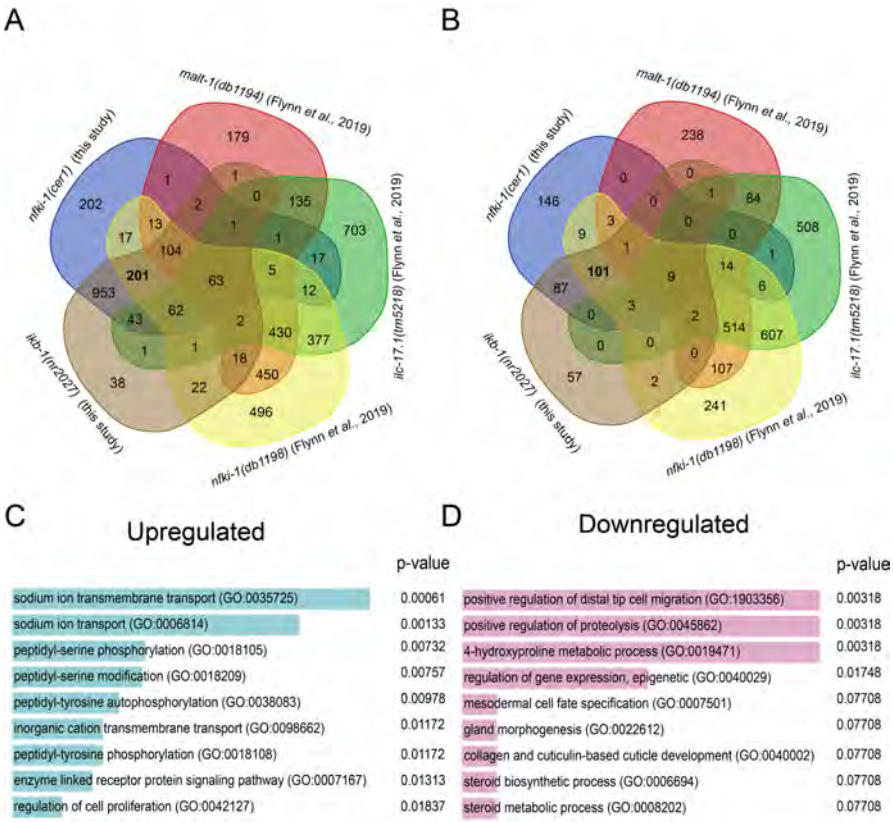

Figure R31. RNA-seq comparison with IL-17 mutants. (A, B) Venn diagrams showing the intersections between the mentioned datasets for upregulated (A) and downregulated (B) genes. Venn diagrams created with the webtool: http://bioinformatics.psb.ugent.be/webtools/Venn/ (C, D). GO-term analyses using WormEnrichr (Kuleshov et al., 2019) for the subset of genes that are in common in *nfki-1(cer1), ikb-1(nr2027),* and *nfki-1(db1198)* datasets and excluded from intersections on any of the other datasets, for upregulated (C) and downregulated (D) genes.

R4.6. IκB mutants display similar alterations in the deposition of H3K27me3 and H3K36me3 chromatin marks

To validate the possibility that NFKI-1 and IKB-1 exert specific functions in the chromatin of *C. elegans* cells, we performed

ChIP-seq experiments from the same worm extracts that were used for RNA-seq assays at L4 stage. It is worth noting that the amount of H3K27me3 in *nfki-1* and *ikb-1* mutants was comparable to wild type, as proved by Western blot analysis performed by our collaborators in the Espinosa-Bigas lab (IMIM, Barcelona) (**Annex R3**).

To know if the patterns of deposition were altered, we used specific antibodies for H3K27me3 and H3K36me3 chromatin marks, and found that the majority of the H3K27me3 (**Figure32A**) and H3K36me3 (**Figure 32B**) deposition was unaffected, but a meaningful percentage of the peaks were altered in an *nfki-1* or *ikb-1* mutant backgrounds.

Interestingly, differentially H3K27me3 marked peaks in *nfki-1* and *ikb-1* display a prominent overlap (56.66% of *nfki-1(cer1)*-specific peaks are present in *ikb-1(nr2027)*-specific dataset) compared to wild type. A gene ontology (GO) analysis of these 1691 differentially methylated genes that are in common using WormEnrichr (Kuleshov et al., 2019) showed epidermal cell differentiation [GO:0009913] and epidermal cell specification [GO:0009957] as well as categories related with metabolic processes as part of the most enriched categories in biological processes (**Figure R32C**). Similarly, differentially marked peaks for H3K36me3 were 48.74% overlapped between *nfki-1(cer1)* and *ikb-1(nr2027)* and GO term analysis included regulation of cell fate commitment [GO:0010453] and

regulation of cell fate specification [GO:0042659] as well as metabolic processes (**Figure R32D**). Such prominent overlaps suggest that NFKI-1 and IKB-1 influence gene expression regulating similarly the deposition of H3K27me3 mark. Moreover, the antagonistic nature of the H3K27me3 and H3K36me3 marks should involve changes in the deposition of H3K36me3, which we also observed (**Figure R32B)**.

These alterations in the deposition of chromatin marks prompted us to explore the possibility that the expression patterns in somatic cells of PRC2-related HMTs such as MES-2 and MES-4 (in charge of the deposition of H3K27me3 and H3K36me3, respectively) would be deregulated, however, we were not able to properly characterize clear differences in the expression with a *mes-2::GFP* and *mes-4::GFP* endogenous reporter strains in *nfki-1* and *ikb-1* mutant backgrounds (data not shown). In a similar approach, we crossed *nfki-1(cer2)* and *ikb-1(cer9)* single and double mutants with the HOX reporters *nob-1::GFP, mab-5::TY1::EGFP::3xFLAG, egl-5::GFP, egl-5::TY1::EGFP::3xFLAG,* and *lin-39::H1-wCherry* but we were not able to observe general qualitative differences compared with wild types (data not shown, performed by Kukhtar, D).

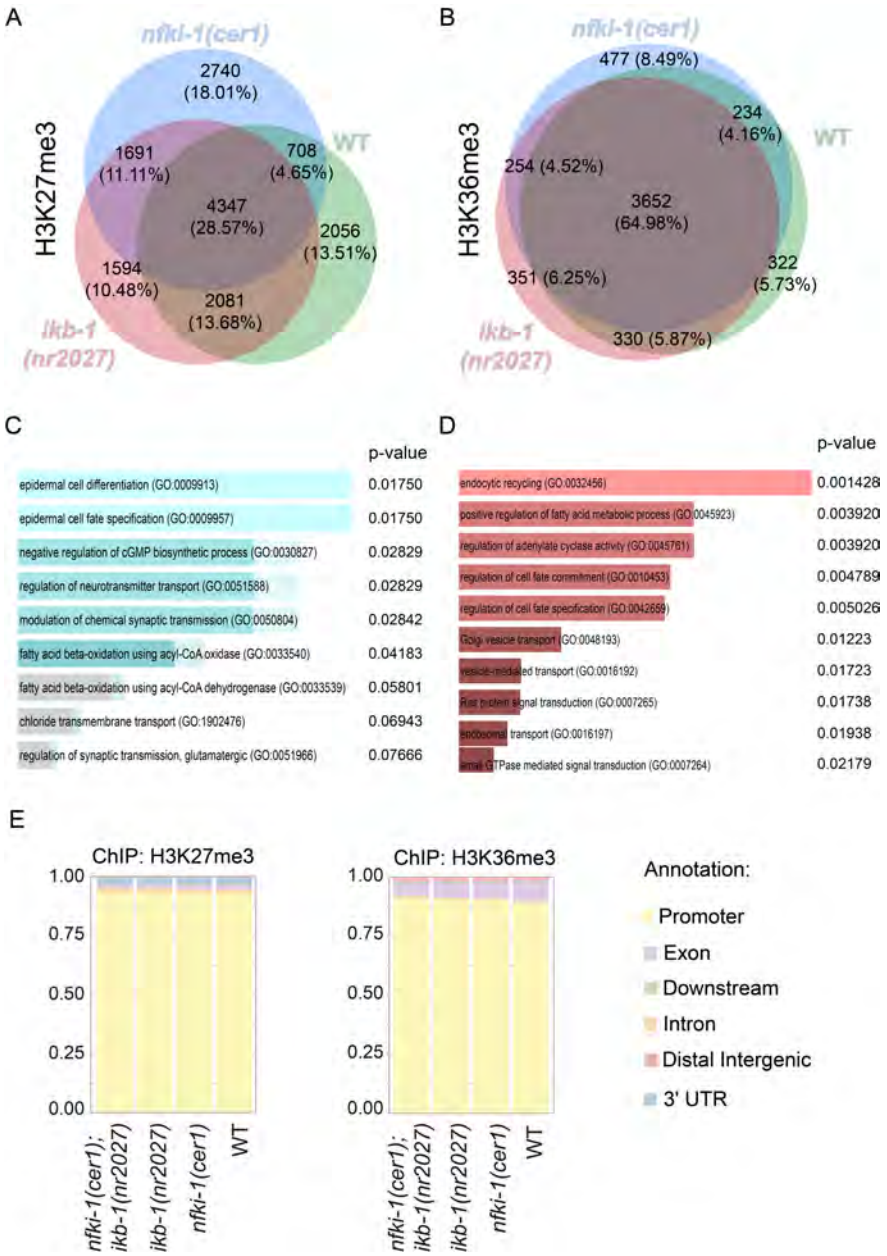

Figure R32. IκB-deficient animals show changes in H3K27me3 and H3K36me3 deposition. (A, B) Venn diagrams showing the proportions of mutant-specific peaks for each chromatin mark. For H3K27me3 (A) *nfki-1(cer1)* shows 2740 (18.01%) specific peaks and *ikb-1(nr2027)* 1594 (10.48%) differentially marked peaks. Similarly, for H3K36me3 (B) we found 477 (8.49%) peaks specific for *nfki-1(cer1)* and 254 (4.52%) for *ikb-1(nr2027).* (C, D) Bar graphs indicating GO analysis with the enriched biological processes in common differentially methylated genes for

H3K27me3 (C) and H3K36me3 (D) in IκB mutants. (E) Plots showing the relative distribution of H3K27me3 and H3K36me3 peaks relative to the closest annotated gene.

R4.7. Gene expression changes in IκB mutants correlate with alterations in chromatin marks

Exploring further the location of the ChIP-seq peaks, we found that most of them were located at promoter regions and displayed a similar distribution among the different IκB-deficient backgrounds (**Figure R32E**). Furthermore, a more detailed analysis of the data indicated that in soma-specific DEGs, the H3K27me3 mark was accumulated at the promoter and intronic regions of genes downregulated in *nfki-1(cer1)*, *ikb-1(nr2027)* and the double mutant, but randomly distributed in the non-differentially expressed group (non- DEG) of genes (**Figure R33A**). In germline genes, which are generally up-regulated in the mutants, both H3K27me3 and H3K36me3 marks were found only in promoter regions and presented a high accumulation of H3K36me3 mark (**Figure R33A and R33B**).

To investigate the extent at which NFKI-1 and IKB-1 regulate chromatin directly or indirectly, we asked if specific transcriptomic alterations corresponded to chromatin-bound regions by endogenous NFKI-1 and IKB-1, and performed chromatin immunoprecipitation followed by qPCR (ChIP-qPCR) in CER425: *ikb-1(syb267[ikb-1::mCherry])* I*; nfki-*

1(cer102[nfki-1::3xFLAG)]) X double endogenously tagged strain under the same growing conditions than the RNA-seq at L4.

Interestingly, we found that there is no general correlation in chromatin binding at the selected deregulated loci under endogenous conditions neither for NFKI-1 (**Figure R34A**) nor IKB-1 (**Figure R34B**), since all the selected DEGs for 3xFLAG::NFKI-1 do not show a significant enrichment in reporter ChIPed samples relative to wild type, and only half of the DEGs presented an enrichment for ChIPed IKB-1::mCHERRY.

This could indicate that the transcriptomic alterations at L4 stage are not directly regulated by IκB orthologs and thus more likely reflect the mean accumulated effect of deregulated networks that involve also a deregulation of chromatin marks (as shown by H3K27me3 and H3K36me3 ChIP-seqs), or that the signal is not sufficient to detect chromatin-bound loci due to the low nuclear proportion displayed by both proteins under endogenous conditions.

To answer this, we performed ChIP-qPCR on the NFKI-1::TY1::EGFP::3xFLAG over-expression strain, since we have previously observed that this condition strongly enhances the NFKI-1 nuclear proportion. As result, we found that NFKI-1 is indeed associated to ten randomly selected deregulated loci (**Figure R35**). These results support the notion that the lack of NFKI-1 leads to transcriptional changes and chromatin

alterations, some of which could be a consequence of deficiencies in its nuclear functions.

In summary, our results demonstrate an ancestral function of NFKI-1 and IKB-1 as regulators of the deposition of chromatin marks and the transcriptional activation of a subset of genes that ultimately have an impact in *C. elegans* development. To our knowledge, this is the first reported evidence of transcriptional regulation imposed by IκB homologues in the absence of a functional NF-κB pathway.

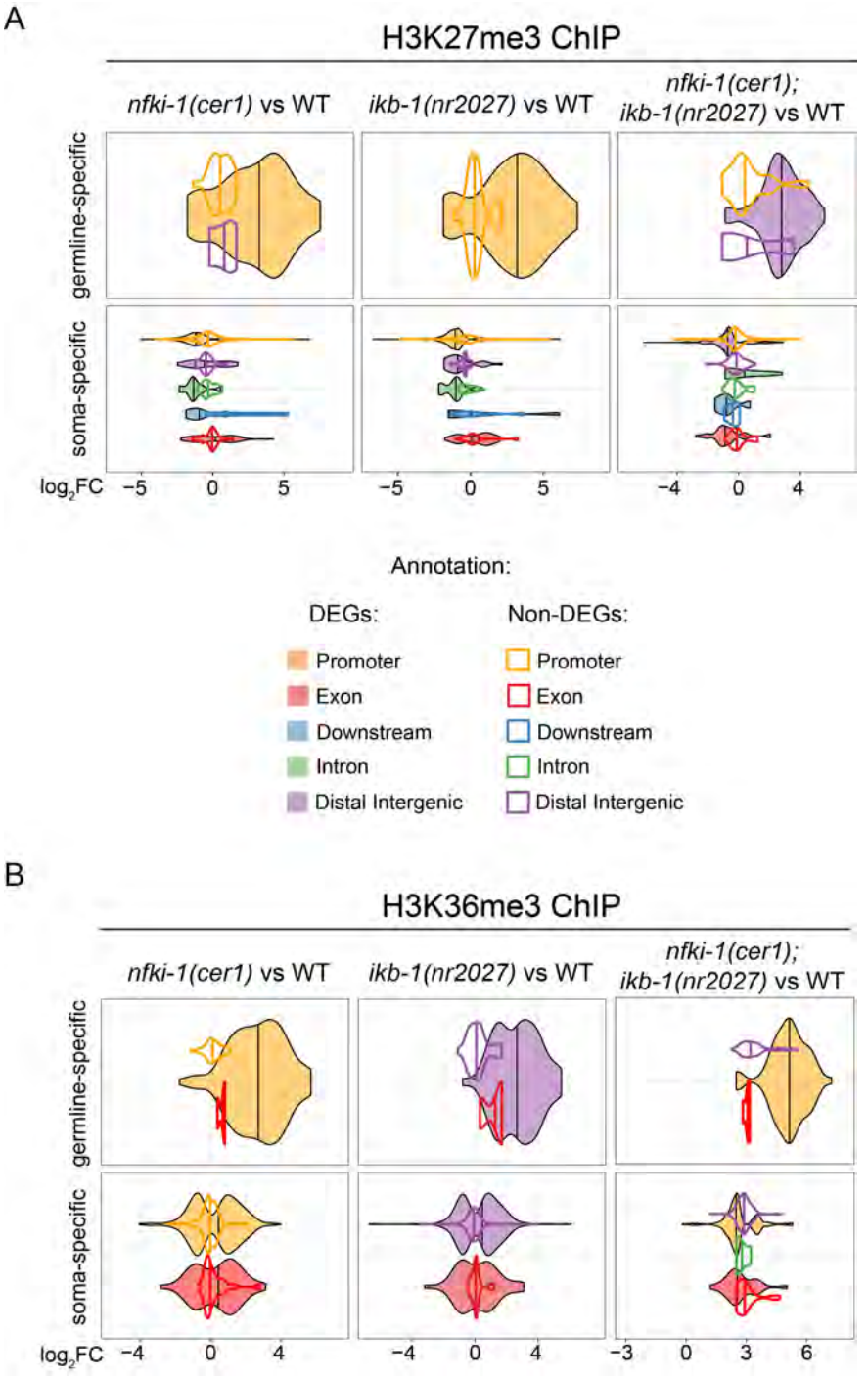

Figure R33. Differentially expressed genes are linked to changes in Polycomb-related chromatin marks. (A, B) Violin plots indicating the

density and distribution of H3K27me3 (A) and H3K36me3 (B) peaks at germline- and soma-specific genes differentially (color-filled/black lines) and not differentially (colored lines) expressed in the indicated genotypes (p-adj < 0.05). x-axis represents the expression levels (log2 fold-change) in mutants relative to the wild type.

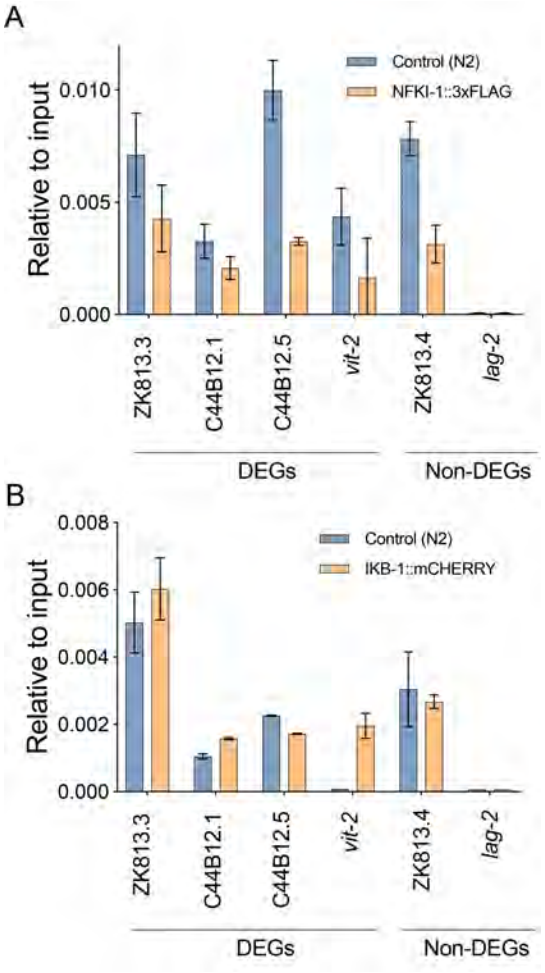

Figure R34. Binding of NFKI-1 and IKB-1 to chromatin regions does not correspond to deregulated gene expression at L4 larval stage under endogenous conditions. (A, B) ChIP-qPCR analyses of endogenous NFKI-1 (A) and IKB-1 (B) of randomly selected common deregulated genes in *nfki-1(cer1)* and *ikb-1(nr2027)* datasets. Data is presented relative to input. N2 (Bristol) is used as specificity control. ChIP-qPCRs were performed at L4 larvae stage (36 hours fed at 25ºC). Bars show the mean of 3 independent experiments. Error lines depict the SD of 3 experiments.

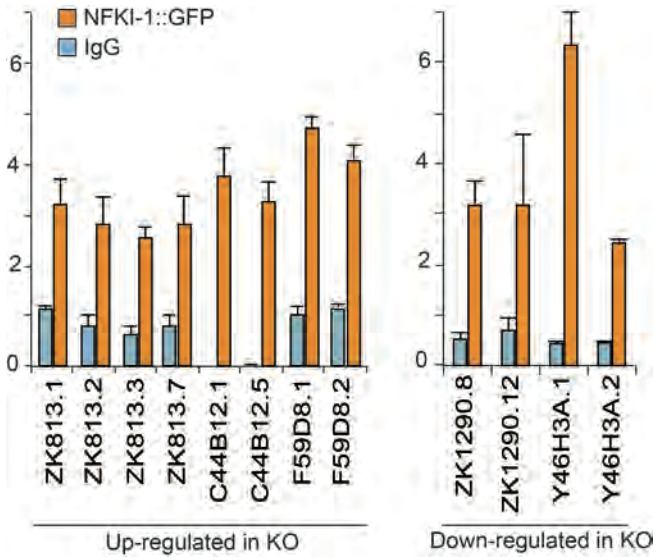

Figure R35. Chromatin-bound NFKI-1 is associated to deregulated loci in over-expression conditions. ChIP-qPCR analysis of transgenic NFKI-1 (CER147: *cerEx35[nfki-1::TY1::EGFP::3xFLAG+unc-119(+)*]) of randomly selected up- and down-regulated genes in *nfki-1* KO dataset. Data is presented relative to input. IgG is presented as specificity control. ChIP-qPCRs were performed at L4 larvae stage (36 hours fed at 25ºC). Bars are representative of one experiment. N=3. Error bars depict SD of 3 replicates in a single experiment.

R4.8. IκB deficiency slightly promotes silencing of an heterochromatin reporter

In order to explore further the impact of IκB mutants in H3K27me3 deposition, we generated strains carrying a *let-858p::GFP* heterochromatic reporter (*pkIs1582[let-858p::GFP:: let-858 3'UTR; rol-6(su1006)]* V) in IκB-deficient genetic backgrounds to assess if the absence of these genes caused changes in the *let-858::GFP* signal either at somatic or germline level. The *let-858p::GFP* reporter is integrated in

several heterochromatic regions, and thus, silenced in the germline and lowly expressed in the nucleus of somatic cells under wild type conditions (Camacho et al., 2018).

Interestingly, IκB-deficient backgrounds displayed a slightly but significant reduction in fluorescence intensity in somatic cells and no germline desilencing (**Figure R36A-B**). Such increment in somatic silencing could be a consequence of an accumulation of the repressive H3K27me3 chromatin mark. Moreover, the double mutant strain seems to have an additive effect. In the same experiment, we also tested if depletion of the H3K27 demethylase *utx-1* by RNAi caused a similar silencing.

Remarkably, we found that *utx-1(RNAi)* indeed provokes silencing at a similar level than the one showed by IκB-deficient strains in *mock(RNAi)* but displays a dim desilencing at the germline, and does not show an additive effect in IκB-deficient backgrounds. This could suggest that both conditions affect similarly the deposition of H3K27me3 in somatic but not germ cells at the sites in which the reporter have inserted copies (and not necessarily at global levels) or that such repression reaches a limiting threshold of detection. We used *lsm-7(RNAi)* as a positive control for germline desilencing (Mattout et al., 2020) and *prp-8(RNAi)* as a positive control for RNAi. Intriguingly but unrelated to our research question, RNAi depletion of the splicing factor *prp-8* caused a prominent

desilencing in both somatic and germ cells of the reporter (**Figure R36A-B**).

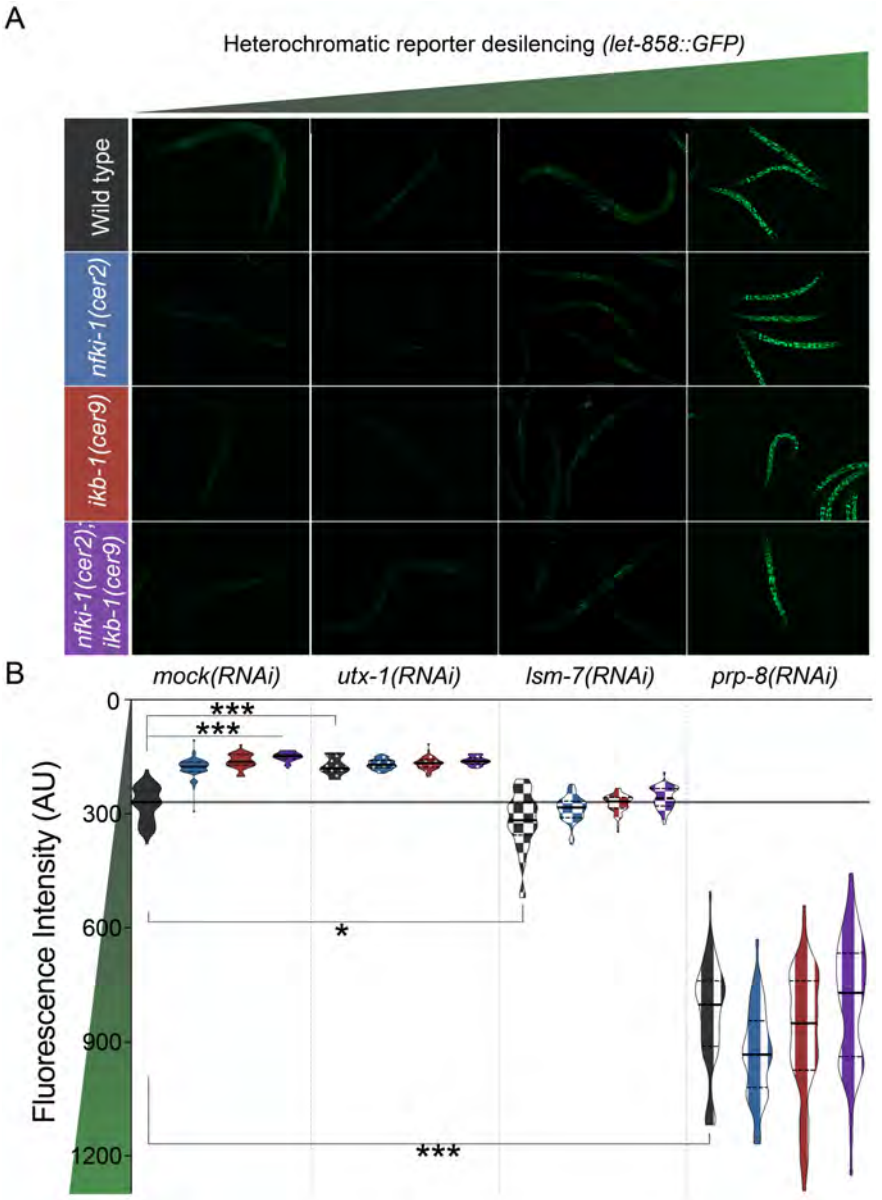

Figure R36. IκB-deficiency silences heterochromatin reporter in somatic cells. (A) Representative fluorescence microscopy images of the *let-858::GFP* heterochromatin reporter strains with an IκB-deficient genetic background and/or RNAi depletion of *utx-1, lsm-7* and *prp-8.* **(B)** Violin plots displaying the fluorescence intensity for

each condition. The horizontal black line depicts the mean intensity of the *let-858::GFP* reporter under a wild type genetic background and *mock(RNAi)* conditions (control conditions). Higher values correspond to desilencing and lower values to silencing. *n>30.* N=1. Significant changes were calculated relative to control conditions with a Kruskal-Wallis test with post-hoc Dunn's correction for multiple comparisons.

DISCUSSION

D1. A kingless kingdom: The IκBs without NF-κB paradox

One of the most relevant conclusions from the last 40 years of research on evolutionary biology is that metazoans have only a restricted collection of signaling pathways that are continually reused during development and other fundamental cellular processes, leading to the broad range of morphologies and major mechanisms that we witness in nature (Pires-daSilva and Sommer, 2003). Consequently, development and pathology are tightly linked, and it is not surprising that many developmental genes also function in innate immunity, and *vice versa* (Partridge et al., 2010).

Prominently, all living systems have the fundamental property of regulating physiological or genetic states in response to environmental stimuli (Çelen et al., 2017). This regulation occurs by means of diverse arrangements of signaling pathways that typically exert their gene regulation through nuclear effectors.

The widely studied transcription factor NF-κB links the reception and transmission of an external signal to the expression of effector proteins in most metazoans, and IκB proteins are mainly known because of their function as

repressors of NF-κB and suppressors of inflammation (Zhang et al., 2017). Therefore, the absence of any NF-κB transcription factors from the nematode genomes is remarkable and opens the possibility of studying non-NF-κB-directed functions for IκB proteins potentially conserved in other species (Engelmann and Pujol, 2010), including IκB nuclear roles and their relationship with alternative signal transduction pathways.

Despite the great research effort to understand IκBs regulation, including their unexpected nuclear role as regulators of stemness and cell differentiation, described in *Drosophila*, the mammalian skin (Mulero et al., 2013) and intestine (Marruecos et al., 2020), the involvement of NF-κB in this function has never been excluded. In this thesis, we have taken advantage of a physiological system lacking NF-κB to discriminate between NF-κB-dependent and -independent functions of the IκB proteins.

The presence of conserved IκB proteins in an NF-κB-deficient organism is at least surprising, in particular when free IκBs are intrinsically unstable in mammalian cells (half-live is 5-10 minutes in the case of IκBα) and require being stabilized through their association with NF-κB (three orders of magnitude prolonged half-live) (Pando and Verma, 2000; O'Dea et al., 2007; Mathes et al., 2008).

In addition, NFKI-1 and IKB-1 present an amino acid stretch highly rich in lysines (K) in the region from aa 31 to 144 (20% of all amino acids). The average K content for non-ribosomal proteins is 5% and 10% for ribosomal proteins (Lott et al., 2013). So, it is plausible that post-translational modifications of the amino-terminal half of the protein, including ubiquitination and/or SUMOylation, are required for compensating the high excess of positive charge imposed by the high proportion of K residues.

Supporting this possibility, we have identified multiple SUMOylation consensus sites in both proteins as well as SUMO-binding regions that could be mediating the potential interaction with other proteins in specific cell types. However, specific *in vitro* and *in vivo* characterization should be performed to validate this hypothesis.

Interestingly, Espinosa-Bigas lab collaborators found that NFKI-1 is only able to phosphorylate at the equivalent region of IκBα S32 (p-S32) **(Annex R1**), and not in p-S36. As a molecular dynamics simulation study suggested that both p-S32 and p-S36 of IκBα are needed to acquire the specific local conformation that makes this region accessible for the recognition by β-TrCP–S phase kinase-associated protein 1 (SKP1)–cullin 1(CUL1)–F-box protein (SCF) complex that leads to the ubiquitination of the protein and thus related to its NF-κB-dependent activity, it is possible that the absence of this

phosphorylation was lost linked to the loss of NF-κB and IKK-like proteins in *C. elegans*. An interesting open question that remains is who phosphorylates NFKI-1 at that residue and if that is still related with nuclear, or even IKK-independent functions.

Furthermore, NFKI-1 has been associated to IL-17 signaling as a member of the complex conformed by MALT-1/MALT1, ACTL-1/Act1 and PIK-1/IRAK (Flynn et al., 2020), signaling downstream of the *C. elegans* IL-17 receptors ILCR-1 and ILCR-2 (Chen et al., 2017). This function may contribute to NFKI-1 stabilization in the cytoplasm, mostly dependent on the association to NF-κB in mammalian cells (Mathes et al., 2008).

Likewise, our collaborators found that *C. elegans* IκBs are unable to bind mammalian p65-NF-κB *in vitro*, but they do bind PRC2 elements MES-2, MES-3 and MES-6 and histones H2A, H3, and H4 by pull-down assays (**Annex R2**) and thus, the association with these proteins and probably to additional yet unidentified protein complexes may contribute to their stabilization in the nucleus (Brena et al., 2020).

D2. NF-κB across evolution

Intriguingly, it is still under debate whether NF-κB was originally present in a common ancestor of vertebrates, arthropods and nematodes and then lost in the latter, or the MyD88-dependent NF-κB signaling was originated in a common ancestor of arthropods and vertebrates after the divergence of nematodes (Kim and Ausubel, 2005).

In this matter, our results suggest two possibilities:

(i) A nuclear function of ancestral IκBs has emerged in an NF-κB-free scenario and has primarily been maintained by BCL3 and other atypical IκBs in mammals, whereas IκBα has functionally diverged to inhibit NF-κB, maintaining the capacity to regulate the chromatin (when phosphorylated and SUMOylated).

(ii) The NF-κB pathway was originally present in *C. elegans* being primarily regulated by NFKI-1 and/or IKB-1, and subsequently lost, thus rewiring NFKI-1 and IKB-1 toward their secondary function as chromatin regulators.

In any case, from the evolutive point of view, according to the cytoplasmic roles of *C. elegans* NFKI-1 and IKB-1, IκB proteins were involved in innate immunity and stress responses even without the existence of NF-κB.

D3. IκBs expression and function in *C. elegans*

We characterized the endogenous expression of NFKI-1 and IKB-1 during post-embryonic development. Notably, NFKI-1 was present in several somatic cell types but specially enriched in cells at the head or anterior part, most of them presumably neuronal cells. Supporting these observations, NFKI-1 was reported to be expressed in RMG, AQR, PQR and URX neurons to regulate O_2 responses, besides other neurons (Chen et al., 2017). Our results together agree with a wide role regulating ancient innate immune responses.

This role includes changes in behavior, as the reported altered response to O_2 that modulates an aggregation social behavior (Chen et al., 2017), an exhibited resistance to *Pseudomonas aeruginosa* PA14, regulation of longevity and associative learning to the exposure of salt, phenocopying IL-17 mutants (Flynn et al., 2020) by a mechanism independent of O_2 sensing, which were recently reported in *nfki-1* mutants.

All this, along with our observations of resistance to the stresses imposed by starvation and high temperature, point out to a broad role in response to environmental perturbations, many of them neuromodulated and having an impact in multiple phenotypes.

In the case of IKB-1, we observed a mainly non-overlapping pattern with NFKI-1, being enriched mostly in cells near the pharynx and body wall muscle. Interestingly, IKB-1 has been reported to be involved in neuronal functions, as there is evidence of IKB-1 functioning downstream of TOL-1-mediated signaling to regulate diverse phenotypes, including the developmental specification of the BAG neurons, and thus affecting CO_2 sensing that ends up in a pathogen avoidance phenotype (Brandt and Ringstad, 2015; Kim, 2015). Moreover, *ikb-1* mutants are less resistant to *S. enterica*-mediated killing (Tenor and Aballay, 2008).

Thus, this notable neuronal and NF-κB-independent role of IκB homologs would be an interesting field to explore in mammalian systems, in which most of the reported phenotypes are associated to a dependency of the NF-κB signaling pathway (Shih et al., 2015).

Outstandingly, both IL-17- and TOL-1-mediated signaling converge into the activation of the p38 MAPK signaling pathway, which is one of the most important and evolutionarily conserved pathways of innate immune response (Huang et al., 2009; Keshet and Seger, 2010). This fact would partially explain why we observe that NFKI-1 and IKB-1 deficiency results in very diverse but almost identical phenotypes at the morphologic, epigenetic, and transcriptional levels, suggesting

that both homologs do not exert overlapping functions but instead they functionally cooperate in gene regulation.

Alternatively, they may perform comparable functions in distinct cell types to regulate a similar set of genes, but whether that is the case and if it is due to a specific nuclear function remains to be explored. Nevertheless, to our knowledge, this is the first evidence of transcriptional regulation imposed by IκB homologs in the absence of a functional NF-κB pathway.

D4. Subcellular localization of IκB homologs

Regarding the subcellular localization of IκB homologs in *C. elegans*, we observed that NFKI-1 and IKB-1 have a predominant presence in the cytoplasm under endogenous conditions, but a low proportion of them would be also present in the nucleus, which agrees with observations in mammalian systems (Mulero et al., 2013b; Marruecos et al., 2020, 2021).

We challenged the NFKI-1 reporter strain with different stresses, but we did not find any condition, besides over-expression, that increases the presence of NFKI-1 in the nucleus. This observation would fit with the notion that as there is no NF-κB effectors in *C. elegans*, there would be no need for NFKI-1 and IKB-1 to have a mechanism of nucleocytoplasmic

shuttle induction or regulation. Furthermore, the existence of other prominent signaling pathways that regulate innate immunity and environmental cues in *C. elegans* would compensate and rewire upon the loss of NF-κB.

Intriguingly, NFKI-1 was recently reported as a protein mainly present in the nucleus, with functions in the cytoplasm (Flynn et al., 2020). However, this affirmation relied on observations of non-endogenous reporters, its prominent nuclear presence in cell fractionation assays and a phylogenetic association with IκBζ/IκBNS, which are atypical IκB proteins that are mainly present in the nucleus in mammalian systems and alter gene expression primarily by regulating chromatin structure by mechanisms that are not well understood (Yamamoto and Gaynor, 2004; Motoyama et al., 2005; Amatya et al., 2017). Thus, our observations reshape the portrait of NFKI-1 being a predominantly cytoplasmatic protein, but also add new evidence of its presence in the nucleus.

Accordingly, we emphasize the importance of studying proteins under endogenous conditions and the utility of the different types of reporters that are available for the *C. elegans* community (reviewed in Nance and Frøkjær-Jensen, 2019), which are constantly updated with new approaches that improve their efficiency, as the example of Nested-CRISPR (Vicencio et al., 2019).

The presence of NFKI-1 and IKB-1 in different cell compartments, and at different proportions, is a common feature of moonlighting protein functions (extensively reviewed in Xu and Massagué, 2004; Min et al., 2016.

Probably, the most appropriate example is the case of the mammalian IκB proteins. Their most prominent role is to sequester NF-κB transcription factors in the cytoplasm, and thus are largely enriched in that subcellular compartment. But they are also able to act in the nucleus performing different functions, one of them being the aforementioned physical interaction with the PRC2 in the nucleus to regulate stemness and development (Mulero et al., 2013; Marruecos et al., 2020) but, importantly, IκB proteins can also inhibit NF-κB activity in the nucleus (Schuster et al., 2013).

The precise mechanism in the nucleus remains an open question, since all IκBs lack a DNA binding domain, but it has been suggested that IκBs act as factors that stabilize diverse NF-κB dimers on the DNA to silence specific genes due to an altered capacity to compete with other activating NF-κB dimers. Alternatively, IκBs would remove NF-κB dimers and relocalize them to the nucleus in dot-like structures that are associated with chromatin remodeling proteins in order to repress transcription (Viatour et al., 2005; Schuster et al., 2013). In any case, both possibilities are dependent of the activity of the NF-κB transcription factors.

Interestingly, we observed similar dot-like structures with IKB-1::mCHERRY reporter, which suggests that the function of those structures may not be entirely dependent of NF-κB or at least that their purpose is not the exclusive regulation of NF-κB, as the structures are conserved in a physiological NF-κB-free system.

D5. Nuclear functions of ancestral IκBs

Certainly, our best evidence supporting a direct nuclear role is the binding of endogenous NFKI-1 and IKB-1 with chromatin *in vivo*. More examples of a nuclear NFKI-1 were reported, such as the detection of NFKI-1 in the nuclear fraction of *C. elegans* cells. Likewise, NFKI-1 interacted directly with the histone acetyl transferase CBP-1/P300, and with a variety of transcription factors (Flynn et al., 2020). Specifically, the physical interaction with CBP-1/P300 would be interesting to explore in the future as it could provide a link with the recent observations of a multiple acetylation marks in the histone H4 associated to the nuclear role of IκBα (Marruecos et al., 2021).

It is important to remark that albeit we focused our work in the involvement of the PRC2 elements MES-2, MES-3, and MES-6, by means of an altered deposition of chromatin marks

H3K27me3 and its antagonist H3K36me3, we can't exclude the possibility and consider likely that other chromatin marks are also involved whether directly or indirectly in the nuclear role of NFKI-1 and IKB-1 since a physical interaction with histones H2A and H4 were also reported (Brena et al., 2020).

These results together with our observations that IκB deficiencies in *C. elegans* result in *(i)* an altered H3K27me3 distribution, *(ii)* a deregulated transcriptome and *(iii)* morphological defects, suggest that nematode IκBs act as modulators of developmental processes, including the animal body patterning, which is also regulated by PRC2, *hox* genes and the UTX-1 demethylase (Agger et al., 2007; Lan et al., 2007; Vandamme et al., 2012).

We observed morphological defects at a very low penetrance (3% – 4.7%), but all the observed aberrations were exclusively found in *nfki-1* and *ikb-1* mutants, consistent between multiple deletion alleles, rescued with a the *nfki-1* wild type single copy insertion, and never present in wild type animals. This is a relatively unusual scenario, but there are several examples of low-penetrance developmental phenotypes in the literature (e.g. (Sumiyoshi et al., 2011; Verghese et al., 2011; Walton et al., 2015; Karabinos et al., 2017).

An intriguing example is the case of *ten-1*, the only homolog of teneurins in *C. elegans* (Trzebiatowska et al., 2008; Topf and

Drabikowski, 2019). Teneurins are transmembrane proteins that assist morphogenetic processes in many organisms, expressed prominently in developing neuronal tissues and are important for neuronal patterning and axon guidance in mammals (Topf and Drabikowski, 2019). In *C. elegans*, *ten-1* is mainly expressed in pharynx neurons and hypodermal cells of the tail and its primary role is organizing the extracellular matrix (ECM) and cell morphogenesis (Drabikowski et al., 2005; Tucker and Chiquet-Ehrismann, 2006; Trzebiatowska et al., 2008). *ten-1* null mutants are mostly viable and display very mild defects in the growth of axons of pharyngeal neurons at a high penetrance (>90%) and sterility at medium penetrance (~39%).

Interestingly, a number of animals present an aberrant migration of the gonads (Drabikowski et al., 2005) and very low morphological defects (<3%) caused by a defective specification of epidermal cells, that are quite similar to some of those observed in *nfki-1* and *ikb-1* mutant animals. Interestingly, a synthetic lethal phenotype results when combined with other mutants of ECM organizers or cytoskeleton remodelers (Mörck et al., 2010).

Since gene ontology analyses of downregulated genes absent in IL-17 mutants but common for *nfki-1* and *ikb-1* suggested categories involved ECM organization and cuticle development, and differentially methylated peaks enriched for

H3K27me3 in both *nfki-1* and *ikb-1* mutants are associated to an epidermal cell fate, it is possible that an aberrant ECM organization could be one of the causes of the morphology defects and is relevant to the aberrant migration of the DTCs. A proper characterization, for instance with a cell adherent junctions reporter like AJM-1::GFP in *nfki-1* and *ikb-1* mutant backgrounds would be useful as a first step to confirm this hypothesis.

As mentioned, another *nfki-1* and *ikb-1* mutant phenotype related to development was the aberrant migration of DTCs. IκB mutants also phenocopy *utx-1* and *ten-1* mutants in this case. Altered migration of DTCs is associated with a defective cellular identity or aberrant signaling of the somatic gonad precursors (Cecchetelli and Cram, 2017; Gordon et al., 2019, 2020). Our transcriptomic analyses revealed that the deregulatory effect of the absence of *nfki-1* and *ikb-1* is higher at L4 stage, when the germline is completely developed.

Thus, it is plausible to speculate that an aberrant signaling arising between L1 and L4 stages is occurring in the DTCs or in the somatic gonad precursors. Interestingly, an abnormal signaling of the somatic gonad has been shown to lead to improper cell differentiation (Trzebiatowska et al., 2008; Jordan et al., 2019). Moreover, somatic gonad deregulation has been associated to stress conditions, such as starvation and L1 diapause, causing an heterochronically discordant

somatic and germline development (Jordan et al., 2019; Tenen and Greenwald, 2019).

This may partially explain the enrichment of germline genes in *nfki-1* and *ikb-1* mutant backgrounds at L4 stage. If this is true, it could also involve defects affecting the germ cells and thus animals' progeny, but we did not specifically address this possibility and hence, should be properly explored in the future.

Considering that in the previously described nuclear roles of the mammalian IκB proteins, the exertion of their functions is as protein factors that cooperate with other proteins in the cytoplasm or in the nucleus (Schuster et al., 2013; Zhang et al., 2017), it is possible that the low phenotypical penetrance is partially caused due to an incomplete functional disruption of the interacting proteins. Additionally, it could also be caused by genetic or functional redundancy, being NFKI-1 and IKB-1 not the only proteins involved in an IκB-like function, but being divergent enough to not be prompted as IκB homologs by phylogenetic databases.

In summary, the body morphology defects as well as the phenotype affecting the DTCs are related to cell fate identity and maintenance, and could be related to nuclear functions of *C. elegans* IκB proteins (**Figure D1**).

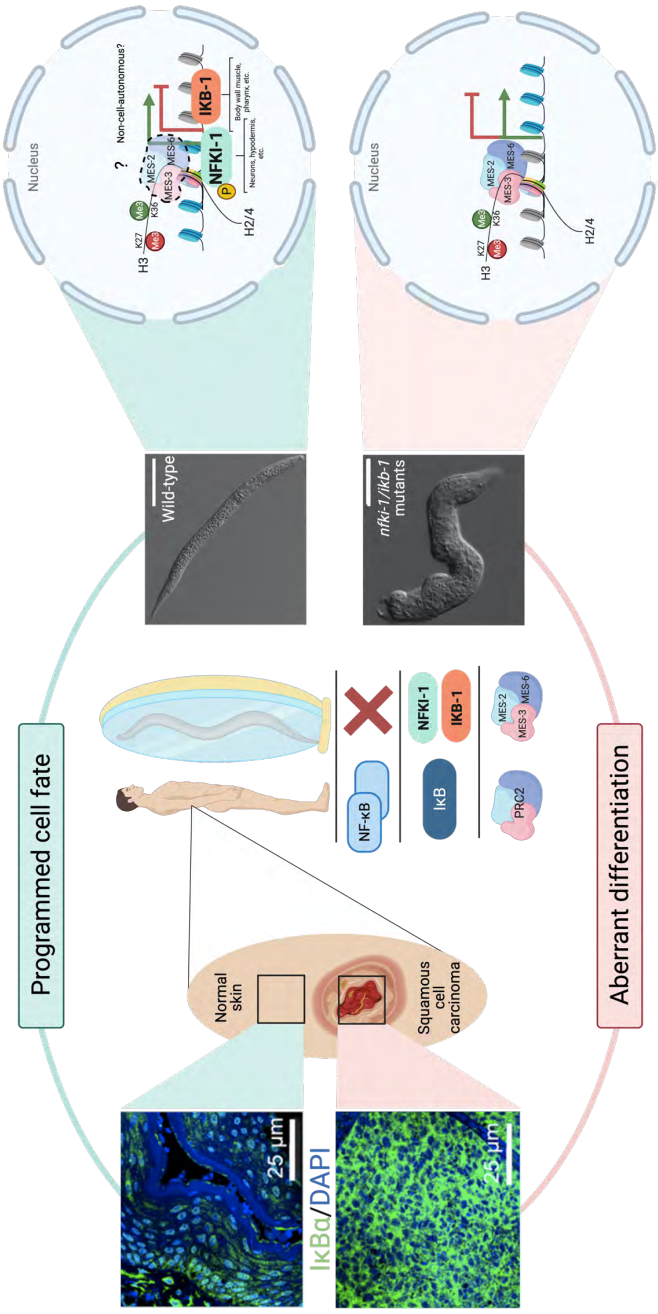

Figure D1. Proposed working model of NFKI-1 and IKB-1 nuclear roles regulating development and analogy with the reported nuclear function in Mulero et al., 2013b.

D6. Future directions

Probably the most prominent future direction of this work could be to study specifically which of the phenotypes that we unraveled are caused by a direct nuclear function. For this, it would be convenient to generate mutant animals that carry a *C. elegans* optimized optogenetic tag named LANS (light-activated nuclear shuttle), which has a constitutive NES and a light-inducible NLS (Yumerefendi et al., 2015). LANS::EGFP::NFKI-1 animals grown in the dark would exclude NFKI-1 from the nucleus, conversely, exposing animals to blue light during development would induce NFKI-1 nuclear translocation. The same methodology is applicable for IKB-1. Alternatively, by adding NLS tags as SV40 or *egl-13* NLS (Lin et al., 2019)to our endogenous reporters would generate a more stable nuclear translocation at physiological levels.

Another way to explore cell fate regulation would be to particularly focus on neuronal development. A recent study generated the NeuroPAL system, which consists in a set of strains carrying 41 reporters and a software that helps to identify the specific neuronal identities in the anatomy of the worm by using an unambiguous color coding (Yemini et al., 2021). Identifying exactly the neurons in which NFKI-1 or IKB-

1 are expressed, as well as evaluating if there are changes in neuronal identities under *nfki-1* and *ikb*-1 mutant backgrounds, would help us to understand their functions, especially the ones that are shared.

Likewise, omics scale studies under nuclear-specific versions of NFKI-1 and IKB-1 could expose primary targets, that were unreasonable to infer from our transcriptomic studies because of the vast presence of indirect targets, probably due to secondary consequences of signaling defects, and ultimately help to untangle the enigmatic nuclear role of the ancient IκB proteins.

The fact that most of the phenotypes that we observed, especially the ones that are closely related with development were lowly penetrant prevented us to easily explore further possible genetic interactors by means of RNAi screens. However, it would be interesting to further explore *nfki-1* and *ikb-1* role in cell fate regulation by performing a targeted RNAi screen including *hox* genes or genes associated to Polycomb function, looking for synthetic lethal phenotypes.

Additionally, our observations suggest a role of NFKI-1 and IKB-1 in innate immunity regulating the response to different stresses (Brena et al., 2020), but it would be interesting to explore the response of *nfki-1* and *ikb-1* mutants to different pathogens and additional stresses, as well as epistasis

analyses with different mutants of TLR and other innate immune signaling participants to elucidate their specific hierarchical place in these critical signaling pathways.

As previously mentioned, since our collaborators detected the presence of a phosphorylated form of NFKI-1 at the equivalent of serine 32 of IκB (Brena et al., 2020), another key unsolved question is how this phosphorylation is regulated, as in mammals that role corresponds to the IKK family of proteins (Zhang et al., 2017), and if it is part of an inducible system to regulate gene expression, which is characteristic of the NF-κB pathway in mammals (Hayden and Ghosh, 2008; Zhang et al., 2017) and could be mediated by alternative signal transduction effectors in *C. elegans*. This question could be approached by CRISPR-generating phosphomimetic mutants (Dickinson et al., 2013; Dickinson and Goldstein, 2016) replacing the serines in the equivalent position of p-S32 and even p-S36 of IκB to aspartic or glutamic acids, which would generate a constitutively phosphorylated NFKI-1, as well as a mutant that cannot be phosphorylated by deleting those residues.

Another evident open question is the functional relationship between NFKI-1 and IKB-1, specifically if whether the shared phenotypes that we observed are occurring because of a cooperative function in some cell(s) in the head of the animal and/or in the DTCs, or whether the mechanism is non-cell-autonomous.

Finally, the present body of work illustrates the use of *C. elegans* as a model to help to explain questions that arise not only from basic biological conceptions, but also from discoveries made in flies, mice, and humans, remarking this fundamental interdependency of research in model organisms, and contributing to the area of developmental biology.

CONCLUSIONS

CONCLUSIONS

1. NFKI-1 and IKB-1 are the *C. elegans* homologs of human IκB proteins.
2. NFKI-1 and IKB-1 are expressed in different cell types, and their expression patterns are mainly complementary.
3. NFKI-1 and IKB-1 are expressed predominantly in the cytoplasm but are also present in the nucleus of *C. elegans* cells.
4. NFKI-1 and IKB-1 role in the cytoplasm is involved in innate immunity and stress response.
5. NFKI-1 and IKB-1 role in the nucleus would be associated to development and chromatin regulation.
6. There is an ancestral nuclear role of the IκB proteins, that act independently of NF-κB activity to regulate developmental cues.

MATERIALS AND METHODS

MATERIALS AND METHODS

M1. Phylogenetic analyses

Phylogenetic trees were generated using the TreeFam project resource (Schreiber et al., 2014) and the BlastP program (Camacho et al., 2009). Ortholog search was done using OrthoList 2 (Kim, Underwood, Greenwald, & Shaye, 2018, http://ortholist.shaye-lab.org)

M2. *Caenorhabditis elegans* strains

C. elegans strains were cultured on Nematode Growth Medium (NGM) agar plates and maintained by standard methods (Stiernagle, 2006; Porta-de-la-Riva et al., 2012). We used N2 (Bristol) as wild type strain. All experiments were conducted at 25ºC, unless otherwise stated. Before performing assays, strains' genotype was verified and then animals were grown for at least two generations at the experimental temperature. All strains in this study are listed in **Annex M1**.

M3. PCR genotyping

In order to lysate worms, singled or pooled animals were picked into 0.2 ml PCR tubes containing 20 µl of 1X MyTaq Reaction Buffer and 66.67 µg/ml proteinase K. Then tubes were frozen at -80ºC for 10 minutes and incubated at 60ºC for 1 hour to activate proteinase K activity, followed by 15 minutes at 95ºC to inactivate it. Once animals are lysed, we added 10 µl of water to dilute the samples. 2 µl of worm lysate were used as templates for polymerase chain reaction (PCR) amplification using MyTaq DNA polymerase (Bioline) according to the manufacturer's instructions. All primer sequences are described in **Annex M2**.

M4. CRISPR-Cas9 editing and nematode transgenesis

For CRISPR-Cas9 editing, single guide RNAs (sgRNAs) were designed using *CCTOP* (Stemmer et al., 2015) online tool. We followed a co-CRISPR approach (Kim et al., 2014) using *dpy-10(cn64)* allele as a marker to enrich for successful genome-editing events. Endogenous reporters were obtained using a Nested CRISPR strategy (Vicencio et al., 2019). PHX267: *ikb-1(syb267[ikb-1::mCherry*]) I endogenous reporter was provided by Suny Biotech.

Young adult hermaphrodites were injected using XenoWorks Microinjection System. F_1 progeny was screened by PCR using specific primers and F_2 homozygotes were confirmed by Sanger sequencing. The sequences of the CRISPR reagents

and primers used are available in the **Annex M2** and **Annex M3**.

For the generation of NFKI-1 overexpression reporter lines, fosmid vectors containing an TY1::EGFP::3xFLAG-tagged version of *nfki-1* (C33A11.1) were requested from the TransgeneOme resource (Sarov et al., 2012) and transformation was performed by bombardment with gold particles (Biolistic Helium Gun, Caenotec). *unc-119(ed3)* young adults were shot with 16 µg of the purified DNA of interest (Praitis et al., 2001). Fosmid constructs were verified by digestion with restriction enzymes. Expression patterns were characterized for 2 independent lines with an integrated transgene and 6 with an extrachromosomal array. All generated lines displayed similar expression patterns. Overexpression reporter lines were generated by Dra. Montserrat Porta-de-la-Riva.

M5. RNA isolation

Synchronized animals were collected in M9 buffer after growing for 36 hours (L4s) or 5 hours-fed and 3 hours starved (L1s) at 25ºC. Suspended worms were washed 5 times in M9 buffer to remove all traces of bacteria. Total RNA was isolated using TRI Reagent (MRC, Inc.) and PureLink RNA Mini Kit (Ambion) according to manufacturer's instructions.

M6. *C. elegans* microscopy

Animals were mounted on 2% agar pads with 6 mM tetramisole hydrochloride. Live fluorescence imaging was performed with a Zeiss Axio Observer Z1 inverted fluorescence microscope and confocal imaging was conducted with a Leica TCS SP5 Confocal Laser Scanning Microscope. Imaging was done with 10-63X magnification in Z-stacks with 0.25-1μm distance between planes.

M7. Image processing and figures assembly

We used Zeiss Zen 2012 (Blue Edition), FIJI (ImageJ version 2.0.0-rc-68/1.52p) for image processing. Adobe Illustrator 2021 and Biorender were used for assembly of the figures.

M8. Semiquantitative RT-PCR

RNA integrity was verified by gel electrophoresis and quantified with a Nanodrop 1000 spectrophotometer (Thermo Fisher Scientific). cDNA was synthesized using RevertAid H Minus First Strand cDNA Synthesis Kit (Fermentas) according to manufacturer's instructions. PCR was carried out using specific primers (**Annex M2**) and analyzed by gel electrophoresis.

M9. Phenotypic characterization

For all experiments, gravid adult animals were synchronized by hypochlorite treatment (Porta-de-la-Riva et al., 2012) and resuspended embryos were allowed to hatch by overnight incubation at 20ºC. Then, incubated at 25ºC until animals reached the optimal stage for phenotype evaluation.

M9.1. Morphogenetic defects

Larvae morphology was assessed at L1 in a large, synchronized population by Nomarski (DIC) microscopy. Animals that presented misshapen bodies, mainly at the posterior region and in the tail, which were completely absent in N2 (Bristol) wild type control, were counted as morphologically aberrant.

M9.2. Migration of the gonads

Gonad migration was characterized in a synchronized population at L4 stage (36 h at 25ºC) for wild type and mutant backgrounds by DIC and fluorescence microscopy. To facilitate inspection and counting, knockout mutants were crossed with endogenous DEPS-1::GFP germline reporter. Gonads were considered with an aberrant migration when the expected U-shape was not achieved due to an irregular turn.

M9.3. Number of distal tip cells

Distal tip cell number was examined by microscopy of a synchronous population of wild type and in an IκB-mutant background at L3 stage (24 h at 25ºC). An abnormal distal tip cell number was considered when animals displayed one or three LAG-2::GFP-expressing distal tip cells.

M9.4. Starvation assay

L1 starvation assay was performed as previously described (Zhang et al., 2011; Cornes et al., 2015). Briefly, gravid adult worms were synchronized by hypochlorite treatment and the resulting eggs were resuspended in 4 ml of S-basal without cholesterol. Animals were incubated rotating at 20ºC. Larval viability was determined by placing ~100 worms every 3 days onto NGM plates and incubated at 20ºC for 2 days. Worms that reached at least L4 stage were marked as survivors and survival rates were calculated. Three biological replicates were used for each timepoint.

M9.5. Thermotolerance assay

Thermotolerance assay was performed as previously described (Cornes et al., 2015). A synchronized population of animals were grown at 25ºC until reached L4 (36 hours), then 50 animals per genotype were transferred into OP50-seeded

plates and grown to day 1 of adulthood. 3 plates were used per genotype (n=150). Next, worms were transferred into pre-heated NGM plates without any food and incubated at 36ºC. Viability was scored each hour during at least 8 hours. Animals were counted as dead when they lack movement and no pharyngeal pumping was detected.

M9.6. Ectopic expression of germline reporters

A synchronized population of animals were grown at 25ºC and inspected visually under the fluorescence microscope at different time points during development. Expected expression was restricted to the primordial germ cells during early development and to the developed germline. Best visual inspection was obtained at L1 and L4 stages. An ectopic expression was considered when the signal of the reporters was not only restricted to germ cells.

M10. RNA interference (RNAi)

RNAi was performed by feeding placing synchronized L1 worms obtained by hypochlorite treatment on NGM plates seeded with the specific RNAi clone-expressing bacteria at 25ºC (Timmons et al., 2001). We used L4440 empty vector (Fire vector library) as a mock RNAi control. Phenotypic characterization was assessed at different developmental stages of the F_1 progeny.

M11. Chromatin immunoprecipitation (ChIP)

Larvae were collected as described by Askjaer et al., 2014. Briefly, synchronized animals were grown in *E. coli* OP50-seeded NGM agar 150 mm plates and then collected in M9 buffer after growing for 36 h (L4s) or 5 h-fed and 3h-starved (L1s) at 25ºC. Suspended worms (approximately, 200 µl of L1 pelleted animals and 2 ml for L4s) were washed 5 times in M9 buffer to remove all traces of bacteria, resuspended in FA buffer with protease inhibitors cocktail (Roche) and frozen as drops in liquid nitrogen (N_2).

Then, 1 ml of packed worms was grounded under liquid N_2 and brought to 10 ml with FA buffer (50 mM HEPES/KOH pH7.5, 1 mM EDTA, 1% Triton X-100, 0.1% sodium deoxycholate, 150 mM NaCl). Next, 600 µl of 37% formaldehyde were added and allowed to crosslink for 20 minutes at room temperature. Glycine (600 µl; 2.5M) was used to quench the reaction, for 2 minutes, and nuclei were recovered by centrifugation (4000 rpm, 5 minutes in a microfuge), washed 3 times with FA buffer by resuspending in 5 ml and spinning again. Finally, nuclei were resuspended in 1.6 ml of FA buffer, split into two Eppendorf tubes and sonicated for 10 minutes in a Bioruptor Pico (Diagenode) under standard conditions (30 s on, 30 s off). After sonication, protein extract was quantified and approximately 2 mg of each sample were spun at full speed for 10 minutes at 4ºC and the supernatants (SN) were pooled

again. SN were pre-cleared with FA-equilibrated SPA/G beads (GE Healthcare) by rotating for 30 minutes at room temperature, recovered by spinning at 1200 rpm for 2 minutes and used for immunoprecipitation (IP). An aliquot of 100 µl was kept as input control at this point. The rest of the sample was split into different tubes for IP with the antibodies of choice. After adding the corresponding antibody (3-10 µg), samples were incubated in a rotator overnight at 4ºC and the immunocomplexes were recovered with FA buffer pre-equilibrated SPA/G beads (GE Healthcare) by rotating 2h at 4ºC. Beads were pelleted (1200 rpm; 2 minutes) washed twice with FA buffer (5 minutes each); once with FA + 0.5 M NaCl (10 minutes); once with FA buffer + 1M NaCl (5 minutes); once with lithium buffer (10 minutes); twice with TE buffer (5 minutes each) and the immunoprecipitated material was recovered by incubation in 100 µl elution buffer (Tris-EDTA; 1% SDS plus inhibitors) 1h at RT. DNA was finally purified by reverse crosslinking at 65ºC overnight followed by proteinase K (0.5 or 1 mg/ml, respectively) digestions and purifying with MinElute® PCR purification kit (Qiagen).

Table M1. List of antibodies used for ChIP-seq experiments.

Antibody	Company	Reference	Specie
Flag M2	Sigma	F3165	Mouse
mCherry	Invitrogen	PA5-34974	Rabbit
H3K27me3	Millipore	#07-449	Rabbit
H3K36me3	Abcam	ab95412	Mouse

M11.1. ChIP-qPCR

qPCR was performed using LightCycler 480 SYBR Green I Master (Roche) in a LightCycler 480 II Real-Time PCR system (Roche). All the measurements were performed in triplicate, in three independent assays and values were normalized to input.

M11.2. ChIP-seq data analysis

DNA samples were sequenced using Illumina HiSeq platform. Raw single-end 50-bp sequences were filtered by quality (Q>30) and length (length > 20 bp) with Trim Galore (Krueger, 2015). Filtered sequences were aligned against the *C. elegans* genome (WBcel235) with Bowtie2 (Langmead and Salzberg, 2012). MACS2 software (Zhang et al., 2008) (available at https://github.com/taoliu/MACS/) was run first for each replicate, and then combining all replicates, using unique alignments (q-value < 0.1). Broad peaks calling was set for H3K27me3 and H3K36me3 (--broad option). Peak annotation was performed with ChIPseeker package (version 1.10.2) (Yu et al., 2015). Data analyses were performed by Dr. Yolanda Guillén.

M12. RNA-seq data analysis

cDNA was sequenced using Illumina HiSeq platform, obtaining 30 – 35 million 75-bp single-end reads per sample. Adapter sequences were trimmed with Trim Galore (Krueger, 2015). Sequences were filtered by quality (Q>30) and length (>20 bp). Filtered reads were mapped against *C. elegans* genome (WBcel235) using Bowtie2 (Langmead and Salzberg, 2012). High quality alignments were fed to HTSeq (v.0.9.1) (Anders et al., 2015) to estimate the normalized counts of each expressed gene. Differentially expressed genes between wild type and knockouts were explored using DESeq2 R package (v.1.20.0) (Love et al., 2014) considering a threshold of adjusted p-value<0.01. Data analyses were performed by Dr. Yolanda Guillén.

M13. Statistical analyses

'N' denotes the number of independent replicate experiments performed, while 'n' indicates total number of animals analyzed for each condition. Statistical analyses were performed in GraphPad Prism 8 and R. Statistical tests are reported in figure legends. For all graphs, all the p-values were noted according to APA annotation style. p-value>0.05 not significant (n.s.); p-value<0.05 (*); p-value<0.01(**); p-value<0.001 (***).

M14. Data availability

ChIP-seq and RNA-seq data have been deposited at the Gene Expression Omnibus (GEO) repository and are available under the accession number: GSE146655.

BIBLIOGRAPHY

BIBLIOGRAPHY

- Agger, K., Cloos, P.A.C., Christensen, J., Pasini, D., Rose, S., Rappsilber, J., Issaeva, I., Canaani, E., et al., 2007. UTX and JMJD3 are histone H3K27 demethylases involved in HOX gene regulation and development. Nature 449, 731–734.
- Aguilera, C., Hoya-Arias, R., Haegeman, G., Espinosa, L., Bigas, A., 2004. Recruitment of IκBα to the *hes1* promoter is associated with transcriptional repression. Proc. Natl. Acad. Sci. U. S. A. 101, 16537–16542.
- Ahringer, J., 2006. Reverse genetics. WormBook.
- Ahringer, J., Gasser, S.M., 2018. Repressive chromatin in *Caenorhabditis elegans*: Establishment, composition, and function. Genetics 208, 491–511.
- Altun, Z., Hall, D., 2020. The Handbook of *C. elegans* Anatomy [WWW Document]. WormAtlas.
- Amatya, N., Garg, A. V., Gaffen, S.L., 2017. IL-17 Signaling: The Yin and the Yang. Trends Immunol. 38, 310–322.
- Anders, S., Pyl, P.T., Huber, W., 2015. HTSeq-A Python framework to work with high-throughput sequencing data. Bioinformatics 31, 166–169.
- Apfeld, J., Alper, S., 2018. What Can We Learn About Human Disease from the Nematode *C. elegans*? BT - Disease Gene Identification: Methods and Protocols, in: DiStefano, J.K. (Ed.), . Springer New York, New York, NY, pp. 53–75.
- Arenzana-Seisdedos, F., Turpin, P., Rodriguez, M., Thomas, D., Hay, R.T., Virelizier, J.L., Dargemont, C., 1997. Nuclear localization of IκBα promotes active transport of NF-κB from the nucleus to the cytoplasm. J. Cell Sci. 110, 369–378.
- Askjaer, P., Ercan, S., Meister, P., 2014. Modern techniques for the analysis of chromatin and nuclear organization in *C. elegans*. WormBook 1–35.
- Baeuerle, P.A., Baltimore, D., 1996. Nf-κB: Ten years after. Cell 87, 13–20.
- Baeuerle, Patrick A., Baltimore, D., 1988. Activation of DNA-binding activity in an apparently cytoplasmic precursor of the NF-κB transcription factor. Cell 53, 211–217.
- Baeuerle, P A, Baltimore, D., 1988. I kappa B: a specific inhibitor of the NF-kappa B transcription factor. Science (80-.). 242, 540 LP – 546.
- Baldwin, A.S., 1996. The NF-κB and IκB proteins: New Discoveries and Insights. Annu. Rev. Immunol. 14, 649–681.
- Baltimore, D., 2011. NF-κB is 25. Nat. Immunol.
- Barstead, R., Moulder, G., Cobb, B., Frazee, S., Henthorn, D., Holmes,

J., Jerebie, D., Landsdale, M., et al., 2012. Large-scale screening for targeted knockouts in the *Caenorhabditis elegans* genome. G3 Genes, Genomes, Genet. 2, 1415–1425.
- Baugh, L.R., 2013. To grow or not to grow: Nutritional control of development during *Caenorhabditis elegans* L1 Arrest. Genetics.
- Ben-Neriah, Y., 2002. Regulatory functions of ubiquitination in the immune system. Nat. Immunol. 3, 20–26.
- Bender, L.B., Cao, R., Zhang, Y., Strome, S., 2004. The MES-2/MES-3/MES-6 Complex and Regulation of Histone H3 Methylation in *C. elegans*. Curr. Biol. 14, 1639–1643.
- Bender, L.B., Suh, J., Caroll, C.R., Fong, Y., Fingerman, I.M., Briggs, S.D., Cao, R., Zhang, Y., et al., 2006. MES-4: An autosome-associated histone methyltransferase that participates in silencing the X chromosomes in the *C. elegans* germ line. Development 133, 3907–3917.
- Beutler, B., Wagner, H., 2002. Toll-like receptor family members and their ligands: Preface, Current Topics in Microbiology and Immunology.
- Boeck, M.E., Huynh, C., Gevirtzman, L., Thompson, O.A., Wang, G., Kasper, D.M., Reinke, V., Hillier, L.W., et al., 2016. The time-resolved transcriptome of *C. elegans*. Genome Res. 26, 1441–1450.
- Brandt, J.P., Ringstad, N., 2015. Toll-like Receptor Signaling Promotes Development and Function of Sensory Neurons Required for a *C. elegans* Pathogen-Avoidance Behavior. Curr. Biol. 25, 2228–2237.
- Braukmann, F., Jordan, D., Miska, E., 2017. Artificial and natural RNA interactions between bacteria and *C. elegans*. RNA Biol. 14, 415–420.
- Brena, D., Bertran, J., Porta-de-la-Riva, M., Guillén, Y., Cornes, E., Kukhtar, D., Campos-Vicens, L., Fernández, L., et al., 2020. Ancestral function of Inhibitors-of-kappaB regulates *Caenorhabditis elegans* development. Sci. Rep. 10.
- Brennan, J.J., Gilmore, T.D., 2018. Evolutionary origins of Toll-like receptor signaling. Mol. Biol. Evol. 35, 1576–1587.
- Brenner, S., 1974. The genetics of *Caenorhabditis elegans*. Genetics 77, 71–94.
- Bucher, E.A., Seydoux, G., 1994. Gastrulation in the nematode *Caenorhabditis elegans*. Semin. Dev. Biol.
- Camacho, C., Coulouris, G., Avagyan, V., Ma, N., Papadopoulos, J., Bealer, K., Madden, T.L., 2009. BLAST+: Architecture and applications. BMC Bioinformatics 10, 1–9.
- Camacho, J., Truong, L., Pellegrini, M., Yang, X., Correspondence, P.A., 2018. The Memory of Environmental Chemical Exposure in *C. elegans* Is Dependent on the Jumonji Demethylases jmjd-2 and jmjd-3/utx-1.
- Cao, J., Packer, J.S., Ramani, V., Cusanovich, D.A., Huynh, C., Daza, R., Qiu, X., Lee, C., et al., 2017. Comprehensive single-cell transcriptional profiling of a multicellular organism. Science (80-.). 357, 661–667.
- Capowski, E.E., Martin, P., Garvin, C., Strome, S., 1991. Identification of grandchildless loci whose products are required for normal germ-line

development in the nematode *Caenorhabditis elegans*. Genetics 129, 1061–1072.
- Cecchetelli, A.D., Cram, E.J., 2017. Regulating distal tip cell migration in space and time. Mech. Dev. 148, 11–17.
- Çelen, İ., Doh, J.H., Sabanayagam, C., 2017. Genetic Adaptation of *C. elegans* to Environment Changes I: Multigenerational Analysis of the Transcriptome. Doi.Org 194506.
- Ceron, J., Rual, J.F., Chandra, A., Dupuy, D., Vidal, M., Van Den Heuvel, S., 2007. Large-scale RNAi screens identify novel genes that interact with the *C. elegans* retinoblastoma pathway as well as splicing-related components with synMuv B activity. BMC Dev. Biol. 7.
- Chen, C., Itakura, E., Nelson, G.M., Sheng, M., Laurent, P., Fenk, L.A., Butcher, R.A., Hegde, R.S., et al., 2017. IL-17 is a neuromodulator of *Caenorhabditis elegans* sensory responses. Nature 542, 43–48.
- Chiao, P.J., Miyamoto, S., Verma, I.M., 1994. Autoregulation of IκBα activity. Proc. Natl. Acad. Sci. U. S. A. 91, 28–32.
- Chiba, T., Miyashita, K., Sugoh, T., Warita, T., Inoko, H., Kimura, M., Sato, T., 2011. IκBL, a novel member of the nuclear IκB family, inhibits inflammatory cytokine expression. FEBS Lett. 585, 3577–3581.
- Chin-Sang, I.D., Chisholm, A.D., 2000. Form of the worm: Genetics of epidermal morphogenesis in *C. elegans*. Trends Genet. 16, 544–551.
- Cildir, G., Low, K.C., Tergaonkar, V., 2016. Noncanonical NF-κB Signaling in Health and Disease. Trends Mol. Med. 22, 414–429.
- Cohen-Fix, O., Askjaer, P., 2017. Cell biology of the *Caenorhabditis elegans* nucleus. Genetics 205, 25–59.
- Cook, S.J., Jarrell, T.A., Brittin, C.A., Wang, Y., Bloniarz, A.E., Yakovlev, M.A., Nguyen, K.C.Q., Tang, L.T.H., et al., 2019. Whole-animal connectomes of both *Caenorhabditis elegans* sexes. Nature 571, 63–71.
- Cornes, E., Porta-De-La-Riva, M., Aristizábal-Corrales, D., Brokate-Llanos, A.M., García-Rodríguez, F.J., Ertl, I., Díaz, M., Fontrodona, L., et al., 2015. Cytoplasmic LSM-1 protein regulates stress responses through the insulin/IGF-1 signaling pathway in *Caenorhabditis elegans*. RNA 21, 1544–1553.
- Corsi, A.K., Wightman, B., Chalfie, M., 2015. A transparent window into biology: A primer on *Caenorhabditis elegans*. Genetics 200, 387–407.
- Culver, C., Sundqvist, A., Mudie, S., Melvin, A., Xirodimas, D., Rocha, S., 2010. Mechanism of Hypoxia-Induced NF-κB. Mol. Cell. Biol. 30, 4901–4921.
- De Santa, F., Totaro, M.G., Prosperini, E., Notarbartolo, S., Testa, G., Natoli, G., 2007. The Histone H3 Lysine-27 Demethylase Jmjd3 Links Inflammation to Inhibition of Polycomb-Mediated Gene Silencing. Cell 130, 1083–1094.
- Desterro, J.M., Rodriguez, M.S., Hay, R.T., 1998. SUMO-1 modification of IκBa inhibits NF-κB activation. Mol Cell 2, 233–239.
- Dickinson, D.J., Goldstein, B., 2016. CRISPR-based methods for *Caenorhabditis elegans* genome engineering. Genetics 202, 885–901.
- Dickinson, D.J., Ward, J.D., Reiner, D.J., Goldstein, B., 2013.

Engineering the *Caenorhabditis elegans* genome using Cas9-triggered homologous recombination. Nat. Methods 10, 1028–1034.
- DiDonato, J., Mercurio, F., Rosette, C., Wu-Li, J., Suyang, H., Ghosh, S., Karin, M., 1996. Mapping of the inducible IkappaB phosphorylation sites that signal its ubiquitination and degradation. Mol. Cell. Biol. 16, 1295–1304.
- Domínguez-Andrés, J., Fanucchi, S., Joosten, L.A.B., Mhlanga, M.M., Netea, M.G., 2020. Advances in understanding molecular regulation of innate immune memory. Curr. Opin. Cell Biol. 63, 68–75.
- Drabikowski, K., Trzebiatowska, A., Chiquet-Ehrismann, R., 2005. *ten-1*, an essential gene for germ cell development, epidermal morphogenesis, gonad migration, and neuronal pathfinding in *Caenorhabditis elegans*. Dev. Biol. 282, 27–38.
- Eluard, B., Thieblemont, C., Baud, V., 2020. NF-κB in the New Era of Cancer Therapy. Trends in Cancer.
- Emmons, S.W., 2005. Male development. WormBook 1–22.
- Engelmann, I., Pujol, N., 2010. Chapter R 6 Innate Immunity in *C. elegans* 105–121.
- Ermolaeva, M.A., Schumacher, B., 2014. Insights from the worm: The *C. elegans* model for innate immunity. Semin. Immunol. 26, 303–309.
- Espinosa, L, Bigas, A., Mulero, M.C., 2014. Novel functions of chromatin-bound IκBα in oncogenic transformation. Br. J. Cancer 111, 1688–1692.
- Evans, K.J., Huang, N., Stempor, P., Chesney, M.A., Down, T.A., Ahringer, J., 2016. Stable *Caenorhabditis elegans* chromatin domains separate broadly expressed and developmentally regulated genes. Proc. Natl. Acad. Sci. 113, E7020–E7029.
- Ezhkova, E., Pasolli, H.A., Parker, J.S., Stokes, N., Su, I. hsin, Hannon, G., Tarakhovsky, A., Fuchs, E., 2009. Ezh2 Orchestrates Gene Expression for the Stepwise Differentiation of Tissue-Specific Stem Cells. Cell 136, 1122–1135.
- Fabrizio, P., Garvis, S., Palladino, F., 2019. Histone Methylation and Memory of Environmental Stress. Cells 8, 339.
- Fay, D., 2006. Genetic mapping and manipulation: chapter 6--Mapping with deficiencies and duplications. WormBook 1–3.
- Fire, A., Xu, S., Montgomery, M.K., Kostas, S.A., Driver, S.E., Mello, C.C., 1998. Potent and specific genetic interference by double-stranded RNA in *Caenorhabditis elegans*. Nature 391, 806–811.
- Flynn, S.M., Chen, C., Artan, M., Barratt, S., Crisp, A., Nelson, G.M., Begum, F., Skehel, M., et al., 2019. MALT1 mediates IL-17 neural signaling to regulate *C. elegans* behaviour, immunity and longevity. bioRxiv.
- Flynn, S.M., Chen, C., Artan, M., Barratt, S., Crisp, A., Nelson, G.M., Peak-Chew, S.-Y., Begum, F., et al., 2020. MALT-1 mediates IL-17 neural signaling to regulate *C. elegans* behavior, immunity and longevity. Nat. Commun. 11, 2099.
- Frézal, L., Félix, M.A., 2015. *C. elegans* outside the Petri dish. Elife 4, 1–14.

- Friedland, A.E., Tzur, Y.B., Esvelt, K.M., Colaiácovo, M.P., Church, G.M., Calarco, J.A., 2013. Heritable genome editing in *C. elegans* via a CRISPR-Cas9 system. Nat. Methods 10, 741–743.
- Furuhashi, H., Takasaki, T., Rechtsteiner, A., Li, T., Kimura, H., Checchi, P.M., Strome, S., Kelly, W.G., 2010. Trans-generational epigenetic regulation of *C. elegans* primordial germ cells. Epigenetics and Chromatin 3, 1–21.
- Gay, N.J., Gangloff, M., O'Neill, L.A.J., 2011. What the Myddosome structure tells us about the initiation of innate immunity. Trends Immunol. 32, 104–109.
- Gay, N.J., Symmons, M.F., Gangloff, M., Bryant, C.E., 2014. Assembly and localization of Toll-like receptor signalling complexes. Nat. Rev. Immunol. 14, 546–558.
- Gaydos, L.J., Rechtsteiner, A., Egelhofer, T.A., Carroll, C.R., Strome, S., 2012. Antagonism between MES-4 and Polycomb Repressive Complex 2 Promotes Appropriate Gene Expression in *C. elegans* Germ Cells. Cell Rep. 2, 1169–1177.
- Gaydos, L.J., Wang, W., Strome, S., 2014. H3K27me and PRC2 transmit a memory of repression across generations and during development. Science (80-.). 345, 1515–1518.
- Gerstein, M.B., Lu, Z.J., Van Nostrand, E.L., Cheng, C., Arshinoff, B.I., Liu, T., Yip, K.Y., Robilotto, R., et al., 2010. Integrative analysis of the *Caenorhabditis elegans* genome by the modENCODE project. Science (80-.). 330, 1775–1787.
- Ghosh, S., Baltimore, D., 1990. Activation in vitro of NF-κB by phosphorylation of its inhibitor IκB. Nature.
- Ghosh, S., Hayden, M.S., 2012. Celebrating 25 years of NF-κB research. Immunol. Rev.
- Ghosh, S., May, M.J., Kopp, E.B., 1998. NF-κB AND REL PROTEINS: Evolutionarily Conserved Mediators of Immune Responses. Annu. Rev. Immunol. 16, 225–260.
- Goodman, M.B., Sengupta, P., 2019. How *Caenorhabditis elegans* senses mechanical stress, temperature, and other physical stimuli. Genetics 212, 25–51.
- Gordon, K.L., Payne, S.G., Linden-High, L.M., Pani, A.M., Goldstein, B., Hubbard, E.J.A., Sherwood, D.R., 2019. Ectopic Germ Cells Can Induce Niche-like Enwrapment by Neighboring Body Wall Muscle. Curr. Biol. 29, 823-833.e5.
- Gordon, K.L., Zussman, J.W., Li, X., Miller, C., Sherwood, D.R., 2020. Stem cell niche exit in *C. elegans* via orientation and segregation of daughter cells by a cryptic cell outside the niche. Elife 9, 1–56.
- Harris, T.W., Arnaboldi, V., Cain, S., Chan, J., Chen, W.J., Cho, J., Davis, P., Gao, S., et al., 2020. WormBase: A modern Model Organism Information Resource. Nucleic Acids Res. 48, D762–D767.
- Hayden, M.S., Ghosh, S., 2008. Shared Principles in NF-κB Signaling. Cell.
- Hendriks, G.J., Gaidatzis, D., Aeschimann, F., Großhans, H., 2014. Extensive Oscillatory Gene Expression during *C. elegans* Larval

Development. Mol. Cell 53, 380–392.
- Herman, M., 2006. Hermaphrodite cell-fate specification. WormBook 1–16.
- Hirotani, T., Lee, P.Y., Kuwata, H., Yamamoto, M., Matsumoto, M., Kawase, I., Akira, S., Takeda, K., 2005. The Nuclear IκB Protein IκBNS Selectively Inhibits Lipopolysaccharide-Induced IL-6 Production in Macrophages of the Colonic Lamina Propria. J. Immunol. 174, 3650–3657.
- Hoffmann, A., Leung, T.H., 2003. Genetic analysis of NF-κB/Rel transcription factors defines functional specificities. Embo 22, 5530–5539.
- Hoffmann, A., Levchenko, A., Scott, M.L., Baltimore, D., 2002. The IκB-NF-κB signaling module: Temporal control and selective gene activation. Science (80-.). 298, 1241–1245.
- Hu, P.J., 2007. Dauer. WormBook 1–19.
- Huang, G., Shi, L.Z., Chi, H., 2009. Regulation of JNK and p38 MAPK in the immune system: Signal integration, propagation and termination. Cytokine 48, 161–169.
- Hutter, H., Suh, J., 2016. GExplore 1.4: An expanded web interface for queries on *Caenorhabditis elegans* protein and gene function . Worm 5, e1234659.
- Irazoqui, J.E., Urbach, J.M., Ausubel, F.M., 2010. Evolution of host innate defence: Insights from *Caenorhabditis elegans* and primitive invertebrates. Nat. Rev. Immunol. 10, 47–58.
- Jacobs, M.D., Harrison, S.C., 1998. Structure of an IkappaBalpha/NF-kappaB complex. Cell 95, 749–58.
- Jinek, M., Chylinski, K., Fonfara, I., Hauer, M., Doudna, J.A., Charpentier, E., 2012. A programmable dual-RNA-guided DNA endonuclease in adaptive bacterial immunity. Science 337, 816–21.
- Johnson, C., 1999. An N-terminal nuclear export signal is required for the nucleocytoplasmic shuttling of Ikappa Balpha. EMBO J. 18, 6682–6693.
- Jordan, J.M., Hibshman, J.D., Webster, A.K., Kaplan, R.E.W., Leinroth, A., Guzman, R., Maxwell, C.S., Chitrakar, R., et al., 2019. Insulin/IGF Signaling and Vitellogenin Provisioning Mediate Intergenerational Adaptation to Nutrient Stress. Curr. Biol. 29, 2380-2388.e5.
- Jorgensen, E.M., Mango, S.E., 2002. The art and design of genetic screens: *Caenorhabditis elegans*. Nat. Rev. Genet. 3, 356–369.
- Kamath, R.S., Fraser, A.G., Dong, Y., Poulin, G., Durbin, R., Gotta, M., Kanapin, A., Le Bot, N., et al., 2003. Systematic functional analysis of the *Caenorhabditis elegans* genome using RNAi. Nature 421, 231–237.
- Karabinos, A., Schünemann, J., Parry, D.A.D., 2017. Assembly studies of six intestinal intermediate filament (IF) proteins B2, C1, C2, D1, D2, and E1 in the nematode *C. elegans*. Cytoskeleton 74, 107–113.
- Karin, M., Ben-neriah, Y., 2000. Phosphorylation meets ubiquitination: The Control of NF-kB Activity. Annu. Rev. Immunol. 621–663.
- Kashatus, D., Cogswell, P., Baldwin, A.S., 2006. Expression of the Bcl-3 proto-oncogene suppresses p53 activation. Genes Dev. 20, 225–235.

- Kawai, T., Akira, S., 2007. Signaling to NF-κB by Toll-like receptors. Trends Mol. Med.
- Keshet, Y., Seger, R., 2010. The MAP Kinase Signaling Cascades: A System of Hundreds of Components Regulates a Diverse Array of Physiological Functions, in: Seger, R. (Ed.), MAP Kinase Signaling Protocols: Second Edition. Humana Press, Totowa, NJ, pp. 3–38.
- Kim, D.H., 2018. Signaling in the innate immune response. WormBook 1–35.
- Kim, D.H., 2015. Signal Transduction: A Different Kind of Toll Is in the BAG. Curr. Biol. 25, R767–R769.
- Kim, D.H., Ausubel, F.M., 2005. Evolutionary perspectives on innate immunity from the study of *Caenorhabditis elegans*. Curr. Opin. Immunol. 17, 4–10.
- Kim, H., Ishidate, T., Ghanta, K.S., Seth, M., Conte, D., Shirayama, M., Mello, C.C., 2014. A Co-CRISPR strategy for efficient genome editing in *Caenorhabditis elegans*. Genetics 197, 1069–1080.
- Kim, S.K., Lund, J., Kiraly, M., Duke, K., Jiang, M., Stuart, J.M., Eizinger, A., Wylie, B.N., et al., 2001. A gene expression map for *Caenorhabditis elegans*. Science (80-.). 293, 2087–2092.
- Kim, W., Underwood, R.S., Greenwald, I., Shaye, D.D., 2018. Ortholist 2: A new comparative genomic analysis of human and *Caenorhabditis elegans* genes. Genetics 210, 445–461.
- Kosugi, S., Hasebe, M., Tomita, M., Yanagawa, H., 2009. Systematic identification of cell cycle-dependent yeast nucleocytoplasmic shuttling proteins by prediction of composite motifs. Proc. Natl. Acad. Sci. U. S. A. 106, 10171–10176.
- Krueger, F., 2015. Trim galore. A wrapper tool around Cutadapt FastQC to consistently apply Qual. Adapt. trimming to FastQ files.
- Kuleshov, M. V, Diaz, J.E.L., Flamholz, Z.N., Keenan, A.B., Lachmann, A., Wojciechowicz, M.L., Cagan, R.L., Ma'ayan, A., 2019. modEnrichr: a suite of gene set enrichment analysis tools for model organisms. Nucleic Acids Res. 47, W183–W190.
- L'Herault, S., 2007. Spermatogenesis. WormBook.
- Labrousse, A., Chauvet, S., Couillault, C., Léopold Kurz, C., Ewbank, J.J., 2000. *Caenorhabditis elegans* is a model host for Salmonella typhimurium. Curr. Biol. 10, 1543–1545.
- Lan, F., Bayliss, P.E., Rinn, J.L., Whetstine, J.R., Wang, J.K., Chen, S., Iwase, S., Alpatov, R., et al., 2007. A histone H3 lysine 27 demethylase regulates animal posterior development. Nature 449, 689–694.
- Lander, E.S., 2016. The Heroes of CRISPR. Cell 164, 18–28.
- Langmead, B., Salzberg, S.L., 2012. Fast gapped-read alignment with Bowtie 2. Nat. Methods 9, 357–359.
- Le Bail, O., Schmidt-Ullrich, R., Israël, A., 1993. Promoter analysis of the gene encoding the I kappa B-alpha/MAD3 inhibitor of NF-kappa B: positive regulation by members of the rel/NF-kappa B family. EMBO J. 12, 5043–5049.
- Lenardo, M.J., Fan, C.M., Maniatis, T., Baltimore, D., 1989. The involvement of NF-κB in β-interferon gene regulation reveals its role as

widely inducible mediator of signal transduction. Cell 57, 287–294.
- Lin, J., Vora, M., Kane, N.S., Gleason, R.J., Padgett, R.W., 2019. Human marfan and marfan-like syndrome associated mutations lead to altered trafficking of the type II TGFβ receptor in *Caenorhabditis elegans*. PLoS One 14, 1–20.
- Lin, R., Beauparlant, P., Makris, C., Meloche, S., Hiscott, J., 1996. Phosphorylation of IkappaBalpha in the C-terminal PEST domain by casein kinase II affects intrinsic protein stability. Mol. Cell. Biol. 16, 1401–1409.
- Lisa Timmons, Andrew Fire, 1998. Specific interference by ingested dsRNA. Nature 395, 854.
- Liu, T., Rechtsteiner, A., Egelhofer, T.A., Vielle, A., Latorre, I., Cheung, M.-S.S., Ercan, S., Ikegami, K., et al., 2011. Broad chromosomal domains of histone modification patterns in *C. elegans*. Genome Res. 21, 227–236.
- Loiarro, M., Gallo, G., Fantò, N., De Santis, R., Carminati, P., Ruggiero, V., Sette, C., 2009. Identification of critical residues of the MyD88 death domain involved in the recruitment of downstream kinases. J. Biol. Chem. 284, 28093–28103.
- Lott, B.B., Wang, Y., Nakazato, T., 2013. A comparative study of ribosomal proteins: Linkage between amino acid distribution and ribosomal assembly. BMC Biophys. 6.
- Love, M.I., Huber, W., Anders, S., 2014. Moderated estimation of fold change and dispersion for RNA-seq data with DESeq2. Genome Biol. 15, 1–21.
- Ludewig, A.H., Klapper, M., Döring, F., 2014. Identifying evolutionarily conserved genes in the dietary restriction response using bioinformatics and subsequent testing in *Caenorhabditis elegans*. Genes Nutr. 9.
- Luo, J., Kamata, H., Karin, M., Luo, J., Kamata, H., Karin, M., 2005. IKK /NF-κB signaling : balancing life and death – a new approach to cancer therapy Find the latest version : Review series IKK/NF-κB signaling : balancing life and death — a new approach to cancer therapy. J. Clin. Invest. 115, 2625–32.
- Maddox, P.S., Oegema, K., Desai, A., Cheeseman, I.M., 2004. “Holo”er than thou: Chromosome segregation and kinetochore function in *C. elegans*. Chromosom. Res. 12, 641–653.
- Markaki, M., Tavernarakis, N., 2010. Modeling human diseases in *Caenorhabditis elegans*. Biotechnol. J. 5, 1261–1276.
- Marruecos, L., Bertran, J., Álvarez-villanueva, D., Floor, M., Villà-freixa, J., Ghosh, G., Bigas, A., 2021. Dynamic association of IκBα to chromatin is regulated by acetylation and cleavage of histone H4. bioRxiv Mol. Biol.
- Marruecos, L., Bertran, J., Guillén, Y., González, J., Batlle, R., López-Arribillaga, E., Garrido, M., Ruiz-Herguido, C., et al., 2020. IκBα deficiency imposes a fetal phenotype to intestinal stem cells. EMBO Rep. 21, 1–18.
- Martin, C., Zhang, Y., 2005. The diverse functions of histone lysine

methylation. Nat. Rev. Mol. Cell Biol. 6, 838–849.
- Mathes, E., O'Dea, E.L., Hoffmann, A., Ghosh, G., 2008. NF-κB dictates the degradation pathway of IκBα. EMBO J. 27, 1357–1367.
- Mattout, A., Gaidatzis, D., Padeken, J., Schmid, C.D., Aeschimann, F., Kalck, V., Gasser, S.M., 2020. LSM2-8 and XRN-2 contribute to the silencing of H3K27me3-marked genes through targeted RNA decay. Nat. Cell Biol. 22, 579–590.
- Mejetta, S., Morey, L., Pascual, G., Kuebler, B., Mysliwiec, M.R., Lee, Y., Shiekhattar, R., Di Croce, L., et al., 2011. Jarid2 regulates mouse epidermal stem cell activation and differentiation. EMBO J. 30, 3635–3646.
- Min, K.W., Lee, S.H., Baek, S.J., 2016. Moonlighting proteins in cancer. Cancer Lett. 370, 108–116.
- Miura, M., Hasegawa, N., Noguchi, M., 2016. The atypical IκB protein I κBNS is important for Toll-like receptor- induced interleukin-10 production in B cells 453–463.
- Mojica, F.J.M., Díez-Villaseñor, C., García-Martínez, J., Soria, E., 2005. Intervening sequences of regularly spaced prokaryotic repeats derive from foreign genetic elements. J. Mol. Evol. 60, 174–182.
- Mojica, F.J.M., Juez, G., Rodriguez-Valera, F., 1993. Transcription at different salinities of *Haloferax mediterranei* sequences adjacent to partially modified PstI sites. Mol. Microbiol. 9, 613–621.
- Mojica, F.J.M., Montoliu, L., 2016. On the Origin of CRISPR-Cas Technology: From Prokaryotes to Mammals. Trends Microbiol. 24, 811–820.
- Mörck, C., Vivekanand, V., Jafari, G., Pilon, M., 2010. *C. elegans ten-1* is synthetic lethal with mutations in cytoskeleton regulators, and enhances many axon guidance defective mutants. BMC Dev. Biol. 10, 1–17.
- Motoyama, M., Yamazaki, S., Eto-Kimura, A., Takeshige, K., Muta, T., 2005. Positive and negative regulation of nuclear factor-κB-mediated transcription by IκB-ζ, an inducible nuclear protein. J. Biol. Chem. 280, 7444–7451.
- Mulder, K.W., Wang, X., Escriu, C., Ito, Y., Schwarz, R.F., Gillis, J., Sirokmány, G., Donati, G., et al., 2012. Diverse epigenetic strategies interact to control epidermal differentiation. Nat. Cell Biol. 14, 753–763.
- Mulero, M.C., Bigas, A., Espinosa, L., 2013a. IκBα beyond the NF-kB dogma. Oncotarget 4, 1550–1551.
- Mulero, M.C., Ferres-Marco, D., Islam, A., Margalef, P., Pecoraro, M., Toll, A., Drechsel, N., Charneco, C., et al., 2013b. Chromatin-bound IκBα regulates a subset of polycomb target genes in differentiation and cancer. Cancer Cell 24, 151–166.
- Nance, J., Frøkjær-Jensen, C., 2019. The *Caenorhabditis elegans* Transgenic Toolbox. Genetics 212, 959–990.
- Nishikori, M., 2005. Classical and Alternative NF-.KAPPA.B Activation Pathways and Their Roles in Lymphoid Malignancies. J. Clin. Exp. Hematop. 45, 15–24.
- O'Dea, E.L., Barken, D., Peralta, R.Q., Tran, K.T., Werner, S.L.,

Kearns, J.D., Levchenko, A., Hoffmann, A., 2007. A homeostatic model of IκB metabolism to control constitutive NF-κB activity. Mol. Syst. Biol. 3.
- O'Neill, L.A.J., Bowie, A.G., 2007. The family of five: TIR-domain-containing adaptors in Toll-like receptor signalling. Nat. Rev. Immunol. 7, 353–364.
- Ohno, H., Takimoto, G., McKeithan, T.W., 1990. The candidate proto-oncogene *bcl-3* is related to genes implicated in cell lineage determination and cell cycle control. Cell 60, 991–997.
- Okamoto, K., Iwai, Y., Oh-Hora, M., Yamamoto, M., Morio, T., Aoki, K., Ohya, K., Jetten, A.M., et al., 2010. IκBζ regulates TH 17 development by cooperating with ROR nuclear receptors. Nature 464, 1381–1385.
- Packer, J.S., Zhu, Q., Huynh, C., Sivaramakrishnan, P., Preston, E., Dueck, H., Stefanik, D., Tan, K., et al., 2019. A lineage-resolved molecular atlas of *C. elegans* embryogenesis at single-cell resolution. Science (80-.). 365, eaax1971.
- Pando, M.P., Verma, I.M., 2000. Signal-dependent and -independent degradation of free and NF-κb-bound IκBα. J. Biol. Chem. 275, 21278–21286.
- Partridge, F.A., Gravato-Nobre, M.J., Hodgkin, J., 2010. Signal transduction pathways that function in both development and innate immunity. Dev. Dyn. 239, 1330–1336.
- Pasini, D., Di Croce, L., 2016. Emerging roles for Polycomb proteins in cancer. Curr. Opin. Genet. Dev. 36, 50–58.
- Patel, T., Tursun, B., Rahe, D.P., Hobert, O., 2012. Removal of Polycomb Repressive Complex 2 Makes *C. elegans* Germ Cells Susceptible to Direct Conversion into Specific Somatic Cell Types. Cell Rep. 2, 1178–1186.
- Perkins, N.D., 2013. Emerging from NF-κB's Shadow, SUMOylated IκBα represses transcription. Cancer Cell 24, 139–140.
- Pires-daSilva, A., Sommer, R.J., 2003. The evolution of signalling pathways in animal development. Nat. Rev. Genet. 4, 39–49.
- Porta-de-la-Riva, M., Fontrodona, L., Villanueva, A., Cerón, J., 2012. Basic *Caenorhabditis elegans* Methods: Synchronization and Observation. J. Vis. Exp. 1–9.
- Praitis, V., Casey, E., Collar, D., Austin, J., 2001. Creation of low-copy integrated transgenic lines in *Caenorhabditis elegans*. Genetics 157, 1217–1226.
- Pujol, N., Link, E.M., Liu, L.X., Kurz, C.L., Alloing, G., Tan, M.W., Ray, K.P., Solari, R., et al., 2001. A reverse genetic analysis of components of the Toll signaling pathway in *Caenorhabditis elegans*. Curr. Biol. 11, 809–821.
- Rao, P., Hayden, M.S., Long, M., Scott, M.L., West, A.P., Zhang, D., Oeckinghaus, A., Lynch, C., et al., 2010. IκBβ acts to inhibit and activate gene expression during the inflammatory response. Nature 466, 1115–1119.
- Rechtsteiner, A., Ercan, S., Takasaki, T., Phippen, T.M., Egelhofer, T.A., Wang, W., Kimura, H., Lieb, J.D., et al., 2010. The Histone H3K36

Methyltransferase MES-4 acts epigenetically to transmit the memory of germline gene expression to progeny. PLoS Genet. 6.
- Ren, J., Gao, X., Jin, C., Zhu, M., Wang, X., Shaw, A., Wen, L., Yao, X., et al., 2009. Systematic study of protein sumoylation: Development of a site-specific predictor of SUMOsp 2.0. Proteomics 9, 3409–3412.
- Ross, J.M., Zarkower, D., 2003. Polycomb group regulation of Hox gene expression in C. elegans. Dev. Cell 4, 891–901.
- Rual, J.F., Ceron, J., Koreth, J., Hao, T., Nicot, A.S., Hirozane-Kishikawa, T., Vandenhaute, J., Orkin, S.H., et al., 2004. Toward improving *Caenorhabditis elegans* phenome mapping with an ORFeome-based RNAi library. Genome Res. 14, 2162–2168.
- Ruan, J., Li, H., Chen, Z., Coghlan, A., Coin, L.J.M., Guo, Y., Hériché, J.K., Hu, Y., et al., 2008. TreeFam: 2008 Update. Nucleic Acids Res. 36, 735–740.
- Ruland, J., Hartjes, L., 2019. CARD–BCL-10–MALT1 signalling in protective and pathological immunity. Nat. Rev. Immunol. 19, 118–134.
- Russ, B.E., Denton, A.E., Hatton, L., Croom, H., Olson, M.R., Turner, S.J., 2012. Defining the molecular blueprint that drives CD8+T cell differentiation in response to infection. Front. Immunol. 3, 1–11.
- Saccani, S., Pantano, S., Natoli, G., 2003. Modulation of NF-κB activity by exchange of dimers. Mol. Cell 11, 1563–1574.
- Sarov, M., Murray, J.I., Schanze, K., Pozniakovski, A., Niu, W., Angermann, K., Hasse, S., Rupprecht, M., et al., 2012. A genome-scale resource for in vivo tag-based protein function exploration in *C. elegans.* Cell 150, 855–866.
- Scheibel, M., Klein, B., Merkle, H., Schulz, M., Fritsch, R., Greten, F.R., Arkan, M.C., Schneider, G., et al., 2010. IκBβ is an essential co-activator for LPS-induced IL-1β transcription in vivo. J. Exp. Med. 207, 2621–2630.
- Schierenberg, E., Miwa, J., von Ehrenstein, G., 1980. Cell lineages and developmental defects of temperature-sensitive embryonic arrest mutants in *Caenorhabditis elegans*. Dev. Biol. 76, 141–159.
- Schreiber, F., Patricio, M., Muffato, M., Pignatelli, M., Bateman, A., 2014. TreeFam v9: A new website, more species and orthology-on-the-fly. Nucleic Acids Res. 42, 922–925.
- Schulenburg, H., Ewbank, J.J., 2007. The genetics of pathogen avoidance in *Caenorhabditis elegans*. Mol. Microbiol. 66, 563–570.
- Schulenburg, H., Félix, M.A., 2017. The natural biotic environment of *Caenorhabditis elegans.* Genetics 206, 55–86.
- Schuster, M., Annemann, M., Plaza-Sirvent, C., Schmitz, I., 2013. Atypical IκB proteins - Nuclear modulators of NF-κB signaling. Cell Commun. Signal. 11, 1–11.
- Sen, R., 2011. The origins of NF-κB. Nat. Immunol.
- Sen, R., Baltimore, D., 1986a. Multiple Nuclear Factors Interact with the Immunoglobulin Enhancer Sequences, Cell.
- Sen, R., Baltimore, D., 1986b. Inducibility of κ immunoglobulin enhancer-binding protein NF-κB by a posttranslational mechanism. Cell 47, 921–928.

- Senftleben, U., Cao, Y., Xiao, G., Greten, F.R., Krähn, G., Bonizzi, G., Chen, Y., Hu, Y., et al., 2001. Activation by IKKα of a second, evolutionary conserved, NF-κB signaling pathway. Science (80-.). 293, 1495–1499.
- Serrat, X., Kukhtar, D., Cornes, E., Esteve-Codina, A., Benlloch, H., Cecere, G., Cerón, J., 2019. CRISPR editing of sftb-1/SF3B1 in *Caenorhabditis elegans* allows the identification of synthetic interactions with cancer-related mutations and the chemical inhibition of splicing. PLoS Genet. 15, 1–24.
- Shi, Y., Whetstine, J.R., 2007. Dynamic Regulation of Histone Lysine Methylation by Demethylases. Mol. Cell 25, 1–14.
- Shih, R.H., Wang, C.Y., Yang, C.M., 2015. NF-kappaB signaling pathways in neurological inflammation: A mini review. Front. Mol. Neurosci. 8, 1–8.
- Shirane, M., Hatakeyama, S., Hattori, K., Nakayama, K., Nakayama, K.I., 1999. Common pathway for the ubiquitination of IκBα, Iκbβ, and IκBε mediated by the F-box protein FWD1. J. Biol. Chem. 274, 28169–28174.
- Siebenlist, U., Franzoso, G., Brown, K., 1994. Structure, regulation and function of NF-κB. Annu. Rev. Cell Biol. 10, 405–455.
- Siebold, A.P., Banerjee, R., Tie, F., Kiss, D.L., Moskowitz, J., Harte, P.J., 2010. Polycomb Repressive Complex 2 and Trithorax modulate *Drosophila* longevity and stress resistance. Proc. Natl. Acad. Sci. U. S. A. 107, 169–174.
- Steinbrecher, K.A., Harmel-Laws, E., Sitcheran, R., Baldwin, A.S., 2008. Loss of Epithelial RelA Results in Deregulated Intestinal Proliferative/Apoptotic Homeostasis and Susceptibility to Inflammation. J. Immunol. 180, 2588–2599.
- Stemmer, M., Thumberger, T., Del Sol Keyer, M., Wittbrodt, J., Mateo, J.L., 2015. CCTop: An intuitive, flexible and reliable CRISPR/Cas9 target prediction tool. PLoS One 10, 1–11.
- Sternberg, S.H., Redding, S., Jinek, M., Greene, E.C., Doudna, J.A., 2014. DNA interrogation by the CRISPR RNA-guided endonuclease Cas9. Nature 507, 62–67.
- Stiernagle, T., 2006. Maintenance of *C. elegans*. WormBook 1–11.
- Sulston, J.E., Horvitz, H.R., 1977. Post-embryonic cell lineages of the nematode, *Caenorhabditis elegans*. Dev. Biol. 56, 110–156.
- Sulston, J.E., Schierenberg, E., White, J.G., Thomson, J.N., 1983. The embryonic cell lineage of the nematode *Caenorhabditis elegans*. Dev. Biol. 100, 64–119.
- Sumiyoshi, E., Takahashi, S., Obata, H., Sugimoto, A., Kohara, Y., 2011. The β-catenin HMP-2 functions downstream of Src in parallel with the Wnt pathway in early embryogenesis of *C. elegans*. Dev. Biol. 355, 302–312.
- Sun, S.C., Ganchi, P.A., Ballard, D.W., Greene, W.C., 1993. NF-κB controls expression of inhibitor IκBα: Evidence for an inducible autoregulatory pathway. Science (80-.). 259, 1912–1915.
- Swigut, T., Wysocka, J., 2007. H3K27 Demethylases, at Long Last. Cell

131, 29–32.
- Tabara, H., Grishok, A., Mello, C.C., 1998. RNAi in *C. elegans*: Soaking in the Genome Sequence. Science (80-.). 282, 430 LP – 431.
- Tenen, C.C., Greenwald, I., 2019. Cell Non-autonomous Function of daf-18/PTEN in the Somatic Gonad Coordinates Somatic Gonad and Germline Development in *C. elegans* Dauer Larvae. Curr. Biol. 29, 1064-1072.e8.
- Tenor, J.L., Aballay, A., 2008. A conserved Toll-like receptor is required for *Caenorhabditis elegans* innate immunity. EMBO Rep. 9, 103–109.
- The *C. elegans* Sequencing Consortium, 1998. Genome Sequence of the Nematode *C. elegans*: A Platform for Investigating Biology. Science (80-.). 282, 2012–2018.
- Tie, F., Banerjee, R., Fu, C., Stratton, C.A., Fang, M., Harte, P.J., 2016. Polycomb inhibits histone acetylation by CBP by binding directly to its catalytic domain. Proc. Natl. Acad. Sci. U. S. A. 113, E744–E753.
- Timmons, L., Court, D.L., Fire, A., 2001. Ingestion of bacterially expressed dsRNAs can produce specific and potent genetic interference in *Caenorhabditis elegans*. Gene 263, 103–112.
- Topf, U., Drabikowski, K., 2019. Ancient Function of Teneurins in Tissue Organization and Neuronal Guidance in the Nematode *Caenorhabditis elegans*. Front. Neurosci. 13, 1–7.
- Toshchakov, V.Y., Szmacinski, H., Couture, L.A., Lakowicz, J.R., Vogel, S.N., 2011. Targeting TLR4 Signaling by TLR4 Toll/IL-1 Receptor Domain-Derived Decoy Peptides: Identification of the TLR4 Toll/IL-1 Receptor Domain Dimerization Interface. J. Immunol. 186, 4819–4827.
- Truhlar, S.M.E., Mathes, E., Cervantes, C.F., Ghosh, G., Komives, E.A., 2008. Pre-folding IκBα Alters Control of NF-κB Signaling. J. Mol. Biol. 380, 67–82.
- Trzebiatowska, A., Topf, U., Sauder, U., Drabikowski, K., Chiquet-Ehrismann, R., 2008. *Caenorhabditis elegans* teneurin, *ten-1*, is required for gonadal and pharyngeal basement membrane integrity and acts redundantly with integrin ina-1 and dystroglycan dgn-1. Mol. Biol. Cell 19, 3898–3908.
- Tucker, R.P., Chiquet-Ehrismann, R., 2006. Teneurins: A conserved family of transmembrane proteins involved in intercellular signaling during development. Dev. Biol. 290, 237–245.
- Tursun, B., 2017. PcG Proteins in *Caenorhabditis elegans*, Polycomb Group Proteins. Elsevier Inc.
- Uhlen, M., Oksvold, P., Fagerberg, L., Lundberg, E., Jonasson, K., Forsberg, M., Zwahlen, M., Kampf, C., et al., 2010. Towards a knowledge-based Human Protein Atlas. Nat. Biotechnol. 28, 1248–1250.
- Uhlen, M., Zhang, C., Lee, S., Sjöstedt, E., Fagerberg, L., Bidkhori, G., Benfeitas, R., Arif, M., et al., 2017. A pathology atlas of the human cancer transcriptome. Science (80-.). 357.
- Van Auken, K., Weaver, D., Robertson, B., Sundaram, M., Saldi, T., Edgar, L., Elling, U., Lee, M., et al., 2002. Roles of the

homethorax/Meis/Prep homolog UNC-62 and the Exd/Pbx homologs CEH-20 and CEH-40 in *C. elegans* embryogenesis. Development 129, 5255–5268.
- Van Auken, K., Weaver, D.C., Edgar, L.G., Wood, W.B., 2000. *Caenorhabditis elegans* embryonic axial patterning requires two recently discovered posterior-group Hox genes. Proc. Natl. Acad. Sci. U. S. A. 97, 4499–4503.
- Vandamme, J., Lettier, G., Sidoli, S., Di Schiavi, E., Nørregaard Jensen, O., Salcini, A.E., 2012. The C. elegans H3K27 demethylase UTX-1 is essential for normal development, independent of its enzymatic activity. PLoS Genet. 8, 1–16.
- Vandamme, J., Sidoli, S., Mariani, L., Friis, C., Christensen, J., Helin, K., Jensen, O.N., Salcini, A.E., 2015. H3K23me2 is a new heterochromatic mark in *Caenorhabditis elegans*. Nucleic Acids Res. 43, 9694–9710.
- Verghese, E., Schocken, J., Jacob, S., Wimer, A.M., Royce, R., Nesmith, J.E., Baer, G.M., Clever, S., et al., 2011. The tailless ortholog nhr-67 functions in the development of the *C. elegans* ventral uterus. Dev. Biol. 356, 516–528.
- Viatour, P., Merville, M.P., Bours, V., Chariot, A., 2005. Phosphorylation of NF-κB and IκB proteins: Implications in cancer and inflammation. Trends Biochem. Sci. 30, 43–52.
- Vicencio, J., Cerón, J., 2021. A Living Organism in your CRISPR Toolbox: *Caenorhabditis elegans* Is a Rapid and Efficient Model for Developing CRISPR-Cas Technologies. Cris. J. crispr.2020.0103.
- Vicencio, J., Martínez-Fernández, C., Serrat, X., Cerón, J., 2019. Efficient Generation of Endogenous Fluorescent Reporters by Nested CRISPR in *Caenorhabditis elegans* , Genetics.
- Walton, T., Preston, E., Nair, G., Zacharias, A.L., Raj, A., Murray, J.I., 2015. The Bicoid Class Homeodomain Factors ceh-36/OTX and unc-30/PITX Cooperate in *C. elegans* Embryonic Progenitor Cells to Regulate Robust Development. PLoS Genet. 11.
- Wang, X., Peng, H., Huang, Y., Kong, W., Cui, Q., Du, J., Jin, H., 2020. Post-translational Modifications of IκBα: The State of the Art. Front. Cell Dev. Biol. 8, 1–15.
- Wani, K.A., Goswamy, D., Irazoqui, J.E., 2020. Nervous system control of intestinal host defense in *C. elegans*. Curr. Opin. Neurobiol. 62, 1–9.
- Wani, K.A., Goswamy, D., Irazoqui, J.E., 2019. A Nutrition-Longevity Tradeoff Enforced by Innate Immunity. Mol. Cell 74, 864–865.
- Waterston, R., Thompson, O., Edgley, M., Strasbourger, P., Flibotte, S., Ewing, B., Adair, R., Au, V., et al., 2013. The Million Mutation Project: A new approach to genetics in *Caenorhabditis elegans*. Genome Res. 1749–1762.
- White, J.G., Southgate, E., Thomson, J.N., Brenner, S., 1986. The structure of the nervous system of the nematode *Caenorhabditis elegans*. Philos. Trans. R. Soc. London. B, Biol. Sci. 314, 1–340.
- Wiles, E.T., Selker, E.U., 2017. H3K27 methylation: a promiscuous repressive chromatin mark. Curr. Opin. Genet. Dev. 43, 31–37.

- Wong, M.C., Schwarzbauer, J.E., 2012. Gonad morphogenesis and distal tip cell migration in the *Caenorhabditis elegans* hermaphrodite. Wiley Interdiscip. Rev. Dev. Biol. 1, 519–531.
- Wong, M.C., Schwarzbauer, J.E., Wong, Ming-Ching & Schwarzbauer, J.E., 2012. Gonad morphogenesis and distal tip cell migration in the *Caenorhabditis elegans* hermaphrodite. Wiley Interdiscip. Rev. Dev. Biol. 1, 519–531.
- Xu, L., Massagué, J., 2004. Nucleocytoplasmic shuttling of signal transducers. Nat. Rev. Mol. Cell Biol. 5, 209–219.
- Yamamoto, Y., Gaynor, R.B., 2004. IκB kinases: Key regulators of the NF-κB pathway. Trends Biochem. Sci. 29, 72–79.
- Yamauchi, S., Ito, H., Miyajima, A., 2010. IκBη, a nuclear IκB protein, positively regulates the NF-κB-mediated expression of proinflammatory cytokines. Proc. Natl. Acad. Sci. U. S. A. 107, 11924–11929.
- Yaron, A., Gonen, H., Alkalay, I., Hatzubai, A., Jung, S., Beyth, S., Mercurio, F., Manning, A.M., et al., 1997. Inhibition of NF-κB cellular function via specific targeting of the IκB-ubiquitin ligase. EMBO J. 16, 6486–6494.
- Yazdi, S., Durdagi, S., Naumann, M., Stein, M., 2015. Structural modeling of the N-terminal signal-receiving domain of IκBα. Front. Mol. Biosci. 2, 1–16.
- Yazdi, S., Naumann, M., Stein, M., 2017. Double phosphorylation-induced structural changes in the signal-receiving domain of IκBα in complex with NF-κB. Proteins Struct. Funct. Bioinforma. 85, 17–29.
- Yemini, E., Lin, A., Nejatbakhsh, A., Varol, E., Sun, R., Mena, G.E., Samuel, A.D.T., Paninski, L., et al., 2021. NeuroPAL: A Multicolor Atlas for Whole-Brain Neuronal Identification in *C. elegans*. Cell 184, 272-288.e11.
- Yoshimura, J., Ichikawa, K., Shoura, M.J., Artiles, K.L., Gabdank, I., Wahba, L., Smith, C.L., Edgley, M.L., et al., 2019. Recompleting the *Caenorhabditis elegans* genome. Genome Res. 29, 1009–1022.
- Yu, G., Wang, L.G., He, Q.Y., 2015. ChIP seeker: An R/Bioconductor package for ChIP peak annotation, comparison and visualization. Bioinformatics 31, 2382–2383.
- Yumerefendi, H., Dickinson, D.J., Wang, H., Zimmerman, S.P., Bear, J.E., Goldstein, B., Hahn, K., Kuhlman, B., 2015. Control of protein activity and cell fate specification via light-mediated nuclear translocation. PLoS One 10, 1–19.
- Yuzyuk, T., Fakhouri, T.H.I., Kiefer, J., Mango, S.E., 2009. The Polycomb Complex Protein mes-2/E(z) Promotes the Transition from Developmental Plasticity to Differentiation in *C. elegans* Embryos. Dev. Cell 16, 699–710.
- Zabel, U., Henkel, T., Silva, M.S., Baeuerle, P.A., 1993. Nuclear uptake control of NF-kappa B by MAD-3, an I kappa B protein present in the nucleus. EMBO J. 12, 201–211.
- Zhang, Q., Didonato, J.A., Karin, M., McKeithan, T.W., 1994. BCL3 encodes a nuclear protein which can alter the subcellular location of NF-kappa B proteins. Mol. Cell. Biol. 14, 3915–3926.

- Zhang, Q., Lenardo, M.J., Baltimore, D., 2017. 30 Years of NF-κB: A Blossoming of Relevance to Human Pathobiology. Cell 168, 37–57.
- Zhang, X., Zabinsky, R., Teng, Y., Cui, M., Han, M., 2011. microRNAs play critical roles in the survival and recovery of *Caenorhabditis elegans* from starvation-induced L1 diapause. Proc. Natl. Acad. Sci. U. S. A. 108, 17997–18002.
- Zhang, Y., Liu, T., Meyer, C.A., Eeckhoute, J., Johnson, D.S., Bernstein, B.E., Nussbaum, C., Myers, R.M., et al., 2008. Model-based analysis of ChIP-Seq (MACS). Genome Biol. 9.
- Zhao, Q., Xie, Y., Zheng, Y., Jiang, S., Liu, W., Mu, W., Liu, Z., Zhao, Y., et al., 2014. GPS-SUMO: A tool for the prediction of sumoylation sites and SUMO-interaction motifs. Nucleic Acids Res. 42, 1–6.
- Zhao, Z., Boyle, T.J., Liu, Z., Murray, J.I., Wood, W.B., Waterston, R.H., 2010. A negative regulatory loop between MicroRNA and Hox Gene controls posterior identities in *Caenorhabditis elegans*. PLoS Genet. 6.

LIST OF PUBLICATIONS

LIST OF PUBLICATIONS

- **Brena, D.**, Bertran, J., Porta-de-la-Riva, M., Guillén, Y., Cornes, E., Kukhtar, D., Campos-Vicens, L., Fernández, L., Pecharroman, I., García-López, A., Islam, A. B. M. M. K., Marruecos, L., Bigas, A., Cerón, J., & Espinosa, L. (2020). Ancestral function of Inhibitors-of-kappaB regulates *Caenorhabditis elegans* development. *Scientific Reports*, *10*(1). https://doi.org/10.1038/s41598-020-73146-5

- García-Rodríguez, F. J., Martínez-Fernández, C., **Brena, D**., Kukhtar, D., Serrat, X., Nadal, E., Boxem, M., Honnen, S., Miranda-Vizuete, A., Villanueva, A., & Cerón, J. (2018). Genetic and cellular sensitivity of *Caenorhabditis elegans* to the chemotherapeutic agent cisplatin. *Disease Models & Mechanisms*, *11*(6), dmm033506. https://doi.org/10.1242/dmm.033506

ANNEX

ANNEX

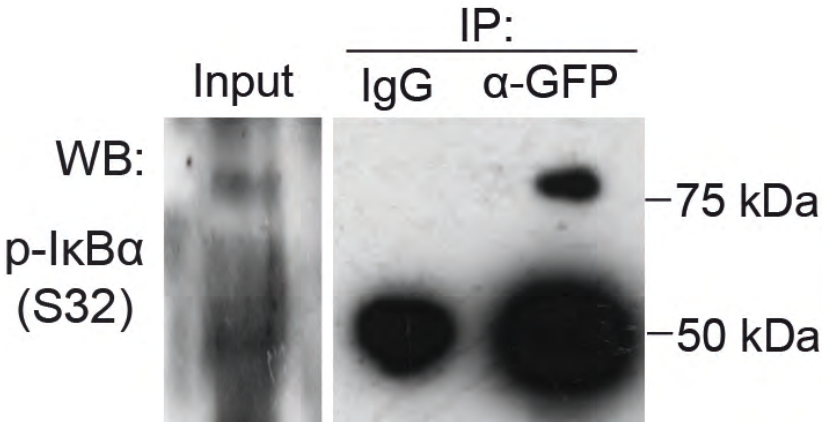

Annex R1. Western blot analysis using the anti-p-S32-IκBα of *C. elegans* protein lysates of endogenous *EGFP::nfki-1* strain (L4 stage) precipitated with α-GFP antibody. IgG precipitation is included as specificity control.

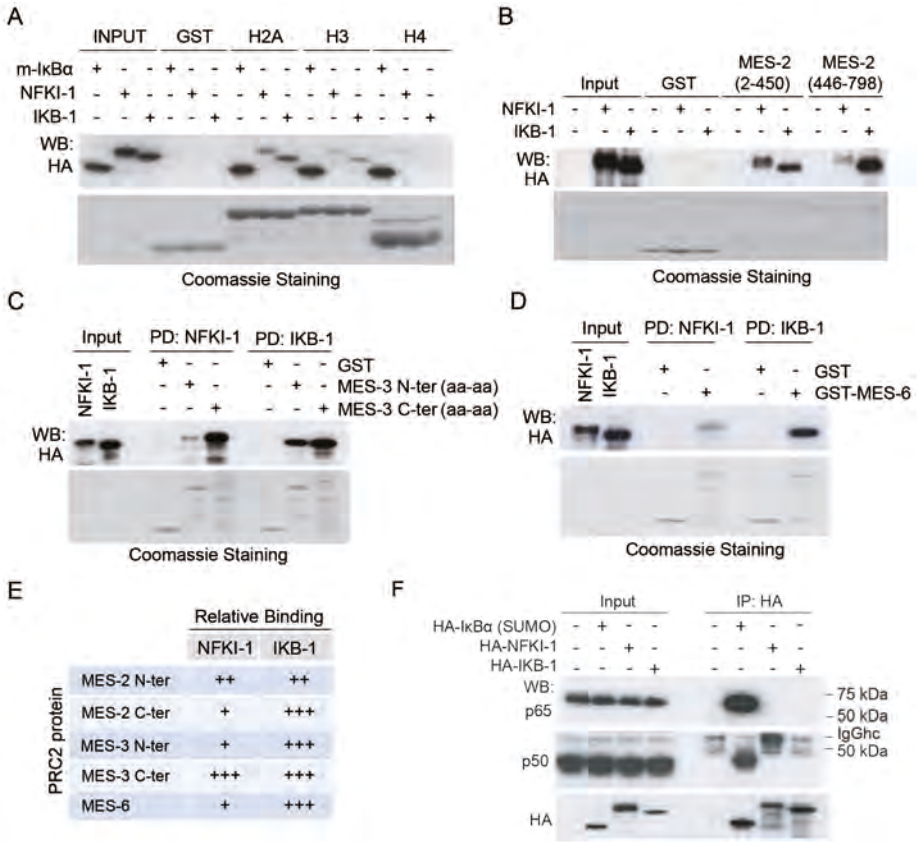

Annex R2. *C. elegans* IκBs physically interact with histones and PRC2 proteins, but not mammalian NF-κB proteins *in vitro*. (A) Pull-down assay using HA-tagged NFKI-1, IKB-1 or mammalian SUMO-IκBα expressed in HEK-293T cells and the indicated GST-fusion histone constructs as bait (B-D) Pull-down assays from HA-tagged NFKI-1 or IKB-1 containing extracts using GST-fusion proteins containing the indicated fragments of MES-2 (B), MES-3 (C) or MES-6 (D). (E) Summary of the data shown in B-D. (F) Extracts from HEK-293T cells transfected with HA-tagged human SUMO-IκBα or *C. elegans* NFKI-1 and IKB-1 were used in co-immunoprecipitation experiments to measure association with the NF-κB proteins p65/RelA and p50. Western blot analysis of a representative experiment is shown.

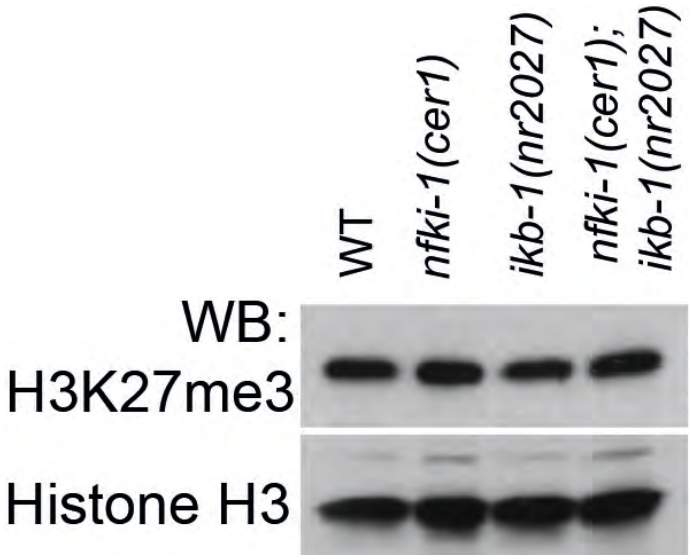

Annex R3. Western blot analysis of total protein lysates of L4 worms with the indicated genotypes using an H3K27me3 antibody. Histone H3 is used as a control.

Annex M1. List of strains used in this thesis.

Strain	Genotype
AX6142	*npr-1(ad609); nfki-1(db1198); dbIs[nfki-1p::nfki-1::gfp; ccRFP]*
AX6670	*ttTi5605 II; unc-119(ed3) III; npr-1(ad609) nfki-1(db1198); MosSCI[unc-119(+); nfki-1p::nfki-1::unc-54 3'UTR]*
BN148	*emr-1(gk119) I; bqSi143[pBN20(unc-119(+) emr-1p::emr-1::mCherry)] II*
BN426	*mel-28(bq5[GFP::mel-28]) III*
BN903	*mel-28(bq6[mkate2::mel-28]) III*
CER144	*cerIs03[fosmidC33A11.1gfp+unc-119(+)]*
CER146	*cerIs04[fosmidC33A11.1gfp+unc-119(+)]*
CER147	*cerEx35[fosmidC33A11.1gfp+unc-119(+)]*
CER178	*nfki-1(cer1) X*
CER185	*ikb-1(nr2027) I*
CER187	*nfki-1(cer2) X*
CER188	*ikb-1(nr2027) I; nfki-1(cer1) X*
CER244	*ikb-1(cer9) I*
CER245	*ikb-1(cer9) I; nfki-1(cer1) X*
CER246	*ikb-1(cer9) I; nfki-1(cer2) X*
CER281	*nfki-1(cer2)* X; *stIs10286*[*nob-1::GFP::unc-54 3'UTR + rol-6(su1006)*]
CER282	*ikb-1(cer9)* I; *nfki-1(cer2)* X; *stIs10286*[*nob-1::GFP::unc-54 3'UTR + rol-6(su1006)*]
CER283	*ikb-1(cer9)* I; *stIs10286*[*nob-1::GFP::unc-54 3'UTR + rol-6(su1006)*]
CER284	*nfki-1(cer2)* X; *wgIs27*[*mab-5::TY1::EGFP::3xFLAG + unc-119(+)*]
CER285	*ikb-1(cer9)* I; *nfki-1(cer2)* X; *wgIs27*[*mab-5::TY1::EGFP*::*3xFLAG + unc-119(+)*]
CER286	*ikb-1(cer9)* I; *wgIs27*[*mab-5::TY1::EGFP*::*3xFLAG + unc-119(+)*]
CER287	*nfki-1(cer2)* X; *bxIs13*[*egl-5::GFP + lin-15(+)*]
CER288	*ikb-1(cer9)* I; *nfki-1(cer2)* X; *bxIs13*[*egl-5::GFP + lin-15(+)*]
CER289	*ikb-1(cer9)* I; *bxIs13*[*egl-5::GFP + lin-15(+)*]
CER290	*nfki-1(cer2)* X; *wgIs54*[*egl-5::TY1::EGFP*::*3xFLAG + unc-119(+)*]

CER291	*ikb-1(cer9)* I; *nfki-1(cer2)* X; *wgIs54*[*egl-5::TY1::EGFP*::*3xFLAG + unc-119(+)*]
CER292	*ikb-1(cer9)* I; *wgIs54*[*egl-5::TY1::EGFP::3xFLAG + unc-119(+)*]
CER293	*nfki-1(cer2)* X; *stIs10224*[*lin-39::H1-wCherry + unc-119(+)*]
CER294	*nfki-1(cer2)* X*; ikb-1(cer9)* I; *stIs10224*[*lin-39::H1-wCherry + unc-119(+)*]
CER295	*ikb-1(cer9)* I; stIs10224 [*lin-39::H1-wCherry + unc-119(+)*]
CER281	*nfki-1(cer2)* X; stIs10286 [*nob-1::GFP*::unc-54 3'UTR + *rol-6(su1006)*]
CER321	*ikb-1(cer9) I; qIs19[lag-2p::GFP::unc-54 3'UTR + rol-6(su1006)]* V*; nfki-1(cer2)* X
CER324	*qIs19[lag-2p::GFP::unc-54 3'UTR + rol-6(su1006)]* V*; nfki-1(cer2)* X
CER325	*ikb-1 (cer9)* I*; qIs19[lag-2p::GFP::unc-54 3'UTR + rol-6(su1006)]* V
CER414	*pgl-1(cer70[pgl-1::mCherry])* IV
CER415	*pgl-1(cer71[pgl-1::mCherry]* IV
CER424	*nfki-1(cer102[nfki-1::3xFLAG)])* X
CER425	*ikb-1(syb267[ikb-1::mCherry])* I*; nfki-1(cer102[nfki-1::3xFLAG)])* X
CER458	*nfki-1(cer2)* X*; pkIs1582[let-858::GFP + rol-6(su1006)]*
CER459	*ikb-1(cer9)* I*; pkIs1582[let-858::GFP + rol-6(su1006)]*
CER461	*nfki-1(cer116[EGFP::nfki-1])* X
CER466	*ikb-1(cer9)* I*; nfki-1(cer2)* X*; pkIs1582[let-858::GFP + rol-6(su1006)]*
CER467	*nfki-1(cer120[EGFP::nfki-1])* X
CER469	*nfki-1(cer121[EGFP1-3::nfki-1])* X
CER474	*pgl-1(cer70[pgl-1::mCherry])* IV*; nfki-1(cer2)* X
CER475	*ikb-1(cer9)* I*; pgl-1(cer70[pgl-1::mCherry])* IV
CER476	*ikb-1(cer9)* I*; pgl-1(cer70[pgl-1::mCherry])* IV*; nfki-1(cer2)* X
CER477	*nfki-1(cer2)* X*; mes-2(ax2059[mes-2::GFP])* II
CER478	*ikb-1(cer9)* I*; mes-2(ax2059[mes-2::GFP])* II

CER479	*ikb-1(cer9)* I*; mes-2(ax2059[mes-2::GFP])* II*; nfki-1(cer2)* X
CER480	*mes-4(sal9[mes-4::GFP::3xFLAG::mes-4 3′ UTR])* V*; nfki-1(cer2)* X
CER481	*ikb-1(cer9)* I*; mes-4(sal9[mes-4::GFP::3xFLAG::mes-4 3′ UTR])* V
CER482	*ikb-1(cer9)* I*; mes-4(sal9[mes-4::GFP::3xFLAG::mes-4 3′ UTR])* V*; nfki-1(cer2)* X
CER485	*deps-1(ax2063[deps-1::GFP])* I*; nfki-1(cer2)* X
CER486	*ikb-1(cer9)* I*; deps-1(ax2063[deps-1::GFP])* I
CER487	*ikb-1(cer9)* I*; deps-1(ax2063[deps-1::GFP])* I*; nfki-1(cer2)* X
CER488	*nfki-1(cer2)* X*; mex-6(ax2065[mex-6::GFP])* II
CER489	*ikb-1(cer9)* I*; mex-6(ax2065[mex-6::GFP])* II
CER490	*ikb-1(cer9)* I*; mex-6(ax2065[mex-6::GFP])* II*; nfki-1(cer2)* X
CER491	*ikb-1(syb267[ikb-1::mCherry])* I*; nfki-1(cer116[EGFP::nfki-1])* X
CER492	*sftb-1(cer114[sftb-1::mCherry])* I*; nfki-1(cer116[EGFP::nfki-1])* X
CER493	*MosSCI[unc-119(+); nfki-1p::nfki-1::unc-54 3'UTR]* II*; nfki-1(cer2)* X
CER509	*ikb-1(syb267[ikb-1::mCherry])* I*; mel-28(bq5[GFP::mel-28])* III
CER523	*daf-2(e1370)* III*; nfki-1(cer116[EGFP::nfki-1])* X
CER524	*ikb-1(syb267[ikb-1::mCherry])* I*; daf-2(e1370)* III
CER525	*ikb-1(syb267[ikb-1::mCherry])* I*; daf-2(e1370)* III*; nfki-1(cer116[EGFP::nfki-1])* X
CER534	*mel-28(bq6[mkate2::mel-28])* III*; nfki-1(cer116[EGFP::nfki-1])* X
CER560	*nfki-1(cer116[EGFP::nfki-1])* X*; mel28(bq6[mKate2::mel-28])* III*; bqSi143[pBN20(unc-119(+) erm-1p::emr-1::mCherry)]* II
CER562	*nfki-1(cer164[nfki-1p::EGFP1-3])* X
CER563	*nfki-1(cer165[nfki-1p::EGFP1-3])* X
CER577	*unc-119(ed3) III; nfki-1(cer2)* X*; cerEx35[fosmidC33A11.1gfp+unc-119(+)]*
CER58	*lsm-3(tm5166)* IV
CER60	*lsm-1(tm3585)* II
JH3203	*mes-2(ax2059[mes-2::GFP])* II
JH3207	*deps-1(ax2063[deps-1::GFP])* I

JH3209	*mex-6(ax2065[mex-6::GFP])* II
JK2049	*qIs19 [lag-2p::GFP::unc-54 3'UTR + rol-6(su1006)]* V
JPM76	*mes-4(sal9[mes-4::GFP::3xFLAG::mes-4 3' UTR])* V
N2	Wild type Bristol strain
NL2507	*pkIs1582[let-858p::GFP:: let-858 3'UTR; rol-6(su1006)]* V
PHX267	*ikb-1(syb267[ikb-1::mCherry])* I

Annex M2. List of primers used in this study.

ID	Sequence (5' - 3')	Target gene	Type	Technique
daf-2(e1370) FW	CGGGATGAGACTGTCAAGATTGGAAGATTTCGG	*daf-2*	Primer FW	PCR
daf-2(e1370) RV	CAACACCTCATCATTACTCAAACCAATCCATG	*daf-2*	Primer RV	PCR
deps-1::GFP FW	TCGGTCTCTGGTGATACGGT	*deps-1*	Primer FW	PCR
deps-1::GFP RV	CTCACGTCTATCGCGATGCT	*deps-1*	Primer RV	PCR
ikb-1(nr2027) FW1	GCGAAAACTGTGTGATCG	*ikb-1*	Primer FW	PCR
ikb-1(nr2027) FW2	ATCGAGATCAGACTCAGAGG	*ikb-1*	Primer FW	PCR

ikb-1(nr2027) int del RV	GAGCTCCACTTCCAATTCTG	*ikb-1*	Primer RV	PCR
RT *ikb-1* 5'UTR FW	ACCCTCATTCTAATATCCTCTCG	*ikb-1*	Primer FW	RT-PCR
RT *ikb-1* exons8-9 FW	CTAGAGAAGAAATATTAAATGACGC	*ikb-1*	Primer FW	RT-PCR
ikb-1(nr2027) RV1	CGACGATGTTGAGGGTCC	*ikb-1*	Primer RV	PCR
RT *ikb-1* exons 2-3 RV	GTTCAGTGGCGTCTCCAG	*ikb-1*	Primer RV	RT-PCR
ikb-1::mCherry FW	TTCTCGCTGAAACTGACTCC	*ikb-1*	Primer FW	PCR
ikb-1::mCherry RV	TGAGTAAGACAGCCATAGGC	*ikb-1*	Primer RV	PCR
ikb-1(cer9) FW	GTCCTCGCGCTCTTTTCCG	*ikb-1*	Primer FW	PCR
ikb-1(cer9) RV	GCGATCACCAGCAGATGC	*ikb-1*	Primer RV	PCR
mel-28 RV	CCCCTCCAACACTCGTATCC	*mel-28*	Primer RV	PCR

mel-28 FW	TGAATGTAGTCGGACGAGCC	*mel-28*	Primer FW	PCR
RT *nfki-1* 3'UTR RV	GATGGCATTATGCAACAACG	*nfki-1*	Primer RV	RT-PCR
RT *nfki-1* exons 9-10 FW	CAATATGGTTGAAGGCCC	*nfki-1*	Primer FW	RT-PCR
nfki-1 5' FW	TATAGTTCAACCGGCAGAG	*nfki-1*	Primer FW	PCR
nfki-1 C-ter SEQ FW	GTGTAGTTCCACCCAGAACG	*nfki-1*	Primer FW	PCR
nfki-1(cer2) RV	CTGTTACGCTGTGCTGGAAA	*nfki-1*	Primer RV	PCR
nfki-1(cer2) FW	CCTGGTTGTCCTTTGCTGTT	*nfki-1*	Primer FW	PCR
GFP JH1986 FW	GCTTCTCGAGATACCCAG	*GFP*	Primer FW	PCR
GFP JH1986 RV	GGTCTGCTAGTTGAACGC	*GFP*	Primer RV	PCR
nfki-1 3'UTR RV	GCTTAACGGTCGTTGTAAGG	*nfki-1*	Primer RV	PCR
nfki-1 ok3681 int FW	ACATGGGTTTGTCCCTTTTT	*nfki-1*	Primer FW	PCR

nfki-1 ok3681 int RV	CCCCCATAATTTTCA TATCACG	*nfki-1*	Primer RV	PCR
EMR-1 3' FW	TTC GTC TTC ATC GCC GTC TT	*emr-1*	Primer FW	PCR
EMR-1 3' RV	AAG ACG GCG ATG AAG ACG AA	*emr-1*	Primer RV	PCR
wrmScarlet Fwd	GTC AGC AAG GGA GAG GCA GTT AT	*wrmScarlet*	Primer FW	PCR
wrmScarlet Rev	CTT GTA GAG CTC GTC CAT TCC T	*wrmScarlet*	Primer RV	PCR
nfki-1 C-ter Fw SEQ	GTG TAG TTC CAC CCA GAA CG	*nfki-1*	Primer FW	PCR
nfki-1 C-ter Fw SEQ 2	TGT CAA CGA AGA CAC GTT CA	*nfki-1*	Primer FW	PCR
nfki-1 C-ter Rv SEQ	TTT AGA CAG GCT TTG CCA AC	*nfki-1*	Primer RV	PCR
nfki-1 Fw (cc1643)	GTC CTT TGC TGT TCT AAT TCT GTC AAG TG	*nfki-1*	Primer FW	PCR

nfki-1 Rv (cc644)	GGA GTG AGA TCA GCG AAC AGA GTC	*nfki-1*	Primer RV	PCR
nfki-1 5' FW	TAT AGT TCA ACC GGC AGA G	*nfki-1*	Primer FW	PCR
nfki-1 5' RV	TGA ATG TCG TGC TGA GAA AT	*nfki-1*	Primer RV	PCR
nfki-1 3' External Rv	TCG AGA GAG AGA GAG GAA G	*nfki-1*	Primer RV	PCR
npr-1(ad609) Fw (cc774)	CAT ATT ATC GCT TCC AAT CAC TCC AAT C	*npr-1*	Primer FW	PCR
npr-1(ad609) Rv (cc775)	GCG GCT ACT TTT GCA CTG AAA A	*npr-1*	Primer RV	PCR
CRISPR *ikb-1* FW	GTCCTCGCGCTCTTT TCCG	*ikb-1*	Primer FW	PCR
CRISPR *ikb-1* RV	GCCCATTCTTCGCTG CC	*ikb-1*	Primer RV	PCR
*mes-4*_FW	AGC TTC ATC TTC AAC ACC AC	*mes-4*	Primer FW	PCR

*mes-4*_RV	GAG TTC AAT TGG GCG AGA CA	*mes-4*	Primer RV	PCR
*ikb-1::mCherry*_ Fw	TTC TCG CTG AAA CTG ACT CC	*ikb-1*	Primer FW	PCR
*ikb-1::mCherry*_ Rv	TGA GTA AGA CAG CCA TAG GC	*ikb-1*	Primer RV	PCR
*mes-2::GFP*_Fw	GCG AAG AGA CGG CTT GAG AT	*mes-2*	Primer FW	PCR
*mes-2::GFP*_Rv	TGG ATC TCG CTG CAA ACT TTC	*mes-2*	Primer RV	PCR
*mex-6::GFP*_Fw	CCT CCA TAT GTA CGT TTC CAT TCG	*mex-6*	Primer FW	PCR
*mex-6::GFP*_Rv	GGT AAA GTA CGC CAG GTT GC	*mex-6*	Primer RV	PCR
ZK813.1 FW	GTCGGGATCCAGTTC ATCCG	*ZK813.1*	Primer FW	ChIP-qPCR
ZK813.1 RV	ATCGTTACCGGTGTT TCCGT	*ZK813.1*	Primer RV	ChIP-qPCR
ZK813.2 FW	TGTGTCCGCCGATGA TTACG	*ZK813.2*	Primer FW	ChIP-qPCR

ZK813.2 RV	TTCGCGGATACGAC GCCTTACTG	*ZK813.2*	Primer RV	ChIP-qPCR
ZK813.3 FW	TCGGACTCCAGAAG CCGTAG	*ZK813.3*	Primer FW	ChIP-qPCR
ZK813.3 RV	TTGAGCTGCTCCACC ATAGG	*ZK813.3*	Primer RV	ChIP-qPCR
ZK813.7 FW	GGCACTATTGACACT TGGGGA	*ZK813.7*	Primer FW	ChIP-qPCR
ZK813.7 RV	GATTGGCCCAGGTTG AGGAC	*ZK813.7*	Primer RV	ChIP-qPCR
C44B12.1 FW	CCTTCCCACTTGTCG GTCTT	*C44B12.1*	Primer FW	ChIP-qPCR
C44B12.1 RV	GGGTTCCGTAGGCTT GTCTC	*C44B12.1*	Primer RV	ChIP-qPCR
C44B12.5 FW	TACAGGCTTCGTATG CGACC	*C44B12.5*	Primer FW	ChIP-qPCR
C44B12.5 RV	GATTAGCTGGGACG GATGGG	*C44B12.5*	Primer RV	ChIP-qPCR
F59D8.1 FW	TCCGCTTTTTGCAAA GTATCAAGA	*F59D8.1*	Primer FW	ChIP-qPCR
F59D8.1 RV	GTTGACCTCAGCCTG GTCTC	*F59D8.1*	Primer RV	ChIP-qPCR
F59D8.2 FW	AGACTCGCGCCAAG GTCA	*F59D8.2*	Primer FW	ChIP-qPCR

F59D8.2 RV	TGGTCCAGAGACCT GAAAGTATTA	*F59D8.2*	Primer RV	ChIP-qPCR
ZK1290.8 FW	CTATATTCCCGCTGC CCTCC	*ZK1290.8*	Primer FW	ChIP-qPCR
ZK1290.8 RV	TGTGCACTGCACTGA GATCCGACAC	*ZK1290.8*	Primer RV	ChIP-qPCR
ZK1290.12 FW	TGATGGCCGTCAAAC TGGAT	*ZK1290.12*	Primer FW	ChIP-qPCR
ZK1290.12 RV	GGAAGGCAGTTCATA CGGGT	*ZK1290.12*	Primer RV	ChIP-qPCR
Y46H3A.1 FW	TCCGCTTGTTTGATC TGC	*Y46H3A.1*	Primer FW	ChIP-qPCR
Y46H3A.1 RV	GAAGAGCAATGGTG GGGTCA	*Y46H3A.1*	Primer RV	ChIP-qPCR
Y46H3A.2 FW	GAAAGCGGGCTCAG AGGAAG	*Y46H3A.2*	Primer FW	ChIP-qPCR
Y46H3A.2 RV	ACAGATCCAGTGAGT TCGTCC	*Y46H3A.2*	Primer RV	ChIP-qPCR
pgl-1 FW	CTACGGGTCTCGAAA CGAAC	*pgl-1*	Primer FW	ChIP-qPCR
pgl-1 RV	TCTCGCTTGTTAGCC TCCAT	*pgl-1*	Primer RV	ChIP-qPCR
glh-1 FW	TAGATCCGGAATCCC ATCAG	*glh-1*	Primer FW	ChIP-qPCR

glh-1 RV	CCATCAGACATTTTC GCAGA	*glh-1*	Primer RV	ChIP-qPCR
gld-1 FW	GAATCGCCGCAGAG TTTAAG	*gld-1*	Primer FW	ChIP-qPCR
gld-1 RV	ATAACGGACGAACGA GATGG	*gld-1*	Primer RV	ChIP-qPCR
glp-1 FW	TTTCGCTTAACCGCA TCTCT	*glp-1*	Primer FW	ChIP-qPCR
glp-1 RV	CGCATTCTCCACCCA TAAGT	*glp-1*	Primer RV	ChIP-qPCR
lag-2 FW	CGCCGTTATGATTTT GGATT	*lag-2*	Primer FW	ChIP-qPCR
lag-2 RV	GACTTCTACTCGGGC TTGGA	*lag-2*	Primer RV	ChIP-qPCR

Annex M3. List of CRISPR reagents used in this study.

ID	Sequence (5' - 3')	Gene	Type	Technique
N-terminal insertion for 3xFLAG and EGFP	CTTGGGGGCAA CGGTTGCCA	*nfki-1*	crRNA	CRISPR-Cas9
C-terminal cut for deletion alleles *cer1* and *cer2*	AATGTTCGTGTT GCCACAGG	*nfki-1*	crRNA	CRISPR-Cas9

N-terminal cut for deletion alleles *cer1* and *cer2*	CTTGTTCGGGA CTGCACCGG	*nfki-1*	crRNA	CRISPR-Cas9
N-terminal cut for deletion allele *cer9* (at promoter before TSS)	ACACACAGTCG AGCAGGCGG	*ikb-1*	crRNA	CRISPR-Cas9
N-terminal cut for deletion allele *cer9* (at exon 4)	AATCCAACGTTC GCATACTC	*ikb-1*	crRNA	CRISPR-Cas9
C-terminal cut for whole *nfki-1* CDS deletion alleles *cer164* and *cer165*	CGACTTGTTCG GGACTGCAC CGG	*nfki-1*	crRNA	CRISPR-Cas9
dpy-10(cn64)	GCTACCATAGG CACCACGAG	*dpy-10*	crRNA	CRISPR-Cas9
dpy-10(cn64)	CACTTGAACTTC AATACGGCAAG ATGAGAATGACT GGAAACCGTAC CGCATGCGGTG CCTATGGTAGC GGAGCTT CACATGGCTTC AGACCAACAGC CTAT	*dpy-10*	ssODN Ultramer Repair template	CRISPR-Cas9

3xFLAG::nfki-1	GTTTTCCAAAATTACGTCGTTTGTTTTCAGCCATGGACTACAAAGACCATGACGGTGATTATAAAGATCATGATATCGATTACAAGGATGACGATGACAAGGCAACCGTTGCCCCCAAGGGAAACTGCCTTGTCGCT	*3xFLAG::nfki-1*	ssODN Ultramer Repair template	CRISPR-Cas9
EGFP::nfki-1	GTTTTCCAAAATTACGTCGTTTGTTTTCAGCCATGTCCAAGGGAGAGGAGCTCTTCACCGGAGTCGTCCCAATCCTCGTCGAGCTCGACGGAGTCAAGGAGTTCGTCACCGCTGCCGGAATCACCCACGGAATGGACGAGCTCTACAAGGCAACCGTTGCCCCCAAGGGAAACTGCCTTGTCGCT	*EGFP::nfki-1*	ssODN Ultramer Repair template	CRISPR-Cas9

nfki-1p::EGFP1-3	GTTTTCCAAAAT TACGTCGTTTGT TTTCAGCCATGT CCAAGGGAGAG GAGCTCTTCAC CGGAGTCGTCC CAATCCTCGTC GAGCTCGACGG AGTCAAGGAGT TCGTCACCGCT GCCGGAATCAC CCACGGAATGG ACGAGCTCTAC AAGGCAGTCCC GAACAAGTCGA GAGCTTGAGCT CTATTC	*nfki-1p::EGFP1-3*	ssODN Ultramer Repair template	CRISPR-Cas9
EGFP::nfki-1 step 2	PCR product amplified from pJJR83 plasmid with the following primers: FW: TCCAAGGGAGA GGAGGACAA RV: CTTGTAGAGCT CGTCCATTC	*EGFP::nfki-1*	PCR product	CRISPR-Cas9